MAGNETOM Flash

Issue Number 97 · 2/2026
ISMRM Edition

magnetomworld.siemens-healthineers.com

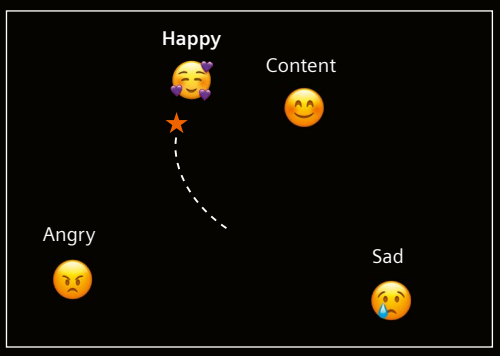

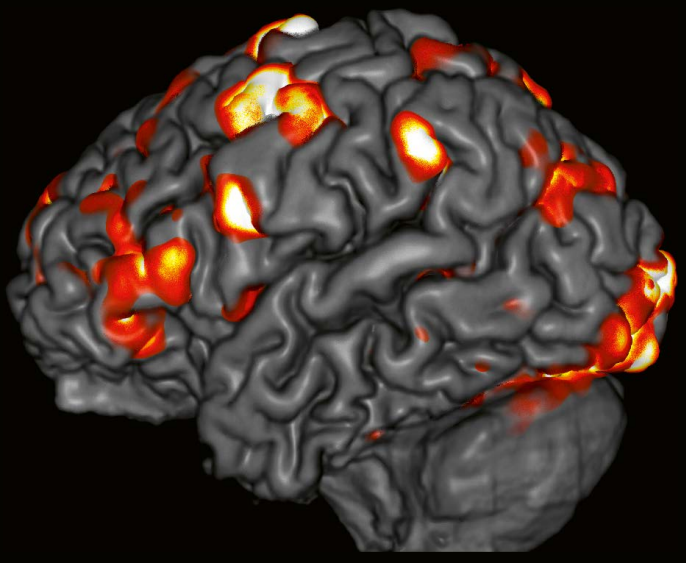

Neurofeedback for Treating Depression

SIEMENS Healthineers

0.55T MAGNETOM Free.Max in Rwanda

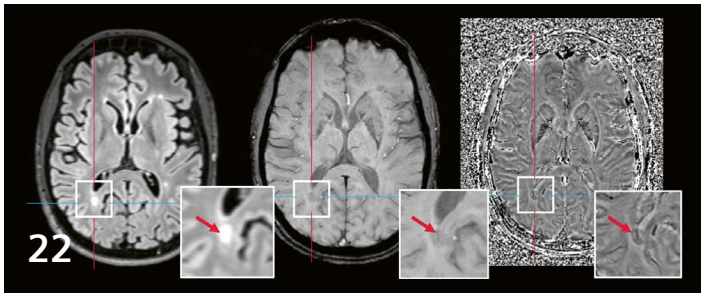

Novel Diagnostic Biomarkers of Multiple Sclerosis

Editorial Comment

Access to MRI / Sustainability

Neurologic Imaging

Interventional MRI / MR in RT

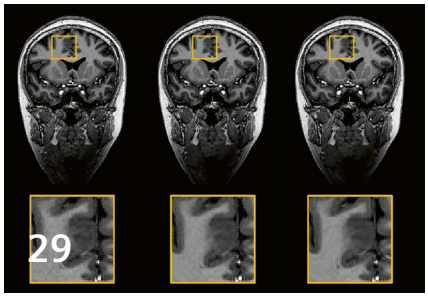

DLR for Submillimeter Neuroimaging at 7T

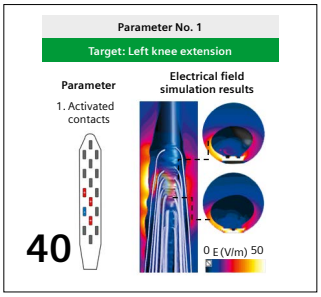

Lumbosacral Spine for Epidural Electrical Stimulation

Intraoperative MRI for Intracranial Lesions

Abdominal Imaging

Fetal Imaging

Cardiovascular Imaging

Meet Siemens Healthineers

[1] Work in progress. The application is currently under development and is not for sale in the U.S. and in other countries. Its future availability cannot be ensured.
[2] MR scanning has not been established as safe for imaging fetuses and infants less than two years of age. The responsible physician must evaluate the benefits of the MR examination compared to those of other imaging procedures.

Ernesta Meintjes is a professor of biomedical engineering at the University of Cape Town (UCT). From 2007 to 2021, she held the prestigious South African Research Chair in Brain Imaging. She completed her Bachelor's Honors and M.Sc. degrees in physics at the University of KwaZulu-Natal (UKZN), Pietermaritzburg campus, in South Africa. Meintjes earned her Ph.D. in physics at Oregon State University in Corvallis, OR, USA. Upon her return to South Africa in 1998, she joined the Biomedical Engineering Department at UCT as a postdoctoral fellow. In this role, she contributed to developing a stereophotogrammetric image-guided neurosurgical navigator. Following the commissioning of the first MRI scanner at Groote Schuur Hospital in November 2001, she embarked on establishing an MRI research stream. In 2004, she implemented the first functional MRI studies in South Africa. These studies led to the establishment of the Cape Universities Brain Imaging Centre (CUBIC), with subsequent expansion to the Cape Universities Body Imaging Centre, of which she has been director since its inception in 2015. Meintjes' research focuses on developing technology to track and correct motion during MRI scanning, and on applying advanced imaging methods to study conditions particularly relevant to South Africa. These include studies on the effects of prenatal insults and diseases — such as HIV, maternal alcohol or drug use during pregnancy, and antiretroviral drugs taken by HIV-infected pregnant women — on brain development. She has authored and coauthored more than 140 peer-reviewed journal papers and more than 250 international conference papers. She has supervised to completion 26 Ph.D. and 31 M.Sc. students, and mentored 22 postdoctoral fellows. She is a fellow of both the University of Cape Town and the American Institute for Medical and Biological Engineering (AIMBE).

"Ubuntu" in the global conversation around MRI access

In the last 50 years, the superior soft tissue contrast of magnetic resonance imaging (MRI) has enabled early, non-invasive detection and characterization of tumors, inflammation, degenerative disease, and congenital abnormalities. As such, it has transformed healthcare across diagnosis, treatment planning, research, and patient safety.

Although I have worked in the MRI field for more than two decades, it wasn't until I attended the 2nd ISMRM Workshop on Accessible MRI in India in 2024 that I became aware of the degree of inequality in access to MRI across the globe. It is estimated that 66% of the world's 8 billion people do not have access to MRI [1–9]. As shown in Figure 1, the scanner density in low- and middle-income countries (LMICs) is significantly lower than in high-income countries (HICs). Further, disparities exist even within countries, with a higher density of scanners located in urbanized regions. Wealthier sectors of the population who can afford private healthcare also enjoy wider access than those relying on public healthcare. This is especially evident in Africa, which has a history of inequality, poverty, and political instability (Fig. 2) [3]. Limited access to MRI causes delays in diagnosis and management of diseases such as stroke, cancer, spinal/joint disease, and congenital heart disease, worsening outcomes and increasing downstream costs.

The need for innovation in the cost of MRI systems

Rapid innovation has been a constant and characteristic feature of the MRI community, but this has not extended to reducing the overall costs of MRI scanners. As such, clinical and research access to MRI remains available primarily to the privileged. I believe this is in part due to most members of our community not being aware of the magnitude of the problem, and to limited resources having been devoted to solving it. To put this in perspective, consider a country like South Africa. South Africa would need to purchase around 355 1.5T MRI scanners to increase the number of MRI scanners in the public sector from currently 0.6 per million population (pmp) to 7 pmp. This would put it on a par with the UK, but would still only be one third of the 22 pmp scanners available in South Africa's private sector. For the 85% of South Africans who rely on public healthcare, such an increase would shorten outpatient wait times for an MRI scan from the current 10–48 months to 1–4 months. Assuming a purchase price of $1 million per Tesla, purchasing these scanners would require the government to invest around $533 million — roughly 3% of South Africa's annual national health budget. Clearly, this is an insurmountable ask for an already stretched economy that struggles to deliver basic healthcare services. The situation in many other African countries is even more dire.

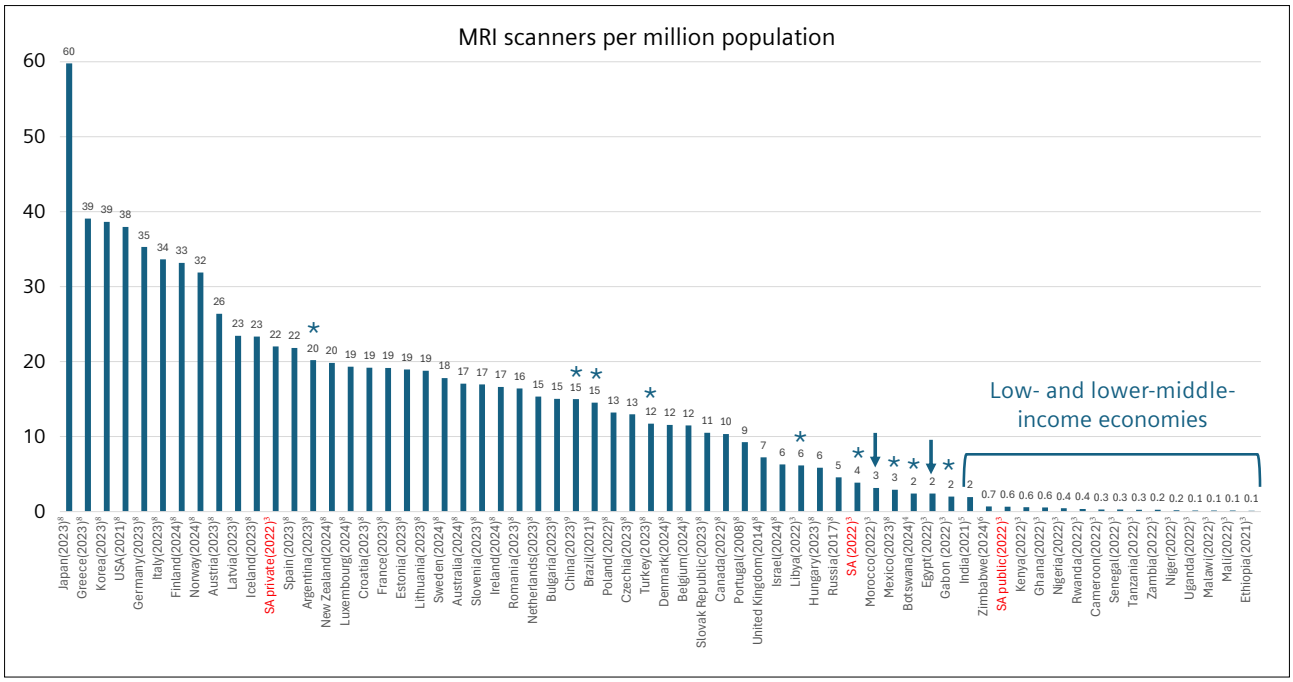

1 MRI scanners per million population by country. The blue bracket and arrows indicate low- and lower-middle-income economies, as defined by the World Bank for the 2026 fiscal year (datahelpdesk.worldbank.org/knowledgebase/articles/906519-world-bank-country-and-lending-groups); asterisks indicate upper-middle income economies. The disparity between the number of MRI scanners in South Africa's (SA) public and private sectors is highlighted. Notably, the public health system serves 85% of South Africans.

Mid-field MRI: Diagnostic images at lower cost

Recently, Synaptive Medical and Siemens Healthineers re-introduced commercial MRI scanners with 0.5–0.6T magnets [2, 10], which fall into the mid-field range (0.3T–1T) as defined by Arnold et al. [11]. These systems exploit increases in magnetic field gradient amplitude and slew rates, parallel imaging, compressed sensing, and improved image reconstruction algorithms that incorporate artificial intelligence (AI) to acquire diagnostic-quality images within acceptable scan times [12–16]. The scanners from Siemens Healthineers also feature DryCool technology, which means they need just 0.7 liters of liquid helium and no quench pipe. The helium-free magnet and the system's smaller footprint reduce siting and maintenance costs, respectively. However, even at an estimated $300,000 to $700,000 [2], the purchase price of these mid-field systems is still a significant barrier to LMICs, which would need to purchase hundreds of these systems to solve their MRI access crisis.

Very-low-field MRI: Promising, but price issues and concerns remain

To bring costs down by an order of magnitude, attention has turned to very-low-field MRI (0.01T–0.1T) [1, 11, 17, 18]. Currently, the only commercially available very-low-field MRI system that has FDA approval for clinical use is the 64 mT Hyperfine Swoop [19–22]. Despite initial optimism for a truly affordable, clinically viable brain MRI scanner that could be rolled out as a screening tool in remote settings, prices quickly soared from an initial $50,000 [21], still well within the $1 million per Tesla heuristic, to somewhere between $250,000 and $600,000 [23, 24]. Additionally, concerns remain regarding the extensive use of black-box AI algorithms by these systems, and the ethics around data sharing and ownership.

It is fortunate that awareness of accessibility-related issues is growing in the MRI community. This has led to tremendous progress in research on very-low-field MRI over a short period of time [25–31]. Additionally, researchers have made the technical details of their developments public through an open-source approach, thereby reducing barriers to entry for new researchers. And although the idea of manufacturing and donating very-low-field MRI scanners to resource-constrained settings is well intentioned, as a researcher based in Africa, I must caution

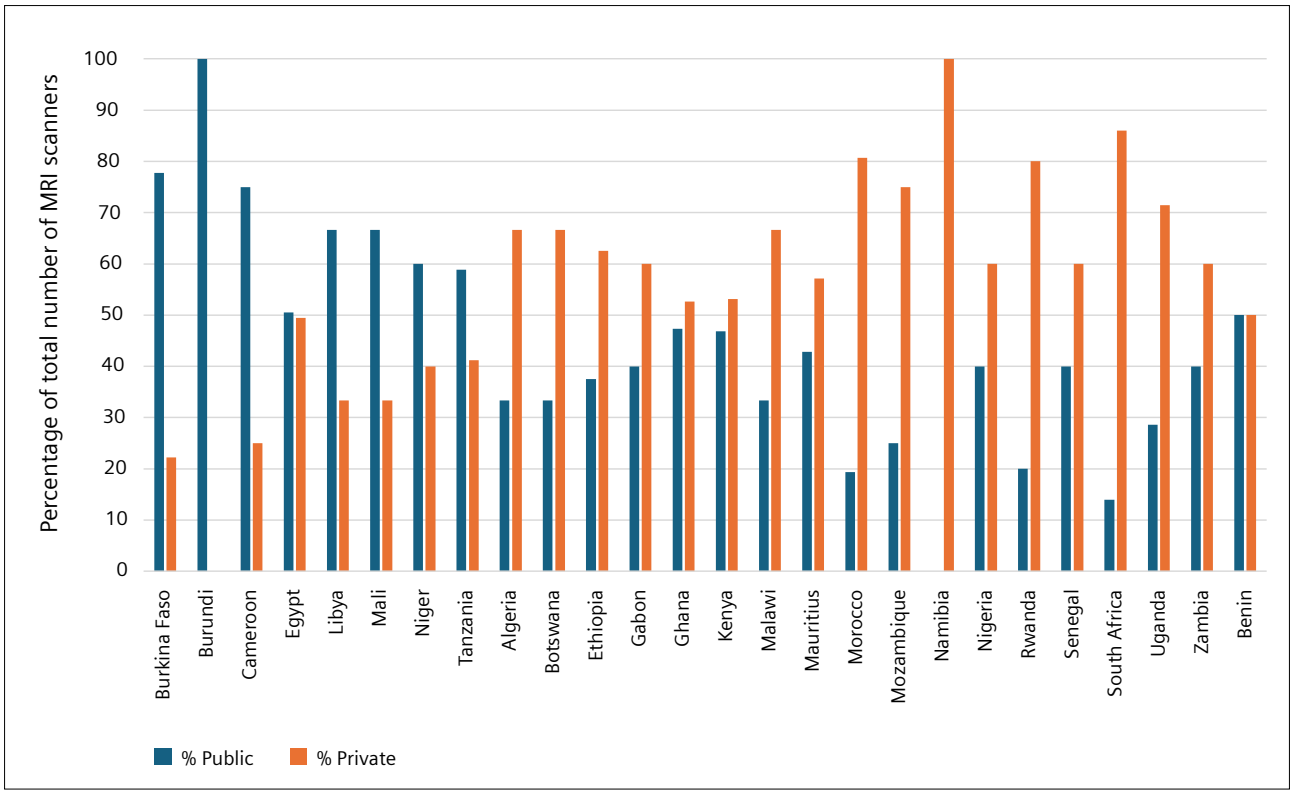

2 Percentage of the total number of MRI scanners in various African countries located in public and private healthcare facilities, respectively. Source: [3].

against donation models that are tied to data extraction or that are not grounded in locally defined needs. Approaches that bypass meaningful engagement with local stakeholders do little to strengthen local capacity building and do not assist under-resourced countries in becoming the architects of their own future. Rather, it makes them dependent on ongoing support or the need to purchase technology manufactured in the Global North [32]. That said, genuinely mutually beneficial donation models — those co-designed with local partners, aligned with local priorities, and coupled with sustained investment in training, maintenance infrastructure, and institutional capacity — can be highly valuable.

A different approach in India

The significant investment by the Indian government in capacity building and local manufacturing of MRI systems that operate at the current standard of performance presents a perfect counterexample. By facilitating in-house serviceability and maintenance [33, 34], India aims to substantially reduce the cost of ownership and address the country's challenges regarding MRI access. India's approach highlights a characteristic that I believe wealthier countries often overlook in under-resourced countries — namely the desire for self-sufficiency rather than dependency. This resonates with the well-known proverb, "Give a man a fish and you feed him for a day; teach a man to fish and you feed him for a lifetime."

Unanswered questions around very-low-field MRI

It remains to be established whether very-low-field MRI is sufficiently robust and reliable for routine clinical use, whether the reliance on AI is too high, and whether the applications are too specific. Another question is whether the reduction in manufacturing and ownership costs justifies the limited usability. It may be that the sweet spot for a system that is widely clinically useful lies somewhere between 0.05T and 0.5T. And even if very-low-field MRI is

deemed to have a role, will it be considered adequate by clinicians and patients, or will it be rejected as a cheap surrogate? These and many other questions remain to be answered before very-low-field portable MRI systems can truly be considered as a clinically feasible solution for rural and under-resourced settings.

Moreover, in addition to solving the numerous technical challenges that arise from operating in the noise-dominated regime, AI pipelines will need to be developed and implemented to simplify workflows and patient positioning to compensate for skills shortages; telemedicine solutions will need to be tailored to settings with fluctuating bandwidth to facilitate remote reporting; and systems that run on alternative energy sources or batteries will need to be employed to combat unstable power supplies. Regulatory processes will also differ in each country and will need to be considered.

The bigger picture

Notably, while this piece focuses on the overall costs of MRI, the principles highlighted also apply to all technical advancements in the field. It is vital for researchers to contemplate the true costs of the solutions they are developing and whether these will be broadly accessible or limited to a privileged few.

Given this context and landscape, it is an exciting time to be working in MRI in Africa. Further, the bold move by the ISMRM to host its annual meeting on the African continent for the first time provides a unique opportunity for scientists from the Global North to be exposed to a less privileged setting and, to some degree, the challenges this presents. The theme of the meeting is "Ubuntu," which loosely translates to "I am what I am because of who we all are." This reminds and compels each of us to consider our responsibility toward and dependence on each other.

Acknowledgments

I am grateful to Associate Professor Frances Robertson for assisting me with this paper.

Ernesta Meintjes

References

1 Murali S, Ding H, Adedeji F, Qin C, Obungoloch J, Asllani I, et al. Bringing MRI to low- and middle-income countries: Directions, challenges and potential solutions. NMR Biomed. 2024; 37(7):e4992.
2 Gulani V, Kandasamy D, Webb AG, Jones DK, Sharma R. Expanding Access to MRI: The Role of All-Purpose Mid-Field and 1.5-T Scanners. Radiology. 2025;316(3):e251406.
3 Hasford F, Mumuni AN, Trauernicht C, Ige TA, Inkoom S, Okeji M, et al. A review of MRI studies in Africa with special focus on quantitative MRI: Historical development, current status and the role of medical physicists. Physica Med. 2022;103:46–58.
4 Nlashwa GD, Sinvula M, Setso SO, Miller W, Lesiamang M, Maboreke T, et al. An audit of licenced radiological equipment and personnel in Botswana. J Coll Med S Afr. 2024;2(1):87. Corrigendum in: J Coll Med S Afr. 2024;2(2):152.
5 Sharma R, Kandasamy D, Goyal A. Current Status of MRI in India. ↗ MAGNETOM Flash. 2021;78(1):4–5.
6 Chinene B, Mudadi LS, Mutasa FE, Nyawani P. A survey of magnetic resonance imaging (MRI) availability and cost in Zimbabwe: Implications and strategies for improvement. J Med Imaging Radiat Sci. 2025;56(2):101819.
7 Geethanath S, Vaughan JT Jr. Accessible magnetic resonance imaging: A review. J Magn Reson Imaging. 2019;49(7):e65–e77.
8 Organisation for Economic Co-operation and Development. Magnetic resonance imaging (MRI) units. Cited March 2, 2026. Available from: https://www.oecd.org/en/data/indicators/magnetic-resonance-imaging-mri-units.html
9 Eastmoney Securities. 2024 China Medical Imaging Equipment Industry Market Prospect Forecast Research Report. August 22, 2024. Cited March 2, 2026. Available from: https://caifuhao.eastmoney.com/news/20240822145921907519450.
10 Hennig J. An evolution of low-field strength MRI. MAGMA 2023;36(3):335–346.
11 Arnold TC, Freeman CW, Litt B, Stein JM. Low-field MRI: Clinical promise and challenges. J Magn Reson Imaging. 2023;57(1):25–44.
12 Hori M, Hagiwara A, Goto M, Wada A, Aoki S. Low-Field Magnetic Resonance Imaging: Its History and Renaissance. Invest Radiol. 2021;56(11):669–679.
13 Breit HC, Obmann M, Schlicht F, Vosshenrich J, Segeroth M, Bach M, et al. New-generation 0.55T MRI in patients with total hip arthroplasty: a comparison with 1.5T MRI. Clin Radiol. 2025; 81:106758.
14 Lavrova A, Mishra S, Kim J, Lobo R, Masotti M, Richardson J, et al. Retrospective comparison of routine brain MRI scans in patients at 0.55 T and 1.5/3T. Eur J Radiol. 2025;184:111929.
15 Lopez Schmidt I, Haag N, Shahzadi I, Frohwein LJ, Schneider C, Niehoff JH, et al. Diagnostic Image Quality of a Low-Field (0.55T) Knee MRI Protocol Using Deep Learning Image Reconstruction Compared with a Standard (1.5T) Knee MRI Protocol. J Clin Med. 2023;12(5):1916.
16 Rusche T, Vosshenrich J, Winkel DJ, Donners R, Segeroth M, Bach M, et al. More Space, Less Noise-New-generation Low-Field Magnetic Resonance Imaging Systems Can Improve Patient Comfort: A Prospective 0.55T-1.5T-Scanner Comparison. J Clin Med. 2022; 11(22):6705.
17 Anoardo E, Rodriguez GG. New challenges and opportunities for low-field MRI. J Magn Reson Open. 2023;14–15:100086.

18 Qin C, Murali S, Lee E, Supramaniam V, Hausenloy DJ, Obungoloch J, et al. Sustainable low-field cardiovascular magnetic resonance in changing healthcare systems. Eur Heart J Cardiovasc Imaging. 2022;23(6):e246–e260.
19 Hyperfine Inc. The Swoop System: Putting AI-powered portable MRI in your hands. 2025. Accessed March 15, 2026. Available from: https://www.hyperfinemri.com/
20 Mazurek MH, Cahn BA, Yuen MM, Prabhat AM, Chavva IR, Shah JT, et al. Portable, bedside, low-field magnetic resonance imaging for evaluation of intracerebral hemorrhage. Nat Commun. 2021; 12(1):5119.
21 Deoni SCL, Medeiros P, Deoni AT, Burton P, Beauchemin J, D'Sa V, et al. Development of a mobile low-field MRI scanner. Sci Rep. 2022;12(1):5690.
22 Hovis G, Langdorf M, Dang E, Chow D. MRI at the Bedside: A Case Report Comparing Fixed and Portable Magnetic Resonance Imaging for Suspected Stroke. Cureus. 2021;13(8):e16904.
23 Cho A. MRI for All. Science. 2023;379(6634)7648–751.
24 Zeidenberg J. Kingston Health Sciences among first to use portable MRI in the ICU. Canadian Healthcare Technology. Jan 31, 2025. Cited March 2, 2026. Available from: https://www.canhealth.com/2025/01/31/kingston-health-sciences-among-first-to-use-portable-mri-in-the-icu/
25 Kimberly WT, Sorby-Adams AJ, Webb AG, Wu EX, Beekman R, Bowry R, et al. Brain imaging with portable low-field MRI. Nat Rev Bioeng. 2023;1(9):617–630.
26 Obungoloch J, Muhumuza I, Teeuwisse W, Harper J, Etoku I, Asiimwe R, et al. On-site construction of a point-of-care low-field MRI system in Africa. NMR Biomed. 2023;36(7):e4917.
27 Guallart-Naval T, O'Reilly T, Algarín JM, Pellicer-Guridi R, Vives-Gilabert Y, Craven-Brightman L, et al. Benchmarking the performance of a low-cost magnetic resonance control system at multiple sites in the open MaRCoS community. NMR Biomed. 2023; 36(1)e4825.
28 Zhao Y, Ding Y, Lau V, Man C, Su S, Xiao L, et al. Whole-body magnetic resonance imaging at 0.05 Tesla. Science. 2024; 384(6696):eadm7168.
29 O'Reilly T, Teeuwisse WM, de Gans D, Koolstra K, Webb AG. In vivo 3D brain and extremity MRI at 50 mT using a permanent magnet Halbach array. Magn Reson Med. 2021;85(1):495–505.
30 de Vos B, Remis RF, Webb AG. An integrated target field framework for point-of-care halbach array low-field MRI system design. MAGMA. 2023;36(3):395–408.
31 Anazodo UC, Ng JJ, Ehiogu B, Obungoloch J, Fatade A, Mutsaerts HJMM, et al. A Framework for Advancing Sustainable MRI Access in Africa. medRxiv. 2022;22274588.
32 Shen FX, Wolf SM, Bhavnani S, Deoni S, Elison JT, Fair D, et al. Emerging ethical issues raised by highly portable MRI research in remote and resource-limited international settings. Neuroimage. 2021;238:118210.
33 Harsh R. Project SAMEER in India: Building a Homegrown MRI Scanner from the Ground Up in an LMIC Environment. Workshop given at the 2nd ISMRM Workshop on Accessible MRI. 16–18 Feb 2024. India International Centre, New Delhi, India.
34 Harsh R. Accessible and Affordable MRI to Make World Healthier: An Indian Initiative. In: Proc Intl Soc Magn Reson Med. 2020;28.

We appreciate your comments.
Please contact us at magnetomworld.team@siemens-healthineers.com

Editorial Board

Review Board

Democratizing Neuroimaging: A Global MRI Training Program to Strengthen Neuroimaging Capacity in Resource-Constrained Settings

Cristian Montalba[1], Abderrazek Zeraii[2], Marina Fernandez Garcia[3,4], Juhi Tulsi[4], Francis Botwe[5], Surendra Maharjan[6], Abdul Nashirudeen Mumuni[7], Jackline Thairu[8], Harrison Aduluwa[9], Guy Poloni[10], Fatade Abiodun[9,11], and Udunna Anazodo[4,9,12]

[1] Biomedical Imaging Center, Pontificia Universidad Católica de Chile, Santiago, Chile
[2] International General Equipment, Tunis, Tunisia
[3] Institute for Molecular Imaging and Instrumentation, Universitat Politenica de Valencia, Spain
[4] Consortium for Advancement of MRI Education and Research in Africa (CAMERA), Montreal, Canada
[5] Clinical Imaging Sciences Centre, University of Sussex, Brighton, United Kingdom
[6] Brain Health Imaging Institute, Weill Cornell Medicine, New York, NY, USA
[7] Diagnostic Imaging Research Centre, University for Development Studies, Tamale, Ghana
[8] Sonar Imaging Centre, Nairobi, Kenya
[9] Medical Artificial Intelligence Laboratory, Lagos, Nigeria
[10] Siemens Healthineers, Erlangen, Germany
[11] Crestview Radiology, Ltd, Lagos, Nigeria
[12] Montreal Neurological Institute, McGill University, Montreal, Canada

Neurological disorders are a public health challenge in low- and middle-income countries (LMICs), particularly in sub-Saharan Africa (SSA). These regions face significant barriers, including limited healthcare resources, shortage of trained medical professionals, and persistent cultural challenges that impact access to care [1]. These challenges are exacerbated by other regional health concerns — such as malnutrition, adverse perinatal conditions, HIV/AIDS, and infectious disease (encephalitis, meningitis, tuberculosis, malaria) — which impact brain health and further compromise the effectiveness of prevention, diagnosis, and treatment strategies for neurological disorders [2].

Take dementia, for example: According to the World Health Organization, more than 68% of individuals living with dementia will reside in LMICs by 2050, with a substantial proportion in African countries [3]. Neuroimaging plays a critical role in improving diagnosis and informing management to reduce the rising health and economic impacts. Magnetic resonance imaging (MRI) is a key tool in managing dementia and other neurological diseases, but its use in LMICs remains limited due to infrastructure constraints, workforce shortages, unreliable power supply, and restricted financing options [4]. Nevertheless, as we will see later with the resource-efficient MAGNETOM Free.Max in Rwanda, new MRI installations are growing across African countries and other LMICs. However, democratizing advanced MRI protocols tailored to these unique health environments remains a challenge.

To help bridge this gap, we partnered with Siemens Healthineers to introduce the Scan With Me (SWiM) training program (Fig. 1) through the Consortium for Advancement of MRI Education and Research in Africa (CAMERA) [5].

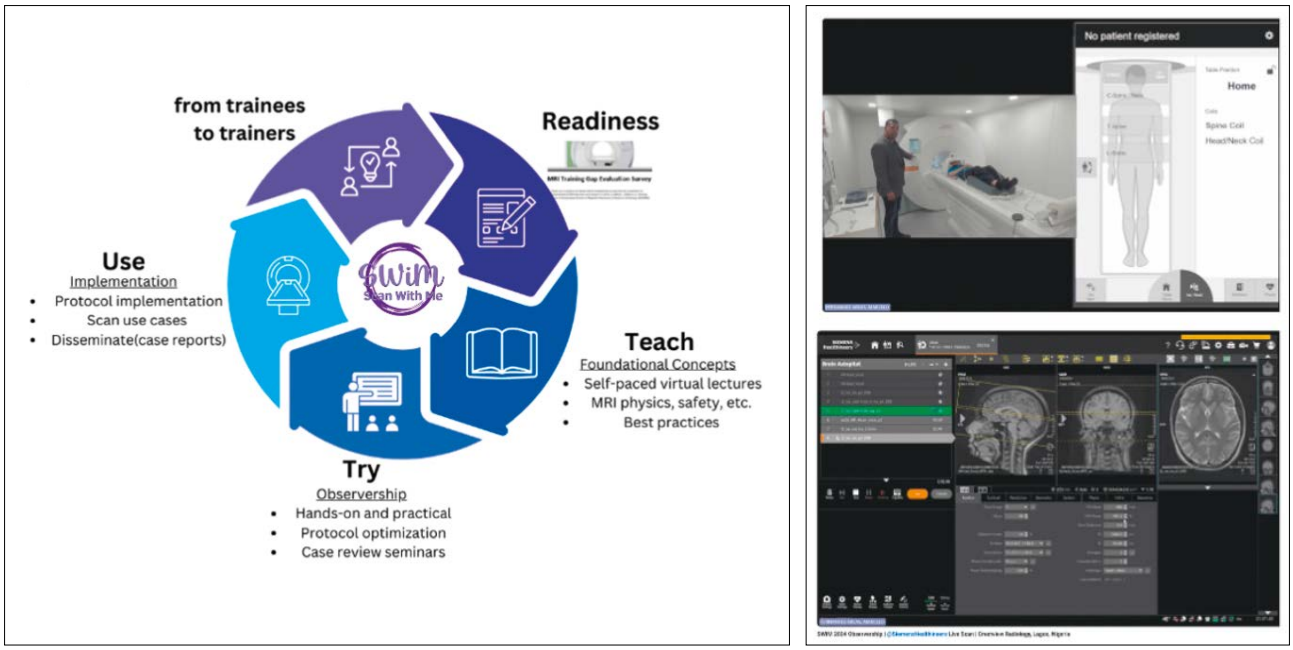

1 The Scan With Me (SWiM) curriculum and its structured training approach upskill practicing MRI technologists. It does this through best practices in MRI acquisition and protocol optimization, as well as hands-on demonstrations of advanced imaging techniques in simulated and live scanning environments. This includes a live scan session from Erlangen, Germany, with MRI technologists and application specialists from Siemens Healthineers.

Scan With Me (SWiM): Optimizing MRI infrastructure by training trainers

The SWiM program is a global initiative designed to strengthen MRI capacity in LMICs through a structured, train-the-trainer model that upskills practicing MRI technologists (Fig. 1) [6]. The annual program delivers an eight-week curriculum that integrates foundational MRI principles, hands-on observerships, expert-led seminars from members of ISMRM and ISMRT, and collaborative team-based capstone projects that are delivered using a case-based and peer-to-peer learning approach based on RAD-AID's Teach-Try-Use framework [7].

Since 2023, SWiM has trained 233 MRI technologists from 25 LMICs across Africa, Latin America, and Southeast Asia (Fig. 2). A total of 30% of the alumni have now joined the program as faculty or are leading local MRI capacity-building and mentorship initiatives, such as ISMRT chapters and divisions.

The 2023 program focused on cardiac imaging, while the following two years emphasized brain imaging, which is the most common MRI indication in LMICs. Over the three-year period, participants received 220 hours of specialized instruction, complemented by 80 hours of weekly peer-to-peer engagement that enabled the technologists to collaboratively implement and share optimized scan protocols for common cardiac and brain indications on their local scanners (Fig. 2).

The structure and outcomes of the 2023 cardiac imaging program have been reported previously [6]. For the 2024/2025 brain imaging programs, 28 of the live online sessions covered advanced techniques such as functional MRI (fMRI), diffusion tensor imaging (DTI), arterial spin labeling (ASL), and magnetic resonance spectroscopy (MRS). Training was delivered through seminars, simulations using the SmartSimulator from Siemens Healthineers, and hybrid live scans in Kenya, Nigeria, and Rwanda (Figs. 1, 2). Despite 80% of participants having fewer than five years of MRI experience, 82.85% reported improved knowledge of brain MRI scanning, including safety, positioning and landmarking, artifact recognition and mitigation, and standard-of-care best practices.

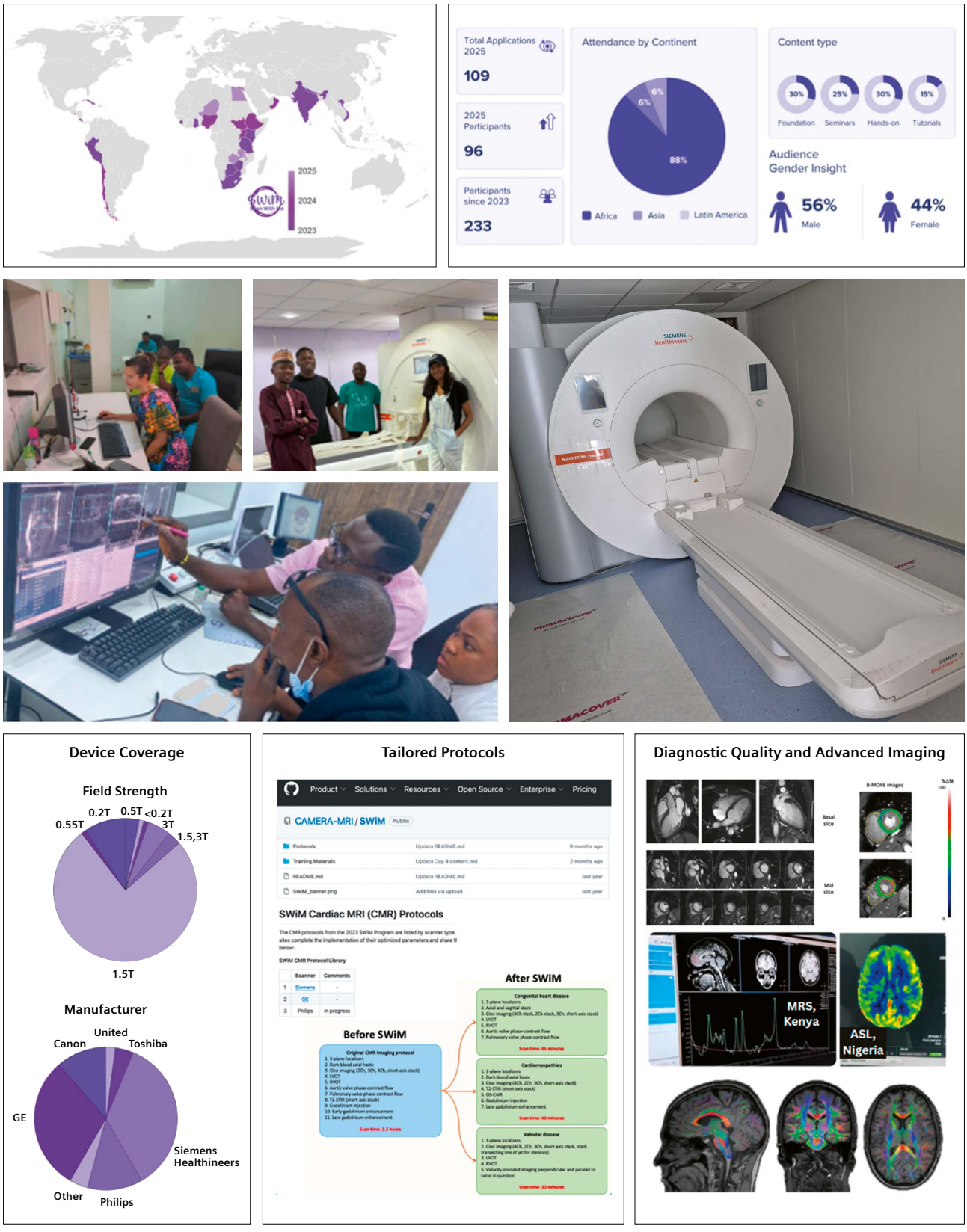

2 The impact of the SWiM program from its inception in 2023 to the most recent program in 2025.

3 A 0.55T MAGNETOM Free.Max with DryCool technology. The system is installed in a mobile unit at the University Teaching Hospital of Kigali, Rwanda.

Breaking barriers across Africa: Rwanda installs its first 0.55T MAGNETOM Free.Max

Limited access to MRI in LMICs is also due to challenges in deploying the scanners themselves. The installation of a 0.55T MAGNETOM Free.Max at CHUK, the University Teaching Hospital of Kigali (Fig. 3), a 519-bed teaching hospital in Rwanda, shows how innovative MRI technology can overcome traditional barriers and expand access to high-quality diagnostic imaging in emerging healthcare environments.

Simplifying installation

Conventional MRI systems often require extensive site preparation, including reinforced flooring, complex radiofrequency (RF) shielding, quench pipe installation, and substantial power and cooling infrastructure. These requirements can pose considerable challenges to healthcare facilities in resource-constrained regions.

The MAGNETOM Free.Max introduces a new paradigm in MRI deployment: Its lightweight design, reduced helium dependency thanks to DryCool technology, and simplified installation requirements make it ideal for clinical environments that would be unsuitable for conventional MRI systems. In Rwanda, these advantages facilitated the smooth installation of a mobile unit (Fig. 3) and minimized infrastructure modifications and costs. This flexibility represents a major step forward in making MRI more accessible across Africa and other resource-constrained settings.

Expanding clinical capabilities

The MAGNETOM Free.Max significantly improves the diagnostic capabilities available to clinicians in Rwanda. The system supports a wide range of clinical applications, including:

- Neurological imaging for stroke, tumors, and neurodegenerative diseases
- Spine imaging for degenerative and traumatic conditions
- Musculoskeletal imaging for orthopedic and sports injuries
- Abdominal and pelvic imaging for comprehensive diagnostic evaluation

The system's design also improves patient comfort, helping reduce motion artifacts and improving overall image quality. By enabling advanced imaging locally, MAGNETOM Free.Max reduces the need for patients to be referred abroad and shortens diagnostic timelines.

Supporting sustainable MRI in Africa

One of the key challenges in expanding MRI across Africa is ensuring sustainability. The MAGNETOM Free.Max addresses this through reduced energy consumption, simplified maintenance, and lower infrastructure demands. These features make MRI operations more sustainable and support long-term healthcare development. The scanner also provides valuable opportunities for local capacity building (Fig. 4). Technologists, radiologists, and MRI specialists gain hands-on experience with advanced MRI technology, strengthening local expertise and supporting the continued growth of medical imaging services.

4 Structured training in MRI acquisition and protocol optimization, as well as hands-on demonstrations of advanced imaging techniques.

A milestone for Rwanda and the African continent

The installation of Rwanda's first MAGNETOM Free.Max represents more than the introduction of a new imaging system. It reflects a broader transformation in how MRI can be deployed in resource-optimized environments. It shows that advanced MRI is no longer limited to highly specialized centers, and can now be successfully implemented in diverse healthcare settings across Africa. It is a model for future installations and highlights the importance of innovation in addressing global healthcare disparities.

Conclusion

Breaking traditional barriers to MRI access requires technological innovation, collaboration, and a commitment to expanding diagnostic capabilities worldwide. The success of the scalable, long-term capacity-building initiatives like SWiM and the installation of the 0.55T MAGNETOM Free.Max in Rwanda are major steps toward this goal. They show how innovative MRI solutions can empower healthcare professionals, democratize access, enhance diagnostic precision and clinical decision-making, and ultimately improve patient outcomes across resource-constrained settings.

Acknowledgment

We gratefully acknowledge the team at Siemens Healthineers for facilitating the live scanning and scan simulator: Jutta Kaiser Gen Rentzing; André Fischer, Ph.D.; Dennis Bogena; Marcelo Fernandes Arêas; Cristiano Panella; Katrin Schmidt-Kaiser; Subin Kottayi; Jing Jing Ling

References

1 GBD 2021 Nervous System Disorders Collaborators. Global, regional, and national burden of disorders affecting the nervous system, 1990-2021: a systematic analysis for the Global Burden of Disease Study 2021. Lancet Neurol. 2024;23(4):344–381. Erratum in: Lancet Neurol. 2024;23(5):e9. Erratum in: Lancet Neurol. 2024;23(7):e11.

2 Ngarka L, Siewe Fodjo JN, Aly E, Masocha W, Njamnshi AK. The Interplay Between Neuroinfections, the Immune System and Neurological Disorders: A Focus on Africa. Front Immunol. 2022; 12:803475.

3 Akinyemi RO, Yaria J, Ojagbemi A, Guerchet M, Okubadejo N, Njamnshi AK, et al. Dementia in Africa: Current evidence, knowledge gaps, and future directions. Alzheimers Dement. 2022;18(4):790–809.

4 Anazodo UC, Ng JJ, Ehiogu B, Obungoloch J, Fatade A, Mutsaerts HJMM, et al. A framework for advancing sustainable magnetic resonance imaging access in Africa. NMR Biomed. 2023; 36(3):e4846.

5 Consortium for Advancement of MRI Education and Research in Africa. SWiM Program. Cited March 26, 2026. Available from: https://www.cameramriafrica.org/swim

6 Mumuni AN, Eyre K, Montalba C, Harrison A, Maharjan S, Botwe F, et al. Scan With Me: A Train-the-Trainer Program to Upskill MRI Personnel in Low- and Middle-Income Countries. J Am Coll Radiol. 2024;21(8):1222–1234.

7 Elahi A, Dako F, Zember J, Ojetayo B, Gerus DA, Schweitzer A, et al. Overcoming Challenges for Successful PACS Installation in Low-Resource Regions: Our Experience in Nigeria. J Digit Imaging. 2020;33(4):996–1001.

8 CAMERA Africa. SWiM 2024 Observership @SiemensHealthineers Live Scan with Crestview Radiology, Lagos, Nigeria. Event held on August 24, 2024 in Erlangen, Germany. Video accessed on March 26, 2026. Available from: https://youtu.be/KMn7Gg1kbpc?si=xE-ToEXnor6QC7Xv

Cristian Montalba, M.Sc. Abderrazek Zeraii, Ph.D. Udunna Anazodo, Ph.D.

Contact

Udunna C. Anazodo, Ph.D.
Assistant Professor of Neurology and Neurosurgery
Montreal Neurological Institute at McGill University
3801 Rue University, Montréal, QC H3A 2B4
Canada
udunna.anazodo@mcgill.ca

Could AI-Driven Acceleration Techniques be One Answer to the Issue of Environmental Sustainability in MRI?

Angela Borella, DipRadDiag (UTas), MRSO (ABMRS), DipMn (Monash)[1]
Justin Warner, BMedRadSc (MedImaging)(CSU), MRSO (ABMRS), MAppSc (MRI)[2]

[1] Monash Health, Melbourne, VIC, Australia
[2] Castlereagh Imaging, Westmead, Sydney, NSW, Australia

Background

Magnetic resonance imaging (MRI) plays a vital role in medical imaging, providing the high-resolution images that are crucial for accurate disease diagnosis and patient management. However, healthcare in general and imaging in particular have a considerable environmental impact: The global healthcare sector accounts for 4.4% of greenhouse gas (GHG) emissions, but here in Australia that figure is 7% [1]. A recent study found that pathology testing and diagnostic imaging in New South Wales, Australia's largest health system, contribute 9% of the carbon footprint from Australian healthcare [1]. As the healthcare industry seeks to reduce its carbon footprint, imaging technologies clearly have a vital role to play here, too.

MRI systems are highly energy-intensive [5]. This poses significant challenges for healthcare sustainability and environmental preservation. One way of addressing the energy issue in MRI is to use artificial intelligence — specifically, deep learning.

While deep learning applications can optimize multiple aspects of MRI operations, their ability to accelerate imaging protocols is especially relevant to sustainability. With advanced denoising techniques, deep learning maintains diagnostic image quality while significantly shortening the time required for each scan. Since faster scans use less energy, deep learning has the potential to minimize greenhouse gas emissions from MRI systems.

Impact of deep learning on scan times at our institution

We recently implemented Deep Resolve, an AI-powered, deep learning image-reconstruction technology from Siemens Healthineers, on our 3 Tesla MAGNETOM Vida system (Siemens Healthineers, Erlangen, Germany). At the time of writing, Deep Resolve has not yet been fully implemented across all MRI scanners in our multi-hospital network.

For the initial implementation, we targeted one of our frequently requested examinations on the MAGNETOM Vida system, to see where we could have the most impact in terms of time savings. To do so, we gathered data on all the MRI examinations performed on the system in 2023. This showed that we most commonly performed brain and spinal cord imaging for multiple sclerosis (MS) and demyelination pathologies. For this examination alone, Deep Resolve enabled us to achieve a 42% time saving, reducing the active scan time from 50 minutes to 29 minutes (Table 1) with comparable, and in some instances improved, image quality (Fig. 1).

Our 3T MAGNETOM Vida is operational for 89.5 hours per week, from 7:30 a.m. to 10:00 p.m. Monday to Friday, and from 8:00 a.m. to 4:30 p.m. on Saturday and Sunday. Therefore, a 42% reduction in active scan time for one of our most frequent examinations effectively means a savings of 228 hours, or approximately 2.5 weeks, per year.

Number of exams in 2023	Pre-AI active scan time	Post-AI active scan time	Active scan time reduction per patient	Active scan time reduction per year (minutes)	Active scan time reduction per year (hours)
651 exams	50 min	29 min	21 min (42%)	13,671 min	228 hrs

Table 1: Retrospective analysis of 2023 data for brain and spinal cord MRI.

The average power consumption of a 3T MAGNETOM Vida during active scanning is 23.4 kW [9]. Using this figure and our 2023 scan data numbers, the kWh required for active scanning in a brain and spinal cord examination is 12,675 kWh across the year. After implementing Deep Resolve on this protocol, the kWh required for active scanning declined to an extrapolated 7,363 kWh for one year. This reduces the average power consumption by 5,312 kWh per year. According to the Carbon intensity of electricity generation in 2023 this would be equivalent to 2.9 metric tons of carbon dioxide-equivalent emissions in Australia [10]. This equivalent to the carbon sequestered by planting and growing 48 tree seedlings for 10 years [11].

These rudimentary numbers are based only on active scanning energy consumption from a single examination after the implementation of Deep Resolve. Given that AI-driven reconstruction leads to some substantial time savings and if similar time savings were extrapolated out across other time-intensive MRI examinations, and across other scanners and sites, the impact on greenhouse gas emissions would speak for itself.

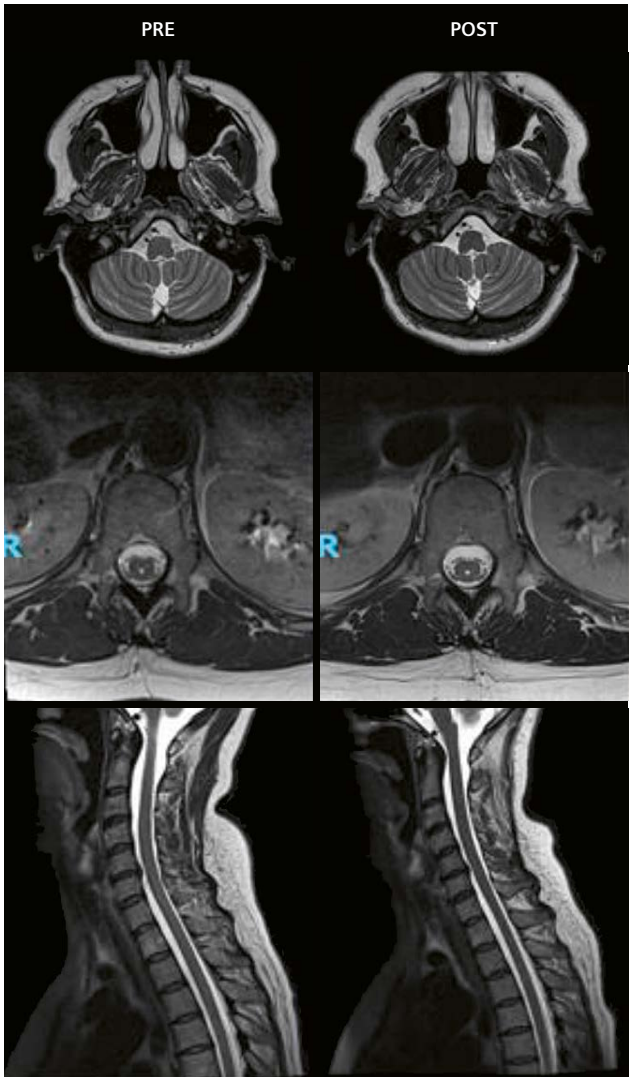

1 Brain and spinal cord images from a patient scanned for demyelination. Imaging was performed both before and after the introduction of AI software (Deep Resolve) from Siemens Healthineers. The left-hand images are before the introduction of Deep Resolve, and the right-hand images are after. Our aim was to achieve equal, if not better, image quality with the AI software.

Co-benefits

In addition, the shortened scan times enabled by Deep Resolve also reduce costs [5] and improve patient comfort [3]. They can increase diagnostic accuracy because faster scans may lead to less movement in patients who find it hard to lie still for long periods. They can also increase patient tolerance and compliance. Technologists benefit as well, with the potential for less stress at work as a result of having more capacity to handle urgent patients, and a reduction in the need for overtime. Furthermore, the newly created space in the schedule could be used to provide technologists with much-needed time for implant investigation, online mandatory training, and continuing professional development. This is what our organization is hoping to do once Deep Resolve has been fully implemented.

Summary

Deep learning technology is a new pathway to improved sustainability within MRI. By decreasing energy consumption and improving imaging efficiency, AI could be the game changer we need at this crucial time in the history of climate change. It also brings co-benefits in the form of lower operational costs, improved patient comfort and diagnostic accuracy, and scope to allocate resources and time more effectively for technologists.

As medical imaging and healthcare in general embrace the digital transformation, leveraging AI is a key cog in the larger strategy required for creating a more sustainable and efficient healthcare system. With AI continuing to develop and transform medical imaging, we must continue to think of ways to harness its potential for improving sustainability.

Acknowledgments

We would like to thank Professor Roland Bammer and Associate Professor Shalini Amukotuwa for their ongoing support.

References

1 McAlister S, McGain F, Petersen M, Story D, Charlesworth K, Ison G, et al. The carbon footprint of hospital diagnostic imaging in Australia. Lancet Reg Health West Pac. 2022;24:100459.
2 Ghotra SS, Champendal M, Flaction L, Ribeiro RT, Sá Dos Reis C. Approaches to reduce medical imaging departments' environmental impact: A scoping review. Radiography (Lond). 2024;30 Suppl 1:108–116.
3 Doo FX, Vosshenrich J, Cook TS, Moy L, Almeida EPRP, Woolen SA, et al. Environmental Sustainability and AI in Radiology: A Double-Edged Sword. Radiology. 2024; 310(2):e232030.
4 Hanneman K, Szava-Kovats A, Burbridge B, Leswick D, Nadeau B, Islam O, et al. Canadian Association of Radiologists Statement on Environmental Sustainability in Medical Imaging. Can Assoc Radiol J. 2025;76(1):44–54.
5 Chaban YV, Vosshenrich J, McKee H, Gunasekaran S, Brown MJ, Atalay MK, Heye T, Markl M, Woolen SA, Simonetti OP, Hanneman K. Environmental Sustainability and MRI: Challenges, Opportunities, and a Call for Action. J Magn Reson Imaging. 2024;59(4):1149–1167.
6 Siemens Healthineers AG. Sustainability in MRI: The power of less is more [Internet]. Erlangen, Germany: Siemens Healthineers [cited 2025 June 26]. Available from: ↗ https://www.siemens-healthineers.com/magnetic-resonance-imaging/sustainability-in-mri
7 Woolen SA, Becker AE, Martin AJ, Knoerl R, Lam V, Folsom J, et al. Ecodesign and Operational Strategies to Reduce the Carbon Footprint of MRI for Energy Cost Savings. Radiology. 2023;307(4):e230441.
8 Siemens Healthineers AG. BioMatrix Fit Upgrades [Internet]. Erlangen, Germany: Siemens Healthineers [cited 2025 June 26]. Available from: ↗ https://www.siemens-healthineers.com/magnetic-resonance-imaging/biomatrix-upgrades
9 Siemens Healthineers AG. MAGNETOM Fit Upgrade with BioMatrix: Environmental Product Declaration [Internet]. Erlangen, Germany: Siemens Healthineers; 2020 [cited 2025 June 26]. Available from: ↗ https://cdn0.scrvt.com/39b415fb07de4d9656c7b516d8e2d907/1800000007344914/20ff121028df/MR_EPD_Broschuere_MAGNETOM_VidaFit_Final_1800000007344914.pdf
10 Ember (2025)Energy Institute - Statistical Review of World Energy (2025) — with major processing by Our World in Data Available from: https://ourworldindata.org/grapher/carbon-intensity-electricity
11 The United States Environmental Protection Agency. Greenhouse Gas Equivalencies Calculator [Internet]. Washington, D.C.: United States Environmental Protection Agency; updated November 2024 [cited 2025 June 26]. Available from: https://www.epa.gov/energy/greenhouse-gas-equivalencies-calculator#results

Contact

Angela Borella, DipRadDiag (UTas), MRSO (ABMRS), DipMn (Monash)
MRI Network Supervisor – Monash Health
Clayton South VIC 3169
Australia
Tel.: 03 9594 2014
angela.borella@monashhealth.org
www.monashhealth.org

Justin Warner, BMedRadSc (MedImaging) (CSU), MRSO (ABMRS), MAppSc (MRI)
MRI Radiographer
Castlereagh Imaging
Westmead, Sydney, NSW 2145
Australia
Tel.: 02 8844 1781
justinwarner@casimaging.com
www.casimaging.com.au

Neurofeedback for Treating Depression: An Emerging Application of Real-Time Functional MRI

Rainer Goebel[1] and David Linden[2]

[1] Maastricht Brain Imaging Center, Department of Cognitive Neuroscience, Faculty of Psychology and Neuroscience, Maastricht University, the Netherlands
[2] Mental Health and Neuroscience Research Institute; Faculty of Health, Medicine and Life Sciences; Maastricht University, the Netherlands

Abstract

In functional MRI (fMRI) neurofeedback, a closed-loop brain-computer interface enables participants to learn self-regulating brain activity using real-time information from their brain (Fig. 1). This method is increasingly being used in scientific and clinical settings. Several 3 Tesla studies have shown the promise of this approach as an add-on treatment for depression, helping patients improve emotion regulation and self-efficacy. Traditional neurofeedback, which uses mean activity from emotion-related areas, cannot distinguish specific emotions. It is therefore unclear whether a patient is engaging in a positive or negative emotional mental state. To address this ambiguity, a new semantic neurofeedback approach maps individual emotions onto a two-dimensional space and visualizes the current emotional state as a moving point on that map. This technique allows participants to navigate their emotional space, thereby offering clearer and potentially more effective therapy for depression. A 7-Tesla proof-of-concept study shows promise for this new real-time fMRI neurofeedback method.

Introduction to functional MRI neurofeedback

Functional magnetic resonance imaging (fMRI) has revolutionized the study of the human brain. By enabling high-resolution, non-invasive recordings of the blood oxygenation level dependent (BOLD) response, it provides indirect measures of neuronal activity [1–4]. While in many cases, the fMRI analysis is being performed quite some time after the data has been acquired, real-time fMRI (rt-fMRI) systems were developed already shortly after the inception of fMRI [5]. They process the data during scanning — i.e., as soon as it is acquired. Although the potential of rt-fMRI for quality assurance, functional localizers, intra-operative studies, and teaching has long been recognized, the uptake has been rather slow. However, the interest in rt-fMRI increased with the invention of fMRI neurofeedback about 20 years ago. One of the first neurofeedback publications [6] describes how optimized brain-imaging software (developed by this paper's co-author, Rainer Goebel) performed incremental data analysis almost as comprehensively as standard offline data

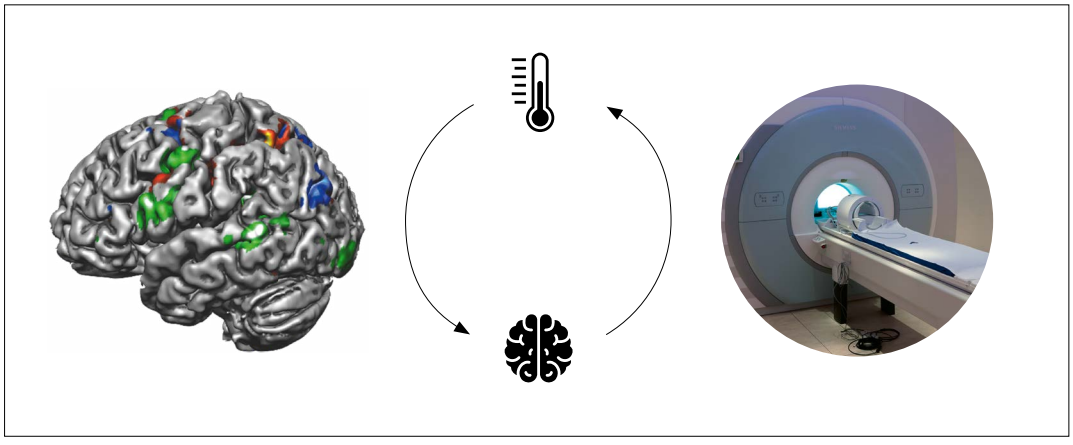

1 Real-time fMRI neurofeedback as a closed-loop system.

analysis. This included motion correction, spatial and temporal filtering, and statistical analysis of the fMRI signals from the entire brain using a recursive general linear model (for an overview of currently employed methods, see [7]). Most importantly, the software allowed to interactively select multiple brain regions, from which the neurofeedback signal was calculated and shown as visual feedback (time-course displays) to the participants in the scanner during ongoing functional scanning. The paper concluded that this novel approach meant fMRI-guided self-regulation would become feasible for healthy participants and patients.

Application in depression treatment

Despite this promising outlook, it took almost 10 years until the first psychiatric application of fMRI neurofeedback was published providing activity feedback from emotion-related brain areas in patients with depression [8]. In this 3-Tesla study, the mean activity from emotion-related areas was provided on a thermometer-like display that showed participants whether they had successfully engaged in emotional mental states during neurofeedback blocks. After only four neurofeedback practice sessions (separated by about a week), patients showed a significantly improved ability to regulate their emotions, which was accompanied in most patients by a substantial reduction of depression symptoms, as measured with the Hamilton Depression Rating Scale (HDRS). This proof-of-concept study laid the foundation for using fMRI neurofeedback to help patients self-regulate emotions in depression, and has had world-wide impact (seven active clinical trials are currently listed on clinicaltrials.gov). More generally, the increasing awareness about the high prevalence of neurological and psychological issues in society, and the limited therapeutic solutions available, has generated excitement for fMRI neurofeedback as a non-pharmacological, brain-driven, and precise treatment option. The rising interest in clinical neurofeedback has been accompanied by large-scale EU funding (e.g., the BRAINTRAIN project [9]) and an increasing number of promising clinical studies on neurofeedback applied to mental disorders such as PTSD [10] and anxiety [11], and to neurological conditions such as Parkinson's disease [12]. Because it provides direct access to (dysfunctional) brain circuits [13], neurofeedback has become a truly disease-modifying intervention, which are currently virtually absent in psychiatry and are rare in neurology.

While neurofeedback has been explored for many clinical disorders [14], depression treatment has proven to be one of its most successful applications in subsequent randomized clinical trials [15, 16]. Its clinical effect (reducing symptoms by approximately 40%) clearly surpasses that of commonly observed placebo or non-specific effects. Furthermore, it has been revealed that the reduction in depression symptoms correlates with an increase in reported self-efficacy, which is an important concept in the psychology of depression. Neurofeedback seems to positively influence two core symptoms of major depression: anhedonia and a perceived loss of control. It does this by teaching patients to engage in positive emotions and by boosting their self-efficacy, respectively. Importantly, after undergoing successful treatment sessions in the scanner, patients were able to apply the learned emotional regulation strategies also outside the scanner. This led to sustained outcome effects, as demonstrated by follow-up measurements recorded weeks or months after the intervention. Most depression neurofeedback studies have used 3-Tesla fMRI, including our studies on 3 Tesla MAGNETOM Prisma scanners in Cardiff (UK) and Maastricht (NL), but a large-scale study currently running at Stanford University is using a 7-Tesla MAGNETOM Terra.X system with impulse gradients to provide optimal feedback signals to patients [17].

Limitations of conventional neurofeedback

There are (at least) two ways of designing clinical protocols for fMRI neurofeedback. On the one hand, one could directly target pathological hyper- or hypoactivation with down- or upregulation. For this approach, stable patterns of abnormal fMRI activity that can be detected and modulated in single trials (without pooling data over longer timeframes) would need to be identified in patients, which is often not possible. On the other hand, one could use the real-time fMRI signal to reinforce particular (desirable) mental states, such as those from positive emotional imagery or memories [8, 15, 16]. This is the approach that most studies on depression have taken so far. However, these clinical studies on fMRI neurofeedback were based on mean activity in a target area or on functional connectivity between brain areas or networks (for example, partial correlation coefficients). In previous studies on neurofeedback for emotion regulation in depression treatment, this conventional approach was "blind" to the type of emotion, since it does not distinguish between specific emotions. Since both positive and negative emotions can lead to an increase in the mean activity in the emotion network, it is thus not automatically known whether a patient is engaging in a positive or negative emotional mental state, despite specific instructions. This lack of specificity presents a challenge for further optimizing therapeutic outcomes, because the feedback should ideally be specific to the targeted emotion. We can now move beyond such low-dimensional feedback signals and harness brain activity patterns that reflect semantic representations in the brain, especially on ultra-high-field (7-Tesla) MRI scanners [16, 18].

Semantic neurofeedback of emotions

To overcome the limitations of conventional neurofeedback for depression, a novel approach termed "semantic neurofeedback of emotions" has been recently proposed [20]. This method leverages multivariate brain activity patterns using representational similarity analysis (RSA) and multi-dimensional scaling (MDS) to capture the semantic structure of emotional representations in the brain (Fig. 2). The experimental protocol begins with an individualized mapping session, in which participants recall autobiographical memories associated with a range of emotions. Brain activation patterns in an emotion-related network are extracted and used to construct a personalized two-dimensional emotion map. In subsequent neurofeedback sessions, a participant's current emotional brain state is visualized as a moving point on the map. Patients are instructed to navigate their mental state toward a target emotion in a series of neurofeedback periods that are interspersed with rest periods. The distance between the current mental state and the other emotions on the map reflects pattern similarity; the size of the visual marker represents the intensity of the evoked emotion brain pattern (Fig. 3).

This semantic ("unblinded") continuous feedback allows participants to consciously explore and regulate their emotional states. It also trains engagement with negative emotions when therapeutically appropriate, particularly to help participants learn how to shift brain activity patterns from negative states toward desired positive emotions.

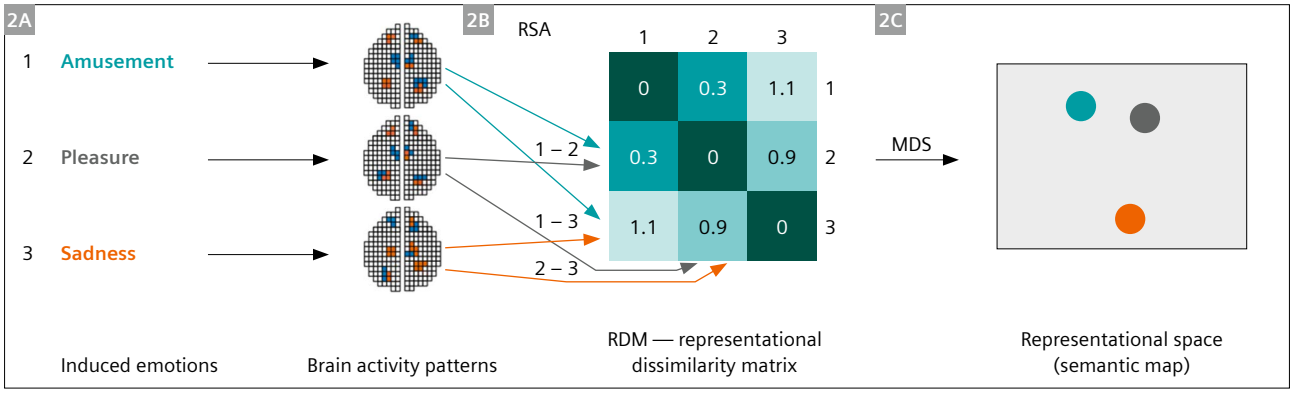

2 Illustration of representational (dis)similarity analysis (RSA) and semantic map creation with N = 3 conditions of induced emotions. **(2A)** Presented stimuli (e.g., pictures or recalled emotional autobiographical memories) evoke distributed activity patterns (N = 3). For voxels in a selected region of interest, the N patterns are compared pairwise (e.g., by calculating a linear correlation value). **(2B)** Similarity (e.g., correlation) values are converted into dissimilarity values d (e.g., d = 1 – correlation, ranging from perfect correlation (d = 0) over no correlation (d = 1) to perfect anticorrelation (d = 2)); pairwise dissimilarity values are placed in respective cells of the representational dissimilarity matrix (RDM) and are often color-coded (here: dark petrol for low dissimilarity, light petrol for high dissimilarity). **(2C)** Using multi-dimensional scaling (MDS), the high-dimensional similarity information in the RDM is projected onto a two-dimensional representational space or semantic map (adapted from [20]).

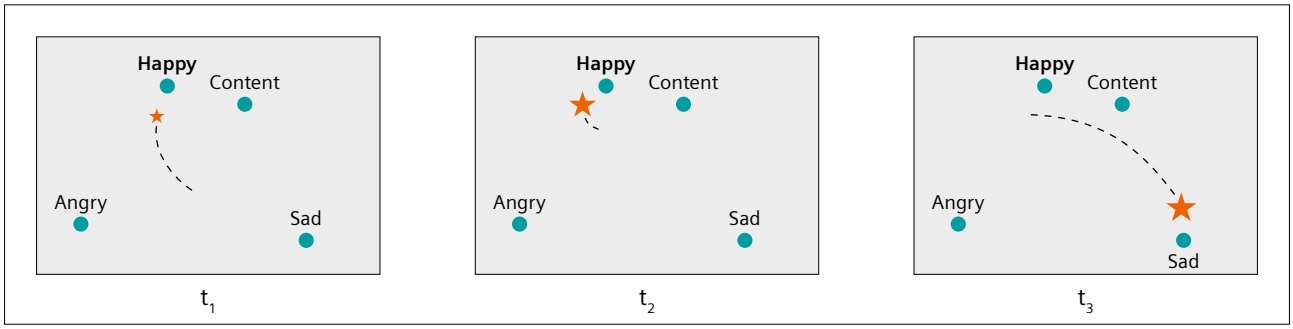

3 Schematic illustration showing semantic neurofeedback of emotions for depression treatment. After a localizer session, the (individual) semantic map contains the four mapped emotions 'happy', 'content', 'angry', and 'sad' as anchor points. After receiving the instruction "navigate to 'happy'", the participant engages in a happy emotional autobiographical memory. The red star, which represents the current mental state, moves from a relatively neutral emotional state (start of dashed line) toward the 'happy' emotion in the semantic map (t_1). By staying close to the target emotion, the participant increases the strength of the 'happy' emotion pattern, as indicated by the larger size of the red star (t_2). After subsequently receiving the instruction "navigate to 'sad'", the participant engages in a sad emotional state, and the current mental state star moves toward the 'sad' emotion in the semantic map (t_3) (adapted from [20]).

Feasibility and benefits of semantic neurofeedback

The feasibility of semantic neurofeedback of emotions has recently been demonstrated in a first proof-of-concept study with five participants [21]. The study consisted of two sessions per participant, conducted at 7 Tesla on a MAGNETOM 7T Plus scanner in Maastricht, the Netherlands. The first session was used to identify the patterns evoked by different emotions. In the second session, the participants practiced navigating to emotions using semantic neurofeedback. Out of nine emotions (contentment, gratitude, friendship love, enthusiasm, surprise, sadness, anger, disgust, and fear), four were selected for each participant to best reflect different valence and arousal categories. In the localizer runs, participants engaged in autobiographical memories matching the selected emotions. An individual mask was created by combining activation from each emotion within the emotional network [22]. Activation patterns were then extracted for the four emotions inside the mask and used to calculate the representational dissimilarity matrix, from which the individual two-dimensional map was created (Fig. 2). During the second session, this map was used to provide the participants with feedback on how their current emotional state was related to the emotion patterns from the first session. The calculated similarity was displayed by a moving red dot, the size of which represented the intensity of pattern activation (Fig. 4). The pilot results demonstrated that participants managed to regulate their brain activation and navigate closely to the emotional target (Fig. 5). These findings indicate the general feasibility of the approach, as high accuracy and

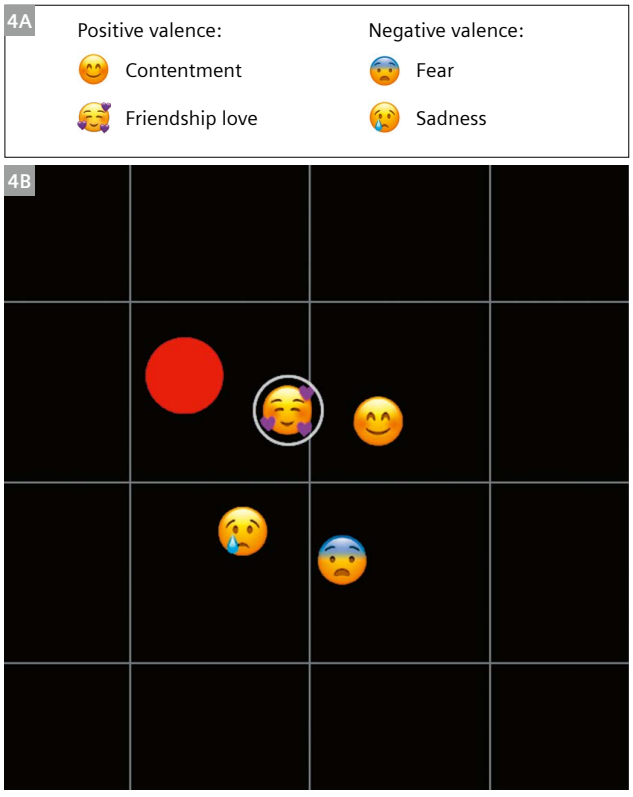

4 Snapshot of real-time fMRI semantic neurofeedback of emotion. **(4A)** Legend showing the four emotions that were selected for the participant and displayed as emojis in the semantic map. **(4B)** Snapshot of the display shown to a participant after they successfully navigated to the cued emotion (white circle) of 'friendship love'. The large size of the red dot indicates that the participant experienced a strong feeling of friendship love.

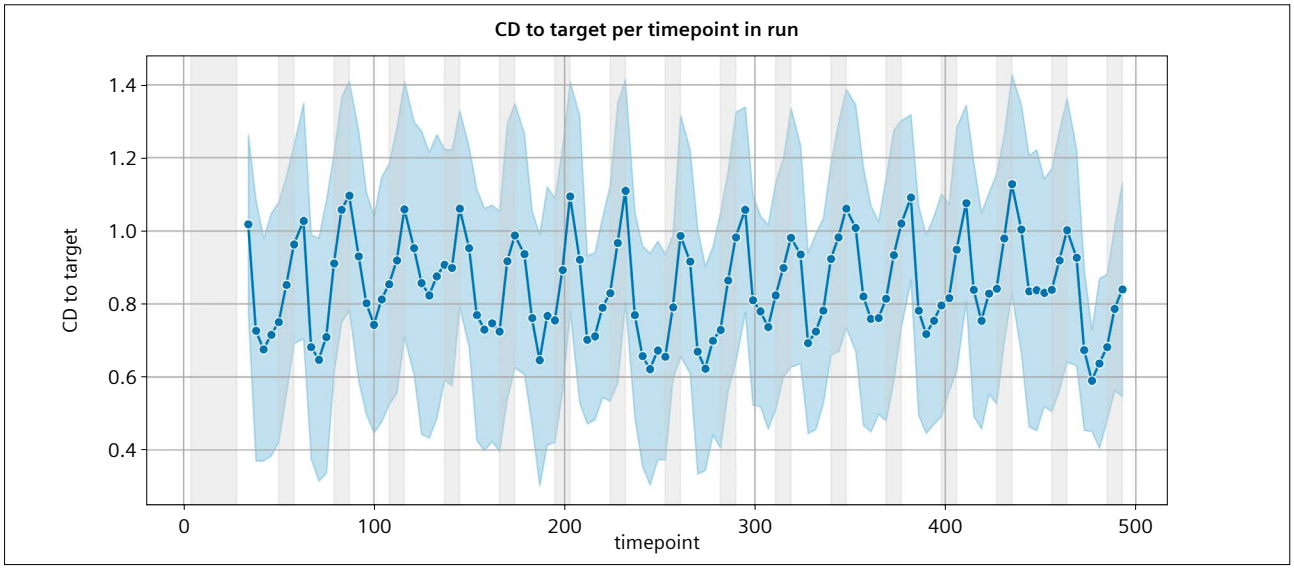

5 These results of semantic neurofeedback of emotion (average of five participants) show that the participants were able to navigate toward the target emotion in individual trials. The distance from the current mental state to the target emotion (y axis) is the correlation distance (CD), which corresponds well with the Euclidean distance (ED) shown on the semantic map. The CD decreases in the white sections (neurofeedback blocks) and rises in the gray sections (rest periods).

engagement were achieved even with non-optimized protocols and methods, suggesting substantial potential for future improvements.

We have not yet systematically compared semantic neurofeedback of emotions at 3-Tesla fMRI versus 7-Tesla fMRI. However, robustly discriminating between different emotion patterns to create a semantic map of emotions is challenging and will likely benefit from the enhanced signal-to-noise ratio or higher spatial resolution at 7 Tesla.

Overall, we believe that this new, transparent technique of navigating one's own emotional space has the potential to enable more specific training for future clinical studies on depression and, more generally, mood disorders.

While fMRI has revolutionized brain research in humans, clinical applications of fMRI are rare. Real-time fMRI neurofeedback for depression has the potential to become a routine application of fMRI in the future, benefitting patients who are not sufficiently responding to conventional interventions.

References

1 Ogawa S, Lee TM, Kay AR, Tank DW. Brain magnetic resonance imaging with contrast dependent on blood oxygenation. Proc Natl Acad Sci U S A. 1990;87(24):9868–72.
2 Ogawa S, Tank DW, Menon R, Ellermann JM, Kim SG, Merkle H, et al. Intrinsic signal changes accompanying sensory stimulation: functional brain mapping with magnetic resonance imaging. Proc Natl Acad Sci U S A. 1992;89(13):5951–5.
3 Bandettini PA, Wong EC, Hinks RS, Tikofsky RS, Hyde JS. Time course EPI of human brain function during task activation. Magn Reson Med. 1992;25(2):390–7.
4 Kwong KK, Belliveau JW, Chesler DA, Goldberg IE, Weisskoff RM, Poncelet BP, et al. Dynamic magnetic resonance imaging of human brain activity during primary sensory stimulation. Proc Natl Acad Sci U S A. 1992;89(12):5675–9.
5 Cox RW, Jesmanowicz A, Hyde JS. Realtime functional magnetic resonance imaging. Magn Reson Med. 1995;33(2):230–6.
6 Weiskopf N, Mathiak K, Bock SW, Scharnowski F, Veit R, Grodd W, et al. Principles of a brain-computer interface (BCI) based on real-time functional magnetic resonance imaging (fMRI). IEEE Trans Biomed Eng. 2004;51(6):966–70.
7 Goebel R. Analysis methods for real-time fMRI neurofeedback. In: Hampson M, editor. fMRI Neurofeedback. London, UK: Academic Press; 2021:23–55.
8 Linden DEJ, Habes I, Johnston SJ, Linden S, Tatineni R, Subramanian L, et al. Real-Time Self-Regulation of Emotion Networks in Patients with Depression. PLoS One. 2012;7(6):e38115.
9 CORDIS. Final Report Summary - BRAINTRAIN (Taking imaging into the therapeutic domain: Self-regulation of brain systems for mental disorders). CORDIS - EU research results. Content archived 2024, June 18. Cited 2026, March 19. Available from: https://cordis.europa.eu/project/id/602186/reporting
10 Fruchtman-Steinbok T, Keynan JN, Cohen A, Jaljuli I, Mermelstein S, Drori G, et al. Amygdala electrical-finger-print (AmygEFP) NeuroFeedback guided by individually-tailored Trauma script for post-traumatic stress disorder: Proof-of-concept. Neuroimage Clin. 2021;32:102859.
11 Zilverstand A, Sorger B, Sarkheil P, Goebel R. fMRI neurofeedback facilitates anxiety regulation in females with spider phobia. Front Behav Neurosci. 2015;9:148.
12 Subramanian L, Morris MB, Brosnan M, Turner DL, Morris HR, Linden DEJ. Functional Magnetic Resonance Imaging Neurofeedback-guided Motor Imagery Training and Motor Training for Parkinson's Disease: Randomized Trial. Front Behav Neurosci. 2016;10:111.
13 Krause F, Linden DEJ, Hermans EJ. Getting stress-related disorders under control: the untapped potential of neurofeedback. Trends Neurosci. 2024;47(10):766–776.
14 Tursic A, Eck J, Lührs M, Linden DEJ, Goebel R. A systematic review of fMRI neurofeedback reporting and effects in clinical populations. Neuroimage Clin. 2020;28:102496.
15 Mehler DMA, Sokunbi MO, Habes I, Barawi K, Subramanian L, Range M, et al. Targeting the affective brain-a randomized controlled trial of real-time fMRI neurofeedback in patients with depression. Neuropsychopharmacology. 2018;43(13):2578–2585.
16 Young KD, Siegle GJ, Zotev V, Phillips R, Misaki M, Yuan H, et al. Randomized clinical trial of real-time fMRI amygdala neurofeedback for major depressive disorder: Effects on symptoms and autobiographical memory recall. Am J Psychiatry. 2017;174(8):748–755.
17 ClinicalTrials.gov. fMRI Neurofeedback With Matter Neuroscience App. ClinicalTrials.gov ID: NCT06735885. National Library of Medicine. Last updated 2025, Dec 17. Cited 2026, March 19. Available from: https://clinicaltrials.gov/study/NCT06735885
18 Russo AG, Lührs M, Di Salle F, Esposito F, Goebel R. Towards semantic fMRI neurofeedback: navigating among mental states using real-time representational similarity analysis. J Neural Eng. 2021;18(4):046015.
19 Ciarlo A, Russo AG, Ponticorvo S, Di Salle F, Lührs M, Goebel R, et al. Semantic fMRI neurofeedback: a multi-subject study at 3 tesla. J Neural Eng. 2022;19(3):036020.
20 Goebel R, Lührs M, Ciarlo A, Esposito F, Linden DE. Semantic fMRI neurofeedback of emotions: From basic principles to clinical applications. Philos Trans R Soc Lond B Biol Sci. 2024;379(1915):20230084.
21 Goblirsch A. Applying Semantic Neurofeedback to Navigate Emotional Space. Master's research thesis. Maastricht University. 2025.
22 Lindquist KA, Wager TD, Kober H, Bliss-Moreau E, Barrett LF. The brain basis of emotion: A meta-analytic review. Behav Brain Sci. 2012;35(3):121–143.

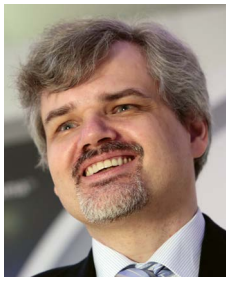

Contact

Professor Dr. rer. nat. Rainer Goebel
Maastricht Brain Imaging Center
Department of Cognitive Neuroscience
Faculty of Psychology and Neuroscience
Maastricht University
Oxfordlaan 55
6229 EV Maastricht
The Netherlands
r.goebel@maastrichtuniversity.nl

David Linden, M.D.
Director Mental Health and
Neuroscience Research Institute
Faculty of Health, Medicine and
Life Sciences
Maastricht University
Universiteitssingel 40
6229 ER Maastricht
The Netherlands
david.linden@maastrichtuniversity.nl

Optimized Susceptibility MRI Sequences for Novel Diagnostic Biomarkers of Multiple Sclerosis

Sreekanth Madhusoodhanan Nair[1], Jin Jin[2], Chang Gao[3], Nader Binesh[4], Thomas Benkert[5], Marcel Maya[4], Pascal Sati[1]

[1] Neuroimaging Program, Department of Neurology, Cedars-Sinai Medical Center, Los Angeles, CA, USA
[2] Siemens Healthineers Pty Ltd, Brisbane, Australia
[3] Siemens Healthineers, Los Angeles, CA, USA
[4] Department of Imaging, Cedars-Sinai Medical Center, Los Angeles, CA, USA
[5] Siemens Healthineers, Erlangen, Germany

Introduction

The 2024 revisions of the international diagnostic criteria for multiple sclerosis (MS) [1] provide an expanded role for magnetic resonance imaging (MRI) by incorporating two novel imaging biomarkers: the central vein sign (CVS) [2] and paramagnetic rim lesions (PRL) [3]. Recent MRI guidelines by the MAGNIMS-CMSC-NAIMS consortia provide practical guidance for the implementation of the different MRI sequences required for the accurate biomarker detection and precise identification of MS [4]. In this article, we focus specifically on the implementation of the susceptibility MRI sequences required for the detection of CVS and PRL.

Due to their paramagnetic properties, CVS and PRL can be detected non-invasively using susceptibility MRI sequences. More specifically, susceptibility-weighted imaging (SWI) has emerged as an important additional sequence to the diagnostic brain MRI protocol for MS since it is highly sensitive to venous features and iron-related signals in the white matter lesions that would be otherwise invisible on conventional T1- and T2-weighted sequences [5, 6]. Although standard SWI provides filtered phase images that are adequate for PRL detection, the SWI magnitude images are not optimized for standalone CVS detection. This complicates the diagnostic interpretation workflow for practitioners. Additionally, standard SWI relies on a gradient echo (GRE) acquisition, which cannot provide in a clinically feasible scan time the recommended submillimeter isotropic resolution for the highest confidence in CVS and PRL detection [4]. An alternative strategy for overcoming this issue for CVS detection is the use of T2*-weighted 3D-segmented echo-planar imaging (3D EPI) [7].

In this article, we will review these techniques and provide guidance for the clinical implementation of an optimized SWI-GRE protocol[1] for concomitant evaluation of CVS and PRL, and of a submillimeter T2* 3D EPI protocol for reaching highest detection confidence for CVS and PRL.

MRI acquisitions

All the cases presented here were imaged on 3T MRI scanners (MAGNETOM Skyra and MAGNETOM Vida) using 20-channel head/neck coils at Cedars-Sinai Medical Center (Los Angeles, CA, USA). Two different brain SWI protocols using the same spatial resolution and coverage were implemented: (a) standard SWI-GRE with a flip angle (FA) of 15°, and (b) optimized SWI-GRE with an FA of 5°. All other sequence parameters were the same in both the standard and optimized SWI-GRE protocols. Additionally, the 3D EPI sequence ('ep_seg_fid'), available in the default sequence tree from Siemens Healthineers (Fig. 1) for recent software versions (≥ VA31), was used to implement submillimeter isotropic T2*-weighted acquisition. Details of the sequence parameters used are shown in Table 1.

[1] 3D EPI SWI processing is provided via a research application[x] resulting in filtered phase images as well as SWI magnitude images.
[x] Work in progress. The application is currently under development and is not for sale in the U.S. and in other countries. Its future availability cannot be ensured.

Protocol	Standard SWI-GRE	Optimized SWI-GRE	T2* 3D EPI
TE (ms)	20	20	35
TR (ms)	27	27	65
FA (deg)	15	5	10
In-plane resolution (mm²)	0.7 × 0.7	0.7 × 0.7	0.7 × 0.7
Slice thickness (mm)	2	2	0.7
FOV Read (mm)	250	250	250
FOV Phase (%)	81.3	81.3	81.3
Base resolution	384	384	384
Acceleration factor	GRAPPA (2)	GRAPPA (2)	None
EPI factor	None	None	15
Bandwidth (Hz/px)	120	120	394
Reconstruction	Magn/Phase	Magn/Phase	Magn/Phase
Coil combination	Adaptive Combine	Adaptive Combine	Adaptive Combine
Scan time	3:50 minutes	3:50 minutes	5:08 minutes

Table 1: MRI acquisition parameters for standard SWI, optimized SWI, and T2* 3D EPI at 3-tesla.

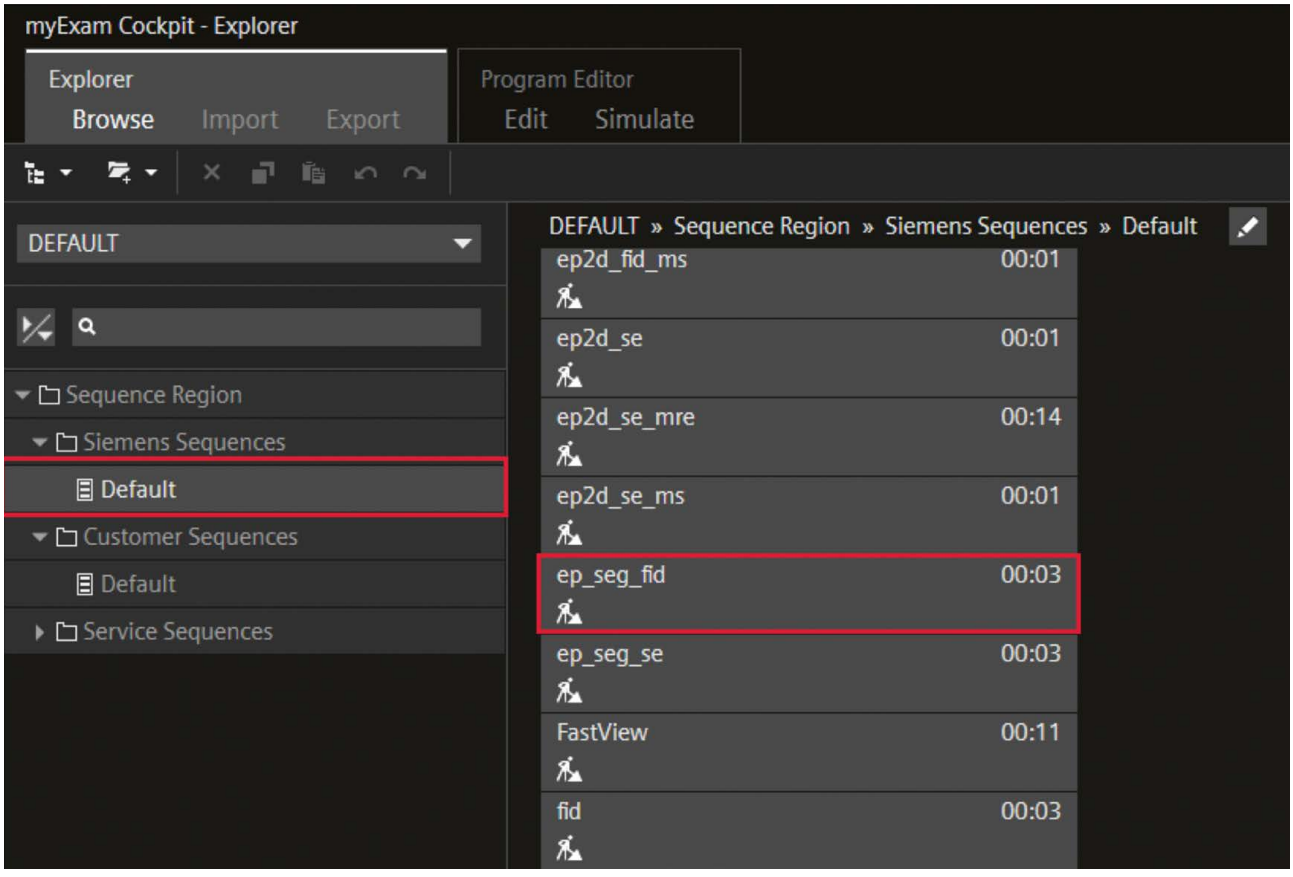

1 Product 3D EPI sequence ('ep_seg_fid') as it appears in the default sequence tree from Siemens Healthineers.

SWI-GRE

As a reminder, the standard SWI-GRE protocol was initially designed for assessing cerebral vasculature and hemorrhage [8, 9]. SWI is particularly useful for evaluating patients with stroke, vascular malformations, and venous diseases [6, 8], but it is not optimized for evaluating the CVS in patients with MS. Indeed, the standard SWI-GRE acquisition prioritizes maximal signal intensity with an FA near to the Ernst angle (between 15° and 20°), which introduces substantial T1-weighted contrast when repetition time (TR) is short. This T1 weighting significantly reduces the lesion-to-white-matter contrast and prevents the co-localization of MS lesions and central veins on SWI magnitude images. This issue is illustrated in Figure 2, where MS lesions appear largely isointense or hypointense on SWI magnitude images, thus requiring the use of T2 FLAIR images to co-localize the presence of T2 hyperintense lesions. In addition, the evaluation of CVS requires establishing the vein centrality using a precise co-registration between T2 FLAIR and SWI. This further complicates the interpretation workflow in clinical practice and reduces the reliability of the CVS rating if the T2 FLAIR and SWI images are inadequately aligned. On the other hand, SWI filtered phase images can be used for PRL evaluation and should be preferred over SWI magnitude images due to their higher sensitivity for PRL detection [10]. In Figure 2, a hypointense rim with isointense core depicting chronic active inflammation in the lesion is clearly visible in the filtered phase image. Note that the image intensity of the filtered phase images is displayed in the left-handed system by default on scanners from Siemens Healthineers. Therefore, the intensity of the filtered phase images needs to be inverted to match the right-handed convention recommended for the detection of PRL (e.g., paramagnetic rims and blood vessels appear dark) [3].

Optimized SWI-GRE

One way to improve diagnostic accuracy and workflow with SWI-GRE is to optimize the acquisition protocol for adequate detection of lesions and central veins on magnitude images. A simple protocol modification is to lower the FA (from 15° to 5° at 3T) to reduce T1 weighting and increase lesion visibility [11]. This single change in the sequence parameter does not affect the scan duration and enables the standalone detection of CVS. This is shown in

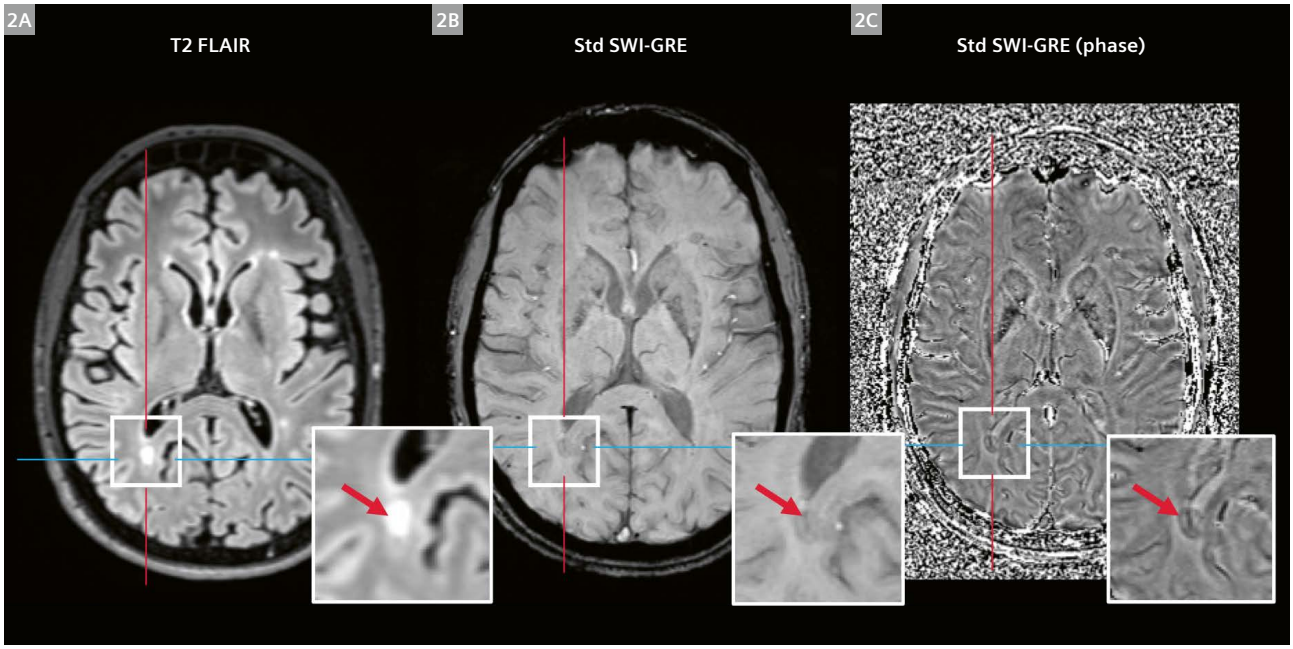

2 **(2A)** Focal hyperintense lesions on T2 FLAIR images, **(2B)** corresponding susceptibility-weighted (SWI) enhanced magnitude image and **(2C)** filtered phase image. Lesions appear isointense on the SWI enhanced magnitude image. For detection of the central vein sign (CVS), centrality of the vein needs to be confirmed using the crosshair. Paramagnetic rim lesion (PRL) is more clearly visible on the filtered phase image than the enhanced magnitude image.

Figure 3, which compares the two SWI protocols (standard and optimized[1]) acquired in the subjects with MS. Hyperintense focal white matter lesions identified on T2 FLAIR are invisible on standard SWI magnitude images but appear hyperintense on the optimized SWI magnitude images (red arrows). As a result, the presence of a central hypointense vein inside these focal white matter lesions can be demonstrated easily with the optimized SWI magnitude images. An important additional observation is that the change in FA does not impact the detection of incidental microbleed (yellow arrows). Moreover, the detection of PRL is not affected by the change in FA, as shown in Figure 3, where both SWI filtered phase images display similar detection sensitivity (white arrows). Additional examples illustrating the superior detection of CVS-positive lesions achieved with the optimized SWI are shown in Figure 4 (top two rows). Examples of the superior detection of PRL-positive lesions achieved with SWI filtered phase images over SWI magnitude images are also shown in Figure 4 (bottom two rows).

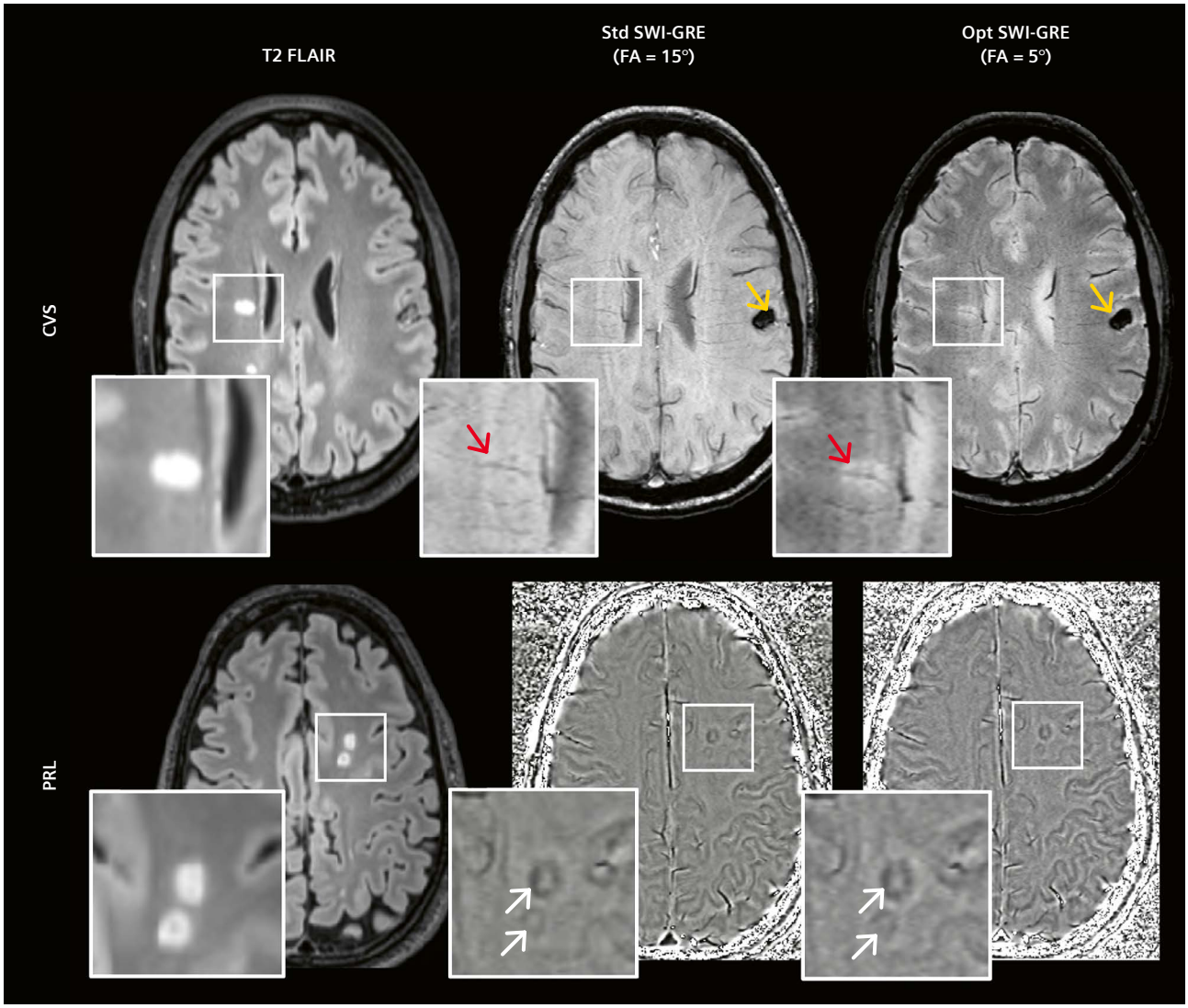

3 Head-to-head comparison of standard and optimized SWI-GRE images acquired in the same subjects with multiple sclerosis. T2 FLAIR images show focal hyperintense lesions in the periventricular and deep white matter areas. Standard SWI-GRE (FA = 15°) shows limited lesion conspicuity with isointense contrast, whereas optimized SWI-GRE (FA = 5°) clearly depicts CVS with high tissue contrast (hyperintense lesion with hypointense vein) (red arrow). A hemorrhagic bleed shows comparable sensitivity on both SWI acquisitions (yellow arrow). Bottom panels: On filtered phase images, PRL demonstrates equal sensitivity with both SWI protocols (white arrows).

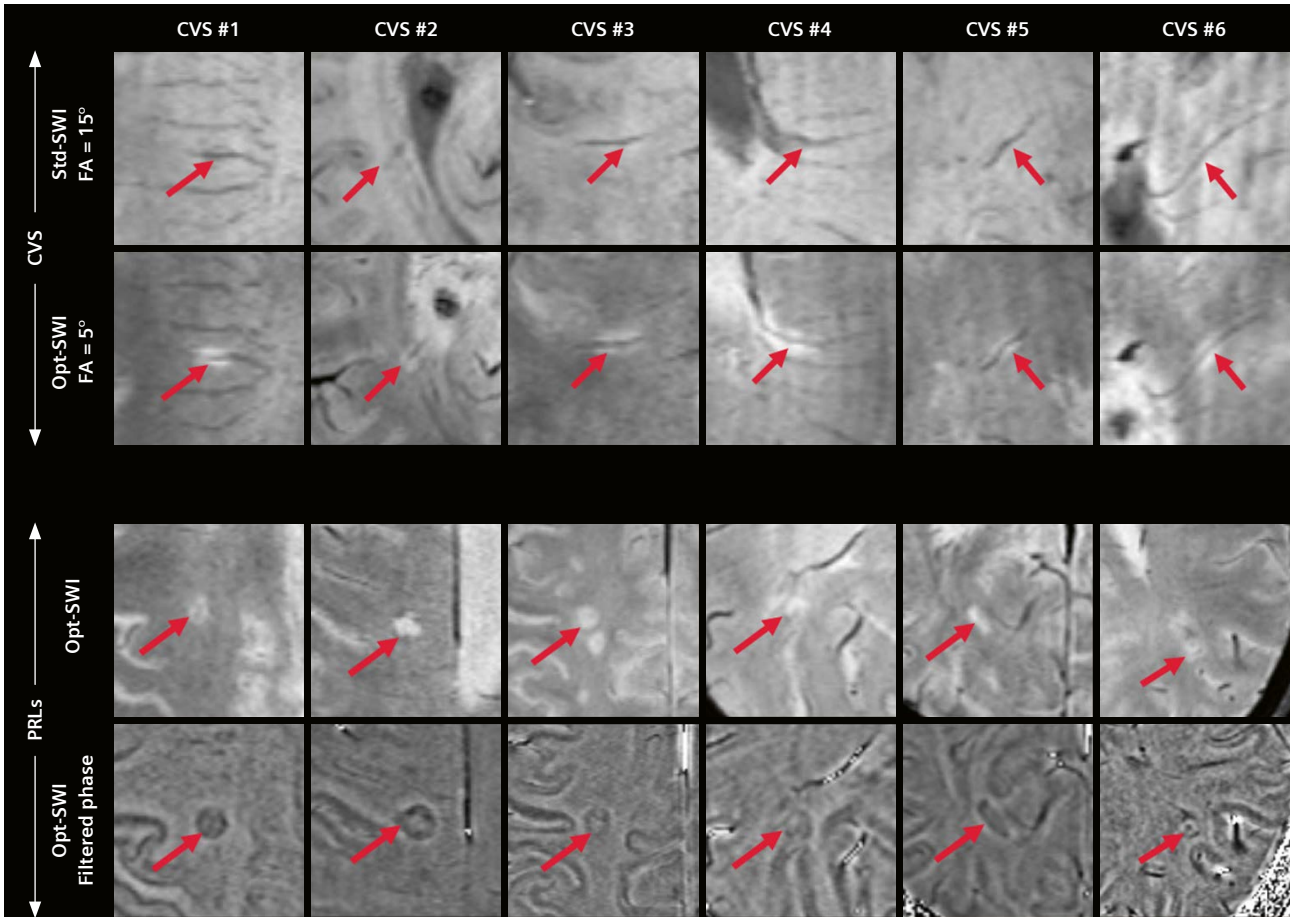

4 The top two rows demonstrate the standalone CVS detection sensitivity of SWI-GRE acquisition at two flip angles, illustrated in the same MS patient evaluated for Select6 criteria (6 or more CVS positive lesions as per the 2024 revised MS diagnostic criteria). The bottom two rows exhibit the superior PRL detection sensitivity, illustrated in six patients with MS. A hypointense rim with an isointense core indicating chronic active inflammation is clearly visible in the filtered phase images, unlike in the SWI magnitude images.

T2*-weighted 3D EPI

The international MRI guidelines recently published by the MAGNIMS-CMSC-NAIMS consortia recommend using submillimeter isotropic T2*-weighted and filtered phase images for more sensitive and reliable detection of the CVS and PRL [2–4]. The product version of the 3D EPI sequence [7, 12] (available for software versions ≥ *syngo* MR VA31) enables the acquisition of magnitude and phase images at 0.65–0.8 mm isotropic in a clinically feasible scan time of 4–6 minutes without the use of parallel imaging acceleration (Table 1). SWI processing is provided via a research application[×], resulting in filtered phase images as well as SWI magnitude images. Representative examples from an MS subject scanned with the 3D EPI protocol are shown in Figure 5. The CVS is clearly visible in all three planes of the T2*-weighted 3D EPI images (red arrows). Similarly, PRL is clearly visible in all three planes of the filtered phase images from 3D EPI (white arrows). This multi-planar evaluation increases reader confidence in rating the CVS and PRL, and reduces any potential false-positive detection. Note the difference in image quality when reformatting the SWI images in coronal and sagittal views. This is due to the anisotropic voxel dimensions which hinders the multi-planar assessment of CVS and PRL (Fig. 5, bottom two rows).

[×] *Work in progress. The application is currently under development and is not for sale in the U.S. and in other countries. Its future availability cannot be ensured.*

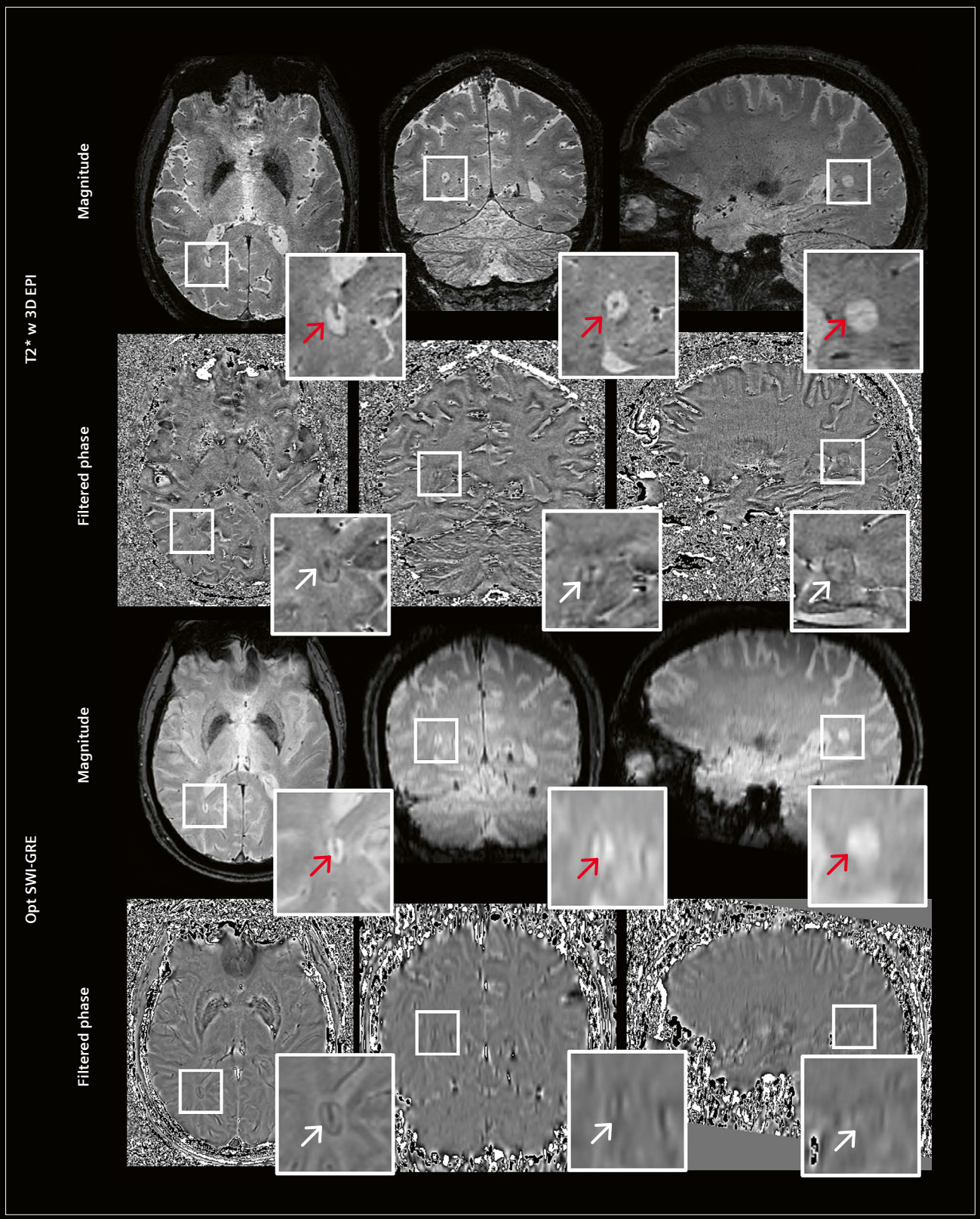

5 Multiplanar view of optimized T2*-weighted 3D EPI (top) and SWI-GRE (bottom) acquired on the same MS patient. High-resolution isotropic acquisition in T2*-weighted 3D EPI enables clear visualization of CVS and PRL in all imaging planes.

Discussion and conclusions

Given the need for rapid clinical adoption of the new imaging biomarkers recently included in the revised diagnostic criteria for MS, we provide here practical strategies to integrate adequate susceptibility MRI sequences into the diagnostic imaging workflow. We recommend using an optimized SWI protocol at 3-tesla to ensure sensitive detection of CVS, and filtered phase images for sensitive detection of PRL. When possible, the more advanced 3D EPI sequence is recommended to acquire submillimeter isotropic images. This enables multi-planar evaluation of T2*-weighted and filtered phase images and increases the radiologist's confidence in interpreting CVS and PRL. Our recommended MRI protocols for these sequences are available for download (see QR code) or can be requested directly via local Siemens Healthineers support. Finally, work is currently underway on technical developments that are using advanced acceleration strategies and deep-learning reconstruction methods to further reduce acquisition time and facilitate wider implementation of these sequences in the clinical setting.

Contact

Sreekanth Madhusoodhanan Nair, Ph.D.
Postdoctoral Scientist
Neuroimaging Program
Department of Neurology
Cedars-Sinai Medical Center
Atrium Building, 2nd Floor
8750 Beverly Blvd
Los Angeles, CA 90048
USA
Sreekanth.madhusoodhanan@cshs.org

Pascal Sati, Ph.D.
Associate Professor
Director of Neuroimaging Program
Department of Neurology
Cedars-Sinai Medical Center
Atrium Building, 2nd Floor
8750 Beverly Blvd
Los Angeles, CA 90048
USA
Pascal.sati@cshs.org

Marcel Maya, M.D.
Professor and Co-Chair
Department of Imaging
Cedars-Sinai Medical Center
8700 Beverly Blvd, Room M335
Los Angeles, CA 90048
USA
Marcel.maya@cshs.org

Acknowledgments

We acknowledge the support of the National Institute of Neurological Disorders and Stroke (NINDS), the National Multiple Sclerosis Society (NMSS), the Department of Defense (DoD), and the Erwin Rautenberg Foundation.

Appendix

Download the optimized SWI and T2* EPI protocol for different scanner models from:

magnetomworld.siemens-healthineers.com/clinical-corner/protocols/neurology-neurography/mri-sequences

References

1 Montalban X, Lebrun-Frénay C, Oh J, Arrambide G, Moccia M, Amato MP, et al. Diagnosis of multiple sclerosis: 2024 revisions of the McDonald criteria. Lancet Neur. 2025;24(10):850–865.
2 Sati P, Oh J, Constable RT, Evangelou N, Guttmann CR, Henry RG, et al. The central vein sign and its clinical evaluation for the diagnosis of multiple sclerosis: a consensus statement from the North American Imaging in Multiple Sclerosis Cooperative. Nat Rev Neurol. 2016;12(12):714–722.
3 Bagnato F, Sati P, Hemond CC, Elliott C, Gauthier SA, Harrison DM, et al. Imaging chronic active lesions in multiple sclerosis: a consensus statement. Brain. 2024;147(9):2913–2933.
4 Barkhof F, Reich DS, Oh J, Rocca MA, Li DK, Sati P, et al. 2024 MAGNIMS-CMSC-NAIMS consensus recommendations on the use of MRI for the diagnosis of multiple sclerosis. Lancet Neurol. 2025;24(10):866–879.
5 Clarke M, Pareto D, Pessini-Ferreira L, Arrambide G, Alberich M, Crescenzo F, et al. Value of 3T susceptibility-weighted imaging in the diagnosis of multiple sclerosis. AJNR Am J Neuroradiol. 2020; 41(6):1001–1008.
6 Mittal S, Wu Z, Neelavalli J, Haacke EM. Susceptibility-weighted imaging: technical aspects and clinical applications, part 2. AJNR Am J Neuroradiol. 2009;30(2):232–52.
7 Sati P, Patil S, Inati S, Wang W-T, Derbyshire JA, Krueger G, et al. Rapid MR susceptibility imaging of the brain using segmented 3D echo-planar imaging (3D EPI) and its clinical applications. ↗ MAGNETOM Flash. 2017;68(2):26–32.
8 Haacke EM, Xu Y, Cheng YCN, Reichenbach JR. Susceptibility weighted imaging (SWI). Magn Reson Med. 2004;52(3):612–8.
9 Haacke EM, Mittal S, Wu Z, Neelavalli J, Cheng Y-C. Susceptibility-weighted imaging: technical aspects and clinical applications, part 1. AJNR Am J Neuroradiol. 2009;30(1):19–30.
10 Lee JD, Renner B, Madhusoodhanan Nair S, Nakamura K, Luskin E, Shinohara RT, et al. Superior visibility of paramagnetic rim lesions on filtered phase versus SWI. AJNR Am J Neuroradiol. 2026:ajnr. A9295.
11 Madhusoodhanan Nair S, Hsu YC, Luskin E, Ayrapetyan D, Liu A, Binesh N, et al. Optimized Susceptibility Weighted Imaging for the Detection of Central Vein Sign in Multiple Sclerosis at 3-tesla. In: Proceedings of the Annual Meeting of ISMRM & ISMRT, Honolulu, Hawai'i, USA. 2025 May 10–15. ISMRM; 2025:3766.
12 Sati P, Thomasson DM, Li N, Pham DL, Biassou NM, Reich DS, et al. Rapid, high-resolution, whole-brain, susceptibility-based MRI of multiple sclerosis. Mult Scler. 2014;20(11):1464–70.

Using Deep Learning Reconstruction to Support the Clinical Adoption of Submillimeter Neuroimaging at 7 Tesla

Jocelyn Philippe[1,2,3], Gabriele Bonanno[4,5,6], Kevin Battistini[7], Caterina Bernetti[7], Roland Wiest[4,8], Marwan El-Koussy[8], Natalia Pato Montemayor[1,2,3], Dominik Nickel[9], Patrick A. Liebig[9], Robin M. Heidemann[9], Felix T. Kurz[7], Jean-Philippe Thiran[2,3], Tom Hilbert[1,2,3], Tobias Kober[9], Gian Franco Piredda[1], Thomas Yu[1,2,3] *, Piotr Radojewski[4,8] *

[1] Swiss Innovation Hub, Siemens Healthineers International AG, Lausanne, Switzerland
[2] Department of Radiology, Lausanne University Hospital and University of Lausanne, Switzerland
[3] LTS5, École Polytechnique Fédérale de Lausanne (EPFL), Lausanne, Switzerland
[4] Translational Imaging Center (TIC), Swiss Institute for Translational and Entrepreneurial Medicine, Bern, Switzerland
[5] Swiss Innovation Hub, Siemens Healthineers International AG, Bern, Switzerland
[6] Magnetic Resonance Methodology, Institute of Diagnostic and Interventional Neuroradiology, University of Bern, Switzerland
[7] Division of Neuroradiology, University Hospitals of Geneva, Switzerland
[8] Support Center for Advanced Neuroimaging, Institute for Diagnostic and Interventional Neuroradiology, Inselspital, University of Bern, Switzerland
[9] Magnetic Resonance, Siemens Healthineers AG, Erlangen, Germany

* Authors contributed equally to the manuscript.

Abstract

Ultra-high-field magnetic resonance imaging (at 7 Tesla and above) enables submillimeter spatial resolution that creates new opportunities for detailed neuroanatomical assessment and lesion characterization. However, long acquisition times are a major barrier to routine clinical use. In this article, we illustrate how deep learning-based reconstruction enables higher acceleration of high-resolution brain imaging while preserving diagnostic image quality and thereby supporting the broader clinical usability of 7T MRI.

Introduction

Ultra–high-field magnetic resonance imaging (UHF MRI) at 7 Tesla (7T) is increasingly transitioning from a research tool to a clinically relevant modality, with specialized centers progressively integrating UHF MRI into routine neuroradiological workflows [1]. This evolution is mainly being driven by substantial improvements in spatial resolution enabled by the increased signal-to-noise ratio at 7T [2]. These improvements have demonstrated clinical value across multiple neurological conditions [1, 3]. Submillimeter-resolution imaging at 7T improves the visualization of cortical and juxtacortical lesions in multiple sclerosis, facilitates the detection of subtle epileptogenic abnormalities, and enhances the assessment of small-vessel pathologies such as cerebral microbleeds and of perivascular spaces [1, 4, 5]. Collectively, these advances have expanded the diagnostic scope of neuroimaging and have motivated the adoption of 7T MRI for targeted clinical indications.

However, the practical use of UHF MRI in routine clinical settings is constrained by long acquisition times, particularly for high-resolution three-dimensional sequences. Achieving submillimeter isotropic resolution often requires five to ten minutes of scanning. This increases sensitivity to patient motion and limits robustness in everyday clinical practice. Even with optimized protocols, scan duration remains a critical bottleneck that restricts broader clinical adoption and complicates the acquisition of larger patient cohorts.

Recent advances in deep learning (DL)-based reconstruction offer new opportunities to address these limitations. By integrating data-driven priors directly into the reconstruction process, DL-based techniques have the potential to enable higher acceleration while preserving image quality [6], which would shorten acquisition times and improve the clinical usability of UHF neuroimaging.

In this article, we illustrate how integrating DL reconstruction into a clinical 7T workflow can help unlock the full potential of submillimeter brain imaging, bringing UHF MRI closer to routine clinical application.

Materials and methods

Forty-five patients with various pathologies (e.g., multiple sclerosis, tumor, epilepsy) were scanned at 7T using a MAGNETOM Terra system (Siemens Healthineers, Erlangen, Germany) with a 1Tx32Rx head coil (Nova Medical, Wilmington, MA, USA). As part of the clinical protocol at the enrolled institution, a 0.6 mm isotropic three-dimensional T1-weighted MP2RAGE sequence [7, 8] (matrix size, 384 × 256 × 384; repetition time, 6000 ms; inversion times, 800 ms and 2700 ms; echo time, 2.06 ms; acquisition time, 7:40 min) was acquired with a sparse undersampling pattern and an acceleration factor of R = 4.

Each acquisition was retrospectively undersampled to simulate acceleration factors of R = 6 (5:06 min), R = 8 (3:50 min), and R = 12 (2:33 min). The original acquisition was reconstructed with compressed sensing (CS) [9] following the institution's clinical protocol. The retrospectively undersampled datasets were reconstructed with a DL-based method [10]. Three radiologists (P.R., K.B., and C.B., with seven years, two years, and one year of experience with UHF brain images, respectively) used a five point Likert scale (1 = very poor, 2 = poor, 3 = adequate, 4 = good, 5 = very good) to rate all the images for overall image quality, pathology conspicuity, and overall clinical value.

Results

Figure 1 presents the distribution of ratings in the four reconstructions (CS with R = 4, and DL with R = 6, 8, and 12) pooled across radiologists. Images reconstructed with DL at R = 6 exhibit statistically significant improvements over the clinical CS reconstruction in all three evaluation criteria. At R = 12, DL performs significantly worse in the three criteria. No statistically significant differences were found between DL reconstruction at R = 8 and CS at R = 4.

Figures 2–6 display representative patient cases, each with four reconstructions. These examples highlight the range of clinical appearances encountered in routine neuroimaging, including cases with subtle cortical abnormalities and fine structural detail. At moderately higher acceleration (R = 6 and R = 8), DL reconstruction consistently preserves anatomical detail, tissue contrast, and lesion morphology, closely matching the clinical reference reconstruction.

At the highest acceleration factor evaluated here (R = 12), image degradation can become apparent, underscoring the importance of balancing acceleration with diagnostic robustness. Collectively, these cases illustrate that DL-based reconstruction enables substantially higher acceleration than conventional compressed sensing and preserves clinically meaningful image quality for submillimeter 7T neuroimaging.

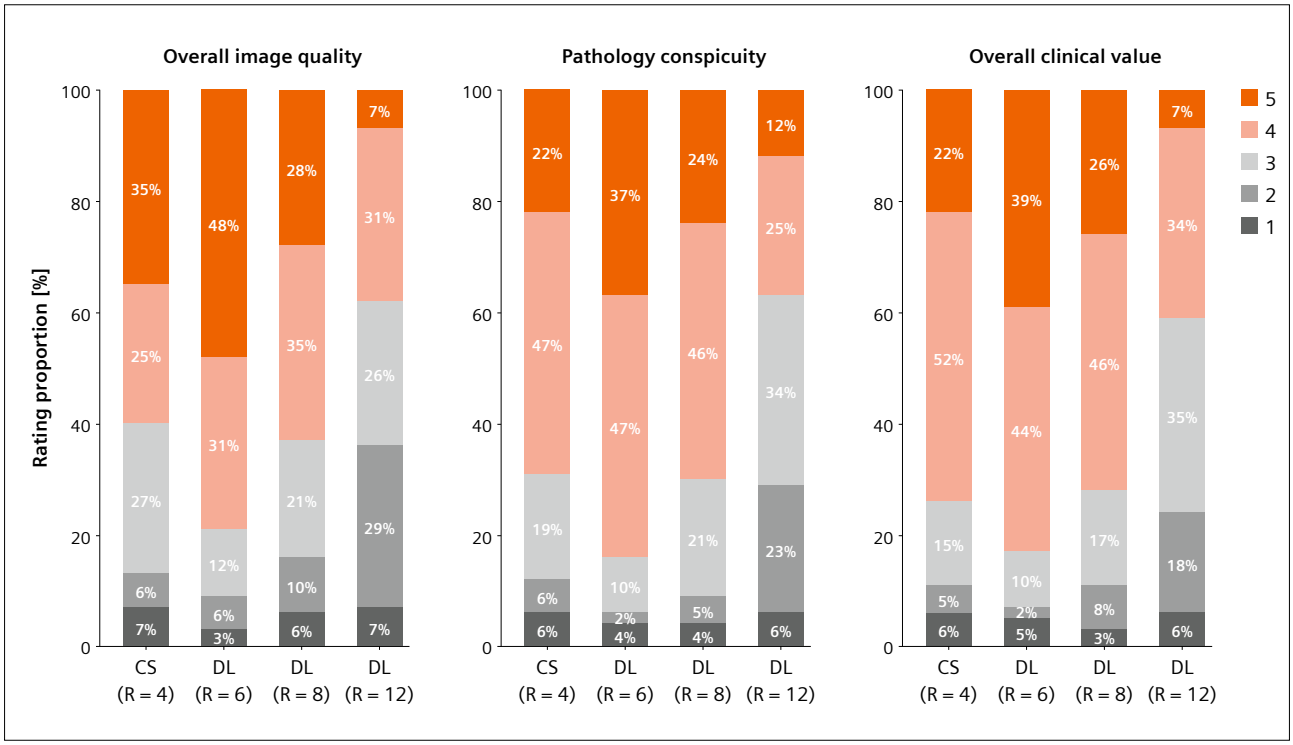

1 Distribution of ratings across reconstruction methods for the three evaluation criteria. Ratings from the three radiologists were pooled. CS = compressed sensing; DL = deep learning

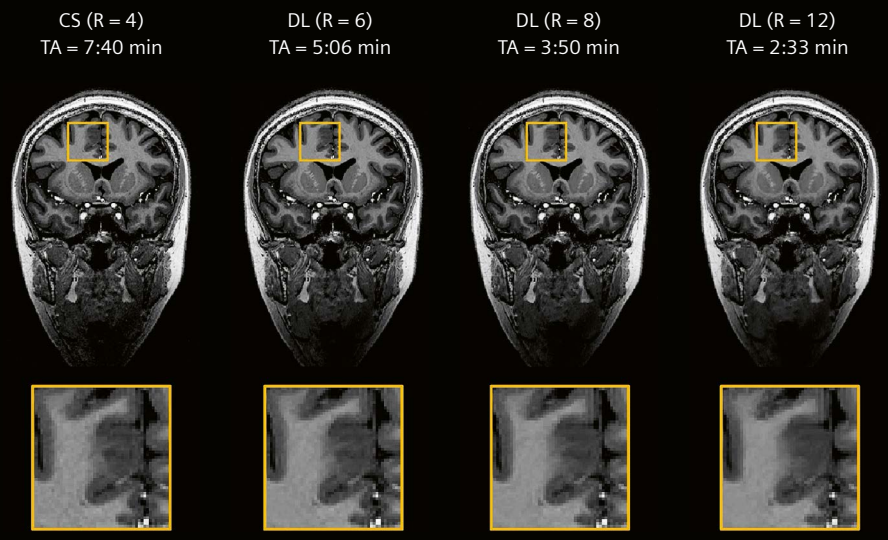

2 T1-weighted MP2RAGE reconstructed images in coronal view of a patient with epilepsy caused by a suspected glioneuronal tumor (WHO Grade 1). DL reconstruction at R = 6 and 8 exhibits a similar level of detail as the compressed sensing image (CS at R = 4).

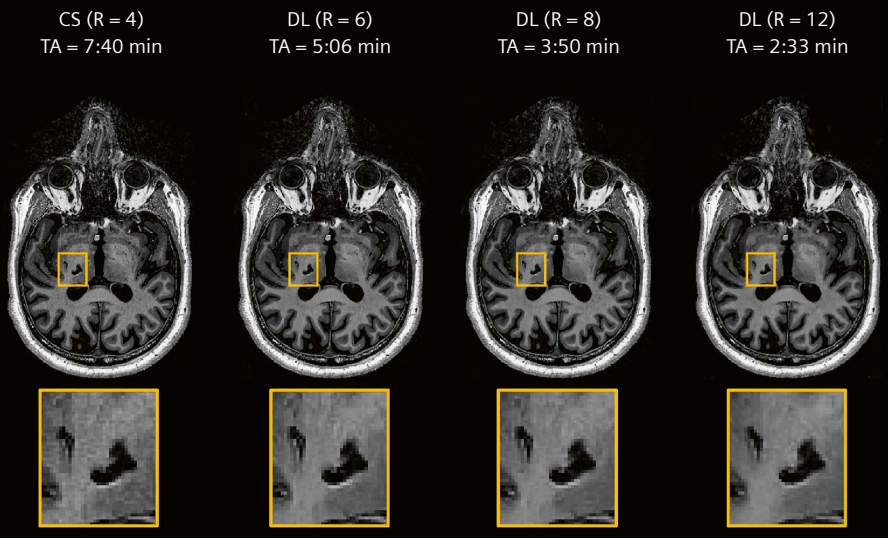

3 T1-weighted MP2RAGE reconstructed images in axial view of a patient with brain hemorrhages. DL-reconstructed images show similar levels of hemorrhage delineation as the compressed sensing image (CS at R = 4).

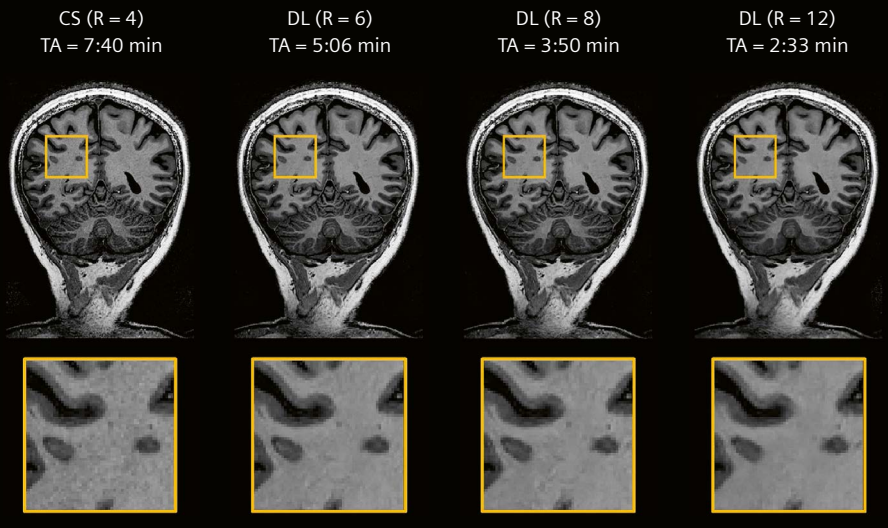

4 T1-weighted MP2RAGE reconstructed images in coronal view of a patient with multiple sclerosis (MS). Lesion conspicuity in images reconstructed with the DL method at R = 6 or 8 is similar to the compressed sensing image (CS at R = 4), while fine structures start to be smoothed out at R = 12.

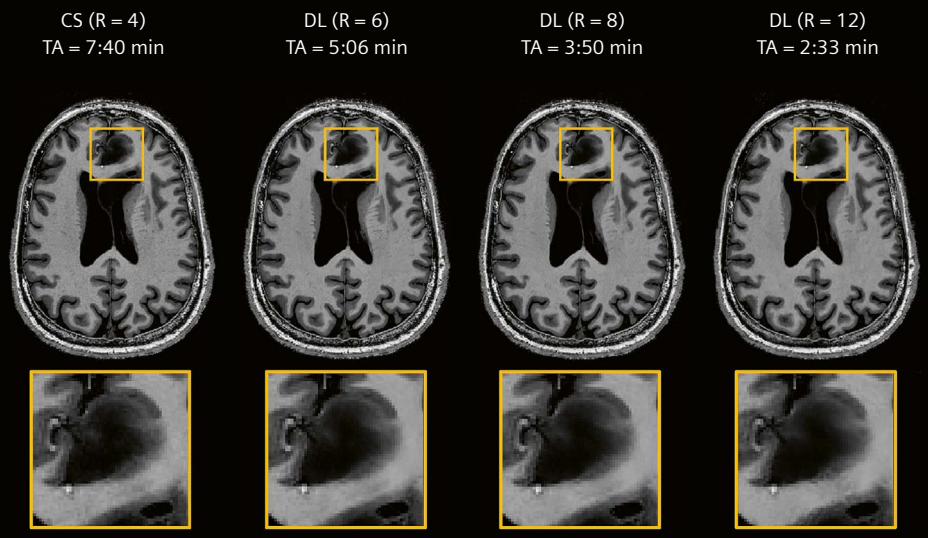

5 T1-weighted MP2RAGE reconstructed images in axial view of a patient with a tumor in the frontal lobe. At the three acceleration factors, the images reconstructed with DL achieve similar image quality and sharpness in the tumor's border as the compressed sensing image (CS at R = 4).

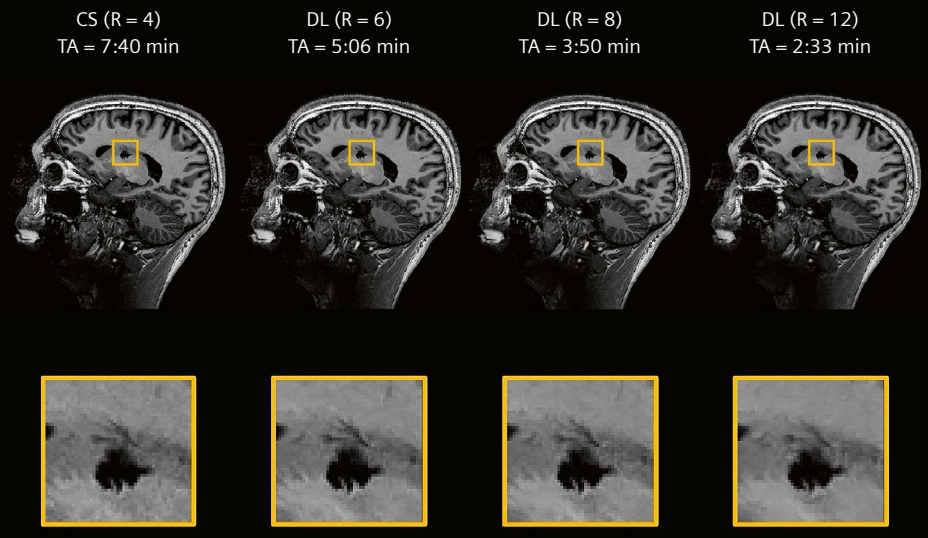

6 T1-weighted MP2RAGE reconstructed images in sagittal view of a patient with vasculitis. At R = 6 and 8, DL reconstruction preserved the sharpness of the ischemic lesion and its surroundings.

Discussion

Submillimeter-resolution imaging is one of the defining strengths of 7T MRI, yet its clinical impact is often limited by long scan times and sensitivity to motion. By enabling higher acceleration without sacrificing diagnostic confidence, DL reconstruction directly addresses a key bottleneck in translating high-resolution imaging into routine clinical practice.

The evaluation presented here demonstrates that DL reconstruction maintains lesion conspicuity and image quality at acceleration levels beyond those typically used in clinical 7T protocols. By reducing the practical barriers associated with long acquisitions, DL-based reconstruction methods may facilitate larger clinical studies, improve patient tolerance, and ultimately broaden access to submillimeter UHF neuroimaging.

Conclusion and outlook

Deep learning (DL) reconstruction enables higher acceleration of submillimeter 7T brain imaging while preserving clinical image quality and diagnostic confidence. By reducing acquisition time constraints, DL-based reconstruction techniques support the broader clinical usability of UHF neuroimaging and help unlock its full diagnostic potential.

Looking ahead, integrating DL reconstruction into routine clinical protocols will be a promising step toward making high-resolution neuroimaging more accessible and practical. As AI-based reconstruction technology continues to evolve, such approaches are poised to play a central role in the development of the next generation of clinical 7T MRI systems.

Acknowledgments

This work was supported by the German Federal Ministry of Research, Technology and Space grant Integrated Deep Learning at 7T (IDL@7T, 13GW0682A).

References

1 Radojewski P, Piredda GF, Bonanno G, Lövblad KO, Vargas MI, Sutter R, et al. Assessment of the available evidence for the use of 7-Tesla (T) magnetic resonance imaging (MRI) in neurological and musculoskeletal disorders, with comparison to 3-T and 1.5-T MRI: A systematic scoping review. Eur J Neurol. 2025;32(1):e16557.

2 Ladd ME, Bachert P, Meyerspeer M, Moser E, Nagel AM, Norris DG, et al. Pros and cons of ultra-high-field MRI/MRS for human application. Prog Nucl Magn Reson Spectrosc. 2018;109:1–50.

3 León Betancourt A, Messmer F, Chan A, Wiest R, Bonanno G, Capiglioni M, et al. 7 Tesla MRI in Multiple Sclerosis: Insights From Its Use in Clinical Routine. Eur J Neurol. 2025;32(8):e70330.

4 Balchandani P, Naidich TP. Ultra-High-Field MR Neuroimaging. AJNR Am J Neuroradiol. 2015;36(7):1204–15.

5 Beck ES, Sati P, Sethi V, Kober T, Dewey B, Bhargava P, et al. Improved Visualization of Cortical Lesions in Multiple Sclerosis Using 7T MP2RAGE. AJNR Am J Neuroradiol. 2018;39(3):459–466.

6 Knoll F, Hammernik K, Zhang C, Moeller S, Pock T, Sodickson DK, et al. Deep-Learning Methods for Parallel Magnetic Resonance Imaging Reconstruction: A Survey of the Current Approaches, Trends, and Issues. IEEE Signal Process Mag. 2020;37(1):128–140. doi:10.1109/MSP.2019.2950640

7 Marques JP, Kober T, Krueger G, Van Der Zwaag W, Van De Moortele PF, Gruetter R. MP2RAGE, a self bias-field corrected sequence for improved segmentation and T1-mapping at high field. Neuroimage. 2010;49(2):1271–81.

8 Mussard E, Hilbert T, Forman C, Meuli R, Thiran J, Kober T. Accelerated MP2RAGE imaging using Cartesian phyllotaxis readout and compressed sensing reconstruction. Magn Reson Med. 2020;84(4):1881–1894.

9 Lustig M, Donoho D, Pauly JM. Sparse MRI: The application of compressed sensing for rapid MR imaging. Magn Reson Med. 2007;58(6):1182–95.

10 Liu Z, Patel V, Zhou X, Tao S, Yu T, Ma J, et al. Deep Learning Reconstruction for 7T MP2RAGE and SPACE MRI: Improving Image Quality at High Acceleration Factors. AJNR Am J Neuroradiol. 2025;46(11):2446–2454.doi:10.3174/ajnr.A8841

Jocelyn Philippe, M.Sc.

Thomas Yu, Ph.D.

Piotr Radojewski, M.D.

Contact

PD Dr. Piotr Radojewski, M.D.
Translational Imaging Center (TIC)
Swiss Institute for Translational and Entrepreneurial Medicine
Freiburgstrasse 3
3010 Bern
Switzerland
piotr.radojewski@insel.ch

Clinical Value of Optimized FLAIR Imaging at 7 Tesla: Neuroimaging Case Examples

Emilie Sleight[1,2], Jose Federico Ojeda Esparza[3], Gian Franco Piredda[4], Jürgen Herrler[5], Tom Hilbert[4,6,7], Karl-Olof Lövblad[3,8], Dimitrios Karampinos[1,2], Frédéric Grouiller[1,8,9], Felix T. Kurz[3,8]

[1] CIBM Center for Biomedical Imaging, Lausanne, Switzerland
[2] Laboratory of Magnetic Resonance Imaging Systems and Methods, Ecole Polytechnique Fédérale de Lausanne, Switzerland
[3] Division of Neuroradiology, Diagnostic Department, Geneva University Hospitals, Geneva, Switzerland
[4] Swiss Innovation Hub, Siemens Healthineers International AG, Lausanne, Switzerland
[5] Siemens Healthineers AG, Erlangen, Germany
[6] Department of Radiology, Lausanne University Hospital and University of Lausanne, Switzerland
[7] LTS5, Ecole Polytechnique Fédérale de Lausanne, Switzerland
[8] Department of Radiology and Medical Informatics, Faculty of Medicine, University of Geneva, Switzerland
[9] Division of Radiology, Diagnostic Department, Geneva University Hospitals, Geneva, Switzerland

Introduction

Fluid-attenuated inversion recovery (FLAIR) is a widely used MRI contrast in clinical neuroimaging. This is due to its high sensitivity for detecting parenchymal lesions, particularly in regions adjacent to cerebrospinal fluid (CSF). By suppressing the CSF signal while preserving T2-weighted contrast, FLAIR improves lesion conspicuity in a wide range of neurological conditions. It is therefore recommended in the assessment of multiple neurological diseases, including multiple sclerosis [1, 2], epilepsy [3, 4], brain tumors [5], and neurodegenerative disorders such as dementia [6].

With the increasing availability of ultra-high-field MRI systems, imaging at 7 Tesla (7T) has created new opportunities for neuroimaging by providing a substantial gain in signal-to-noise ratio compared with lower field strengths [7, 8]. This gain enables higher spatial resolution and improved lesion detection, which is particularly attractive for diseases characterized by subtle or small lesions. Indeed, several studies have demonstrated increased lesion sensitivity at 7T compared with conventional field strengths [9, 10].

Despite these advantages, the clinical implementation of FLAIR at 7T remains challenging and many sites report suboptimal image contrast or limited robustness. These limitations are primarily related to increased specific absorption rate (SAR) [11], changes in tissue relaxation times that reduce contrast between gray and white matter [12, 13], and pronounced B_1^+ field inhomogeneities that can cause regional signal loss [11]. As a result, FLAIR is sometimes omitted from 7T clinical protocols, despite its established diagnostic value at lower field strengths.

This article presents an optimized 3D FLAIR sequence protocol designed to address these challenges on the 7T MAGNETOM Terra.X system. The clinical value is illustrated using selected neuroimaging cases.

FLAIR sequence optimization

At 7T, limitations in SAR restrict the use of 180° refocusing flip angles [11]. However, the 3D SPACE sequence uses variable refocusing flip angles, which substantially reduces SAR while preserving image quality and whole-brain coverage.

A further challenge for ultra-high-field MRI is the reduced intrinsic contrast between gray and white matter on FLAIR images, largely due to prolonged T1 and altered T2 relaxation times. To compensate for this effect, a T2-preparation module was added prior to the inversion recovery [13], with the preparation duration optimized to enhance tissue contrast on FLAIR images. Table 1 provides the parameters for the 7T 3D FLAIR SPACE sequence.

Finally, B_1^+ inhomogeneities at 7T can lead to regional signal loss, particularly in the temporal lobes, cerebellum, and brain stem, and are especially pronounced on FLAIR images. These effects were mitigated using parallel transmission (pTx) technology [14–16]. In this work, fast online-customized (FOCUS) pTx pulses were employed with an 8Tx32Rx head coil (Nova Medical, Wilmington, MA, USA), enabling improved flip-angle homogeneity across the brain with limited SAR exposure by designing subject-specific pTx pulses, resulting in more uniform image quality [17, 18].

Parameter	Value
Orientation	Sagittal
FOV (mm^3)	225 × 180 × 156
Resolution (mm^3)	0.7 × 0.7 × 0.7
Slices per slab	224
Acceleration	CAIPI 3 × 2 (shift 1)
TR (ms)	8000
Magnetization preparation	Non-sel. T2 prep. IR
T2 prep. duration (ms)	200
TI (ms)	1990
Flip angle mode	T2 variable
Tissue T1 (ms)	1500
Tissue T2 (ms)	50
TE (ms)	300
Echo spacing (ms)	4.28
Turbo factor	180
Bandwidth (Hz/Px)	751
RF pulse type	Low SAR
Gradient mode	Normal
Acquisition time (min:s)	8:18

Table 1: Parameters of the 7T FLAIR SPACE sequence with FOCUS pTx pulses.

Conclusion

The clinical cases presented here illustrate the added value of an optimized 7T 3D FLAIR SPACE protocol across a range of neurological pathologies. Compared to standard 3T imaging, 7T FLAIR provided improved lesion conspicuity, sharper lesion delineation, and enhanced visualization of subtle cortical and juxtacortical abnormalities.

In cases with indeterminate lesions, 7T FLAIR enabled the detection of small additional abnormalities that were not visible at 3T, potentially contributing to a more comprehensive assessment of lesion burden.

For suspected low-grade glioma in the temporal lobe, the use of pTx technology mitigated signal loss related to B_1^+ inhomogeneities in lower brain regions, which made it possible to detect the tumor at 7T. Compared with 3T FLAIR, ultra-high-field imaging provided improved delineation of cortical involvement and lesion margins, revealing features of cortical infiltration. This enhanced lesion characterization increased diagnostic confidence in distinguishing an infiltrative glioma from non-infiltrative juxtacortical white matter abnormalities, and may have implications for clinical decision-making.

Similarly, in a case of suspected multinodular and vacuolating neuronal tumors, 7T FLAIR enabled clearer delineation of lesion extent and revealed a characteristic multinodular, aggregated architecture of multiple juxta-cortical and subcortical hyperintense nodules that appeared more confluent on 3T imaging, thereby providing imaging features with potential diagnostic relevance.

In the context of epilepsy, 7T FLAIR demonstrated clear advantages in visualizing focal cortical dysplasia. This allowed more confident identification of abnormalities and more-targeted resection while minimizing the removal of adjacent non-pathological tissue.

These examples highlight the strength of optimized FLAIR imaging at 7T for pathologies where subtle changes or lesion extent are clinically relevant. Overall, with appropriate sequence and RF optimization, FLAIR imaging at 7T can be robustly integrated into clinical neuroimaging protocols. The resulting gains in lesion sensitivity and anatomical detail may provide clinically meaningful information beyond that available at 3T, supporting diagnosis, treatment planning, and patient management.

Case 1

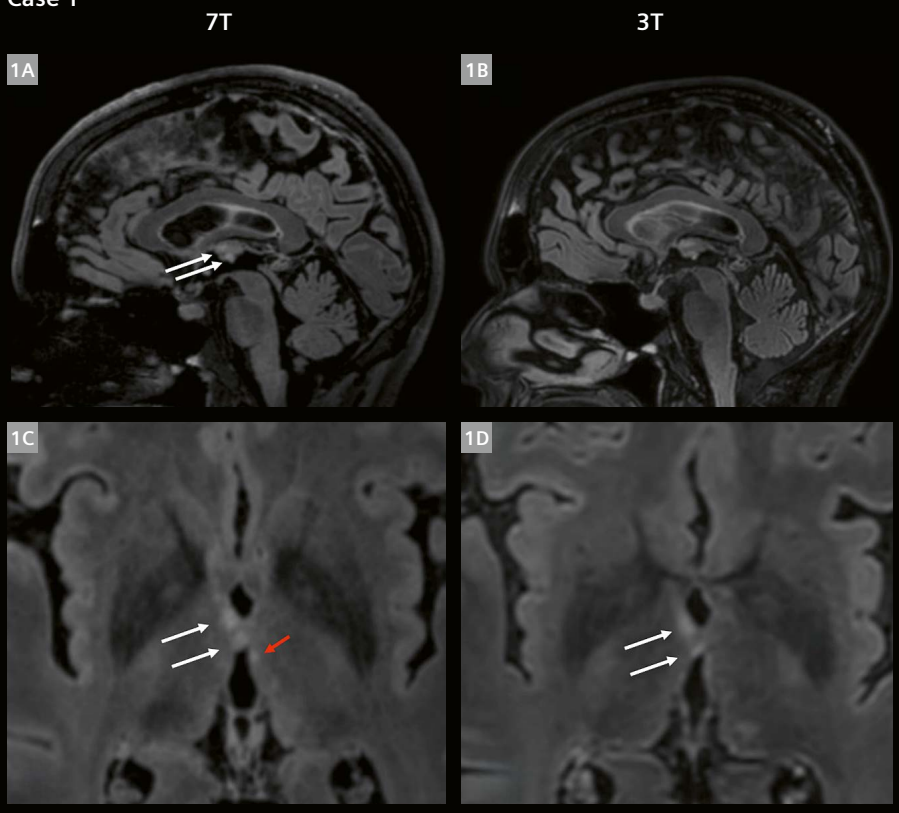

1 Bithalamic lesions of indeterminate origin in a 57-year-old patient. The FLAIR-hyperintense bithalamic lesions are well visible (white arrows) at both 7T **(1A, 1C)** and 3T **(1B, 1D)**, but are more conspicuous at 7T. **(1C)** A small lesion to the left of the third ventricle (red arrow) is only visible on 7T FLAIR, not on 3T FLAIR **(1D)**.

Case 2

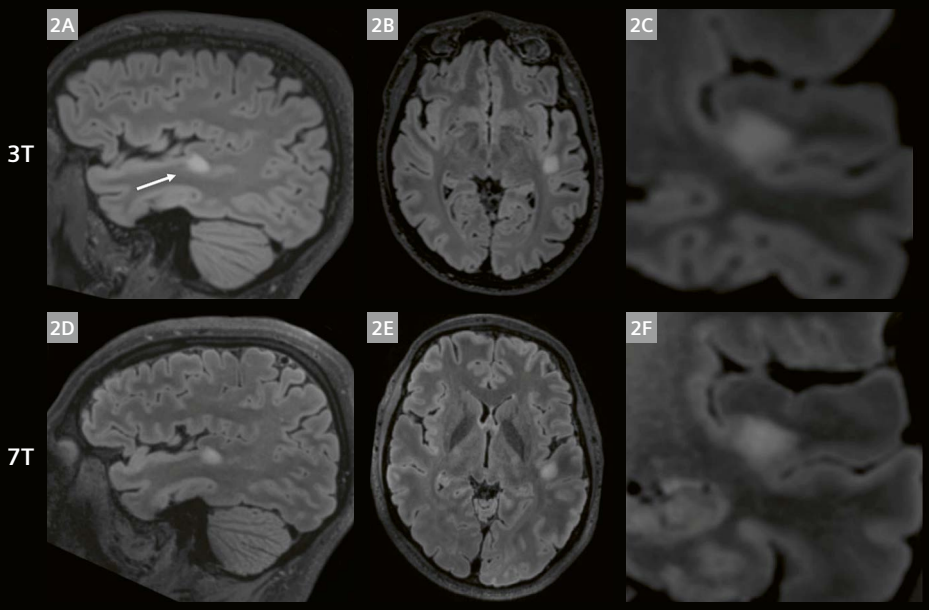

2 Suspected left temporal low-grade glioma. **(2A–2C)** 3T FLAIR-hyperintense left temporal lesion (white arrow) in **(2A)** sagittal, **(2B)** axial, and **(2C)** zoomed-in coronal orientations. **(2D–2F)** 7T images of the same lesion in **(2D)** sagittal, **(2E)** axial, and **(2F)** zoomed-in coronal orientations. Signal in the temporal lobe at 7T is only possible when using pTx pulses. Cortical infiltration was equivocal on 3T FLAIR, but more clearly delineated at 7T, thereby improving lesion characterization and diagnostic confidence when distinguishing an infiltrative lesion such as a low-grade glioma from non-infiltrative juxtacortical white matter abnormalities, and potentially informing surgical indication and planning.

Case 3

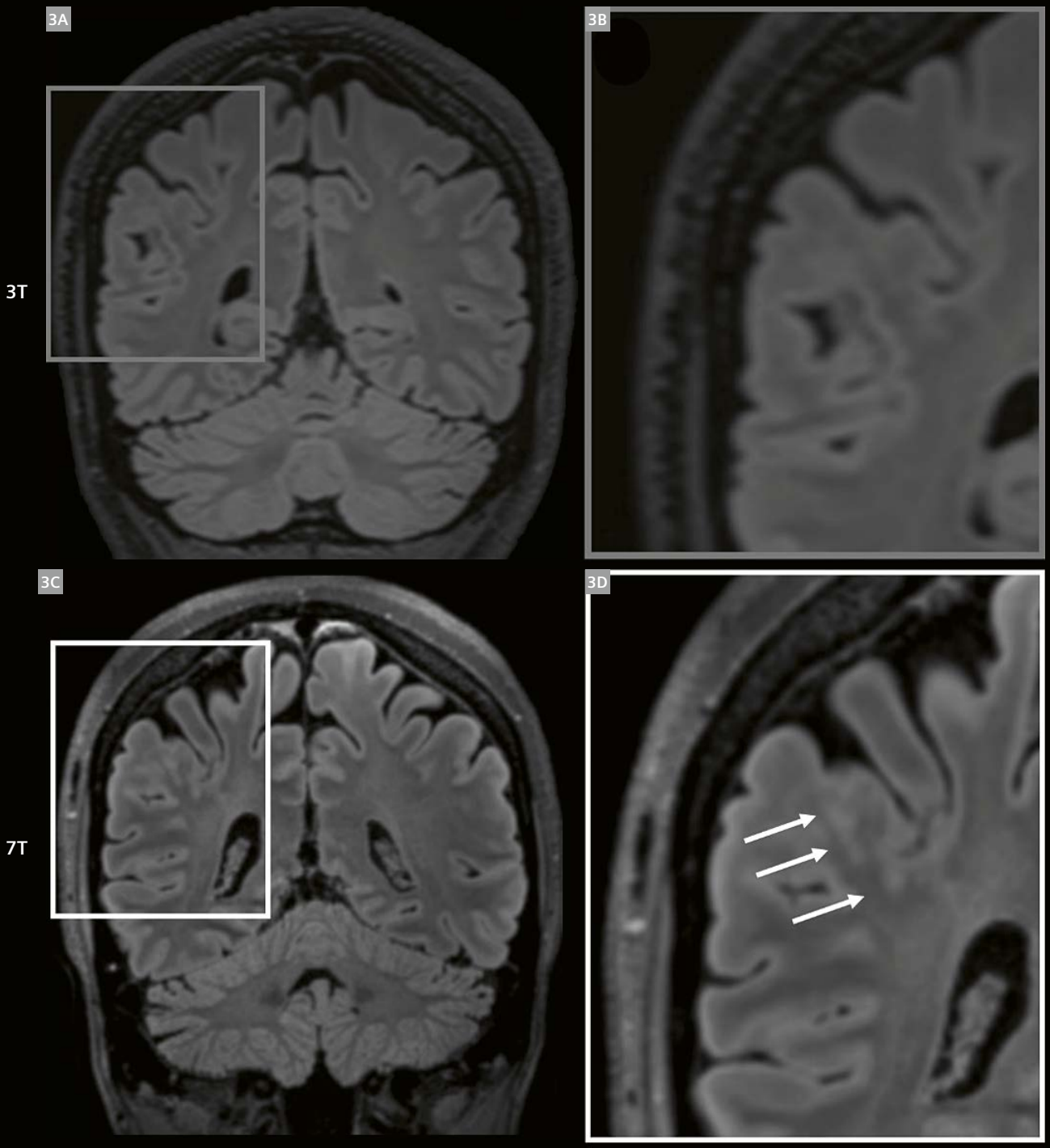

3 Suspicion of a multinodular and vacuolating neuronal tumor (MVNT) in the right superior parietal lobule. **(3A)** 3T FLAIR image in coronal orientation, with a magnified view of the superior parietal lobule subregion shown in **(3B)**. **(3C)** Corresponding 7T FLAIR image, with magnified view shown in **(3D)**, demonstrating multiple juxtacortical and subcortical hyperintense lesions. With 7T FLAIR, the extent of the lesion and its multinodular aggregated architecture are more clearly depicted, in contrast to the more confluent appearance on 3T, a pattern that can have diagnostic implications.

Case 4

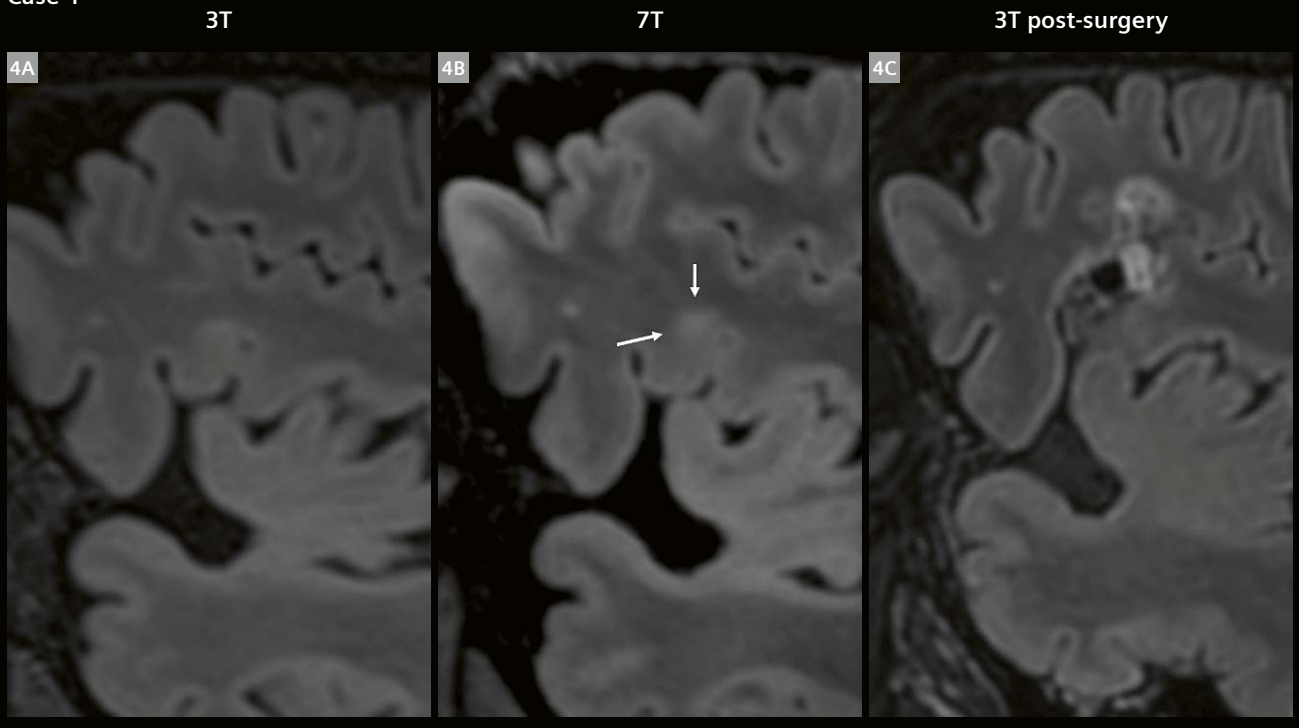

4 Left frontal focal cortical dysplasia type IIb. **(4A)** Magnified view of a 3T sagittal FLAIR image of a patient with focal epilepsy, retrospectively demonstrating subtle cortical and subcortical FLAIR-hyperintense changes involving the left inferior frontal gyrus (Brodmann area 45). **(4B)** 7T FLAIR image of the same area, which shows improved lesion delineation (white arrows) compared to 3T. This allowed for a more precise definition of the dysplastic cortex preoperatively, which facilitated a better targeted resection while minimizing removal of adjacent non-pathological tissue. **(4C)** 3T post-operative FLAIR image following resection of the cortical dysplasia (scan conducted three months after surgery).

Acknowledgments

We acknowledge the MRI Platform of the FCBG (Fondation Campus Biotech Geneva), and the CIBM Center for Biomedical Imaging, for providing expertise and resources to conduct this study. We also acknowledge research support from Siemens Healthineers.

References

1 Traboulsee A, Li DKB. Conventional MR imaging. Neuroimaging Clin N Am. 2008;18(4):651–673. [Multiple Sclerosis, Part I: Background and Conventional MRI].
2 Bakshi R, Ariyaratana S, Benedict RHB, Jacobs L. Fluid-Attenuated Inversion Recovery Magnetic Resonance Imaging Detects Cortical and Juxtacortical Multiple Sclerosis Lesions. Arch Neurol. 2001; 58(5):742–748.
3 Rüber T, David B, Elger CE. MRI in epilepsy: clinical standard and evolution. Curr Opin Neurol. 2018;31(2):223–231.
4 Opheim G, van der Kolk A, Markenroth Bloch K, Colon AJ, Davis KA, Henry TR, et al. 7T Epilepsy Task Force Consensus Recommendations on the Use of 7T MRI in Clinical Practice. Neurology. 2021; 96(7):327–341.
5 Upadhyay N, Waldman AD. Conventional MRI evaluation of gliomas. Br J Radiol. 2011;84 Spec No 2(Spec Iss 2):S107–11.
6 Theysohn JM, Kraff O, Maderwald S, Barth M, Ladd SC, Forsting M, et al. 7 tesla MRI of microbleeds and white matter lesions as seen in vascular dementia. J Magn Reson Imaging. 2011;33(4):782–91.
7 Uğurbil K. Magnetic Resonance Imaging at Ultrahigh Fields. IEEE Trans Biomed Eng. 2014;61(5):1364–1379.
8 van der Kolk AG, Hendrikse J, Zwanenburg JJ, Visser F, Luijten PR. Clinical applications of 7 T MRI in the brain. Eur J Radiol. 2013; 82(5):708–18.
9 Veersema TJ, Ferrier CH, van Eijsden P, Gosselaar PH, Aronica E, Visser F, et al. Seven tesla MRI improves detection of focal cortical dysplasia in patients with refractory focal epilepsy. Epilepsia Open. 2017;2(2):162–171.

10 Wang I, Oh S, Blümcke I, Coras R, Krishnan B, Kim S, et al. Value of 7T MRI and post-processing in patients with nonlesional 3T MRI undergoing epilepsy presurgical evaluation. Epilepsia. 2020; 61(11):2509–2520.
11 Barisano G, Sepehrband F, Ma S, Jann K, Cabeen R, Wang DJ, et al. Clinical 7 T MRI: Are we there yet? A review about magnetic resonance imaging at ultra-high field. Br J Radiol. 2019;92(1094): 20180492.
12 Rooney WD, Johnson G, Li X, Cohen ER, Kim SG, Ugurbil K, et al. Magnetic field and tissue dependencies of human brain longitudinal 1H2O relaxation in vivo. Magn Reson Med. 2007;57(2):308–18.
13 Visser F, Zwanenburg JJ, Hoogduin JM, Luijten PR. High-resolution magnetization-prepared 3D-FLAIR imaging at 7.0 Tesla. Magn Reson Med. 2010;64(1):194–202.
14 Adriany G, Van de Moortele PF, Wiesinger F, Moeller S, Strupp JP, Andersen P, et al. Transmit and receive transmission line arrays for 7 Tesla parallel imaging. Magn Reson Med. 2005;53(2):434–45.
15 Gras V, Vignaud A, Amadon A, Le Bihan D, Boulant N. Universal pulses: A new concept for calibration-free parallel transmission. Magn Reson Med. 2017;77(2):635–643.
16 Faber J, Paech D, Pracht E, Stirnberg R, Ehses P, Völzke Y, et al. Ready for Routine: Homogeneous, High-Resolution, and Multicontrast Whole-Brain MRI at 7 Tesla in Short Scan Time With "plug-and-Play" pTx Sequences. Invest Radiol. 2025. doi: 10.1097/RLI.0000000000001252. Epub ahead of print.
17 Herrler J, Liebig P, Gumbrecht R, Ritter D, Schmitter S, Maier A, et al. Fast online-customized (FOCUS) parallel transmission pulses: A combination of universal pulses and individual optimization. Magn Reson Med. 2021;85(6):3140–3153.
18 Piredda GF, Sleight E, Yu T, Klauser A, Pato Montemayor N, Philippe J, et al. Individually optimized dynamic parallel transmit pulses for 3D high-resolution SPACE imaging at 7T. Magn Reson Med. 2025;94(4):1616–1625.

Contact

Emilie Sleight, Ph.D.
CIBM Center for Biomedical Imaging
EPFL Campus Biotech
Chemin des Mines 9
1202 Geneva
Switzerland
emilie.sleight@epfl.ch

Professor Frédéric Grouiller, Ph.D.
CIBM Center for Biomedical Imaging
Division of Radiology
Diagnostic Department
Geneva University Hospitals (HUG)
Boulevard de la Tour 8
1205 Geneva
Switzerland
frederic.grouiller@hug.ch

Professor Felix T. Kurz, M.D., Ph.D.
Division of Neuroradiology
Diagnostic Department
Geneva University Hospitals (HUG)
Rue Gabrielle-Perret-Gentil 4
1205 Geneva
Switzerland
FelixTobias.kurz@hug.ch

MRI-Based Modeling of the Lumbosacral Spine for Epidural Electrical Stimulation: Toward Personalized Neuromodulation

Jionghui Liu[1], Wenqi Zhang[1], Yuxing Zhou[1], Linhao Xu[1], Ying-Hua Chu[2], Fumin Jia[1,3]

[1] Institute of Science and Technology for Brain-inspired Intelligence, Fudan University, Shanghai, China
[2] MR Research Collaboration Team, Siemens Healthineers Ltd., Shanghai, China
[3] State Key Laboratory of Medical Neurobiology and MOE Frontiers Center for Brain Science, Fudan University, Shanghai, China

Introduction

Spinal cord injuries (SCI) impair motor function and quality of life for millions globally. Spatiotemporal epidural electrical stimulation (EES) has demonstrated the ability to restore movement [1], yet translational progress is hindered by the lack of detailed imaging datasets targeting spinal nerve roots.

One limitation to clinical adoption is the lack of high-resolution imaging data covering the lumbosacral nerve roots [2]. These data are essential for precise stimulation targeting. Our open-access dataset aims to address this unmet need.

Data acquisition and post-processing workflow

Participants

Fourteen healthy adults (12 males, 2 females; mean age: 23 years) participated in this study. All were screened to ensure no history of SCI or related conditions. Ethical approval was obtained from Fudan University, and all participants provided informed consent.

Sequence	Field of view (mm)	Voxel size (mm^3)	TR/TE (ms)	Flip angle	Scan time (min:sec)
T2-TSE	240 × 240	0.63 × 0.63 × 3.00	3500/104	160°	3:22
DESS	243 × 243	1.27 × 1.27 × 1.27	10.95/3.86	25°	2:23
CISS	288 × 288	0.35 × 0.35 × 1.80 or 0.30 × 0.30 × 2.00	9.80/4.46	50°	29:30

Table 1: Imaging protocol overview (3T MAGNETOM Prisma, Siemens Healthineers, Erlangen, Germany).

Workflow

The workflow involved representative MRI data acquired from a healthy adult participant illustrating the human lumbosacral spine from multiple dimensions, and the post-processing pipeline in Figure 1. T2 TSE images delineate the spinal cord contour, while DESS images highlight ganglion localization. Additionally, MR images from the CISS sequence clearly depict the distribution of spinal nerve roots in the lumbosacral spine. The geometry information was obtained through manual annotation and was subsequently utilized to automatically construct a comprehensive human lumbosacral model, encompassing structures such as the dura, cerebrospinal fluid, and the nerve roots spanning from L1 to S2.

Spinal 3D model reconstruction

In CISS images, nerve root trajectories often appear amidst other tissues like arachnoid and denticulate ligaments, and therefore require precise differentiation. The density of nerve roots increases as the spinal cord extends toward the cauda equina, complicating the identification of individual segments. The research team overcame these challenges by developing annotation protocols based on anatomical and physiological expertise. Two independent annotators worked to minimize biases (Fig. 2), ensuring robust and reliable data for constructing 3D models.

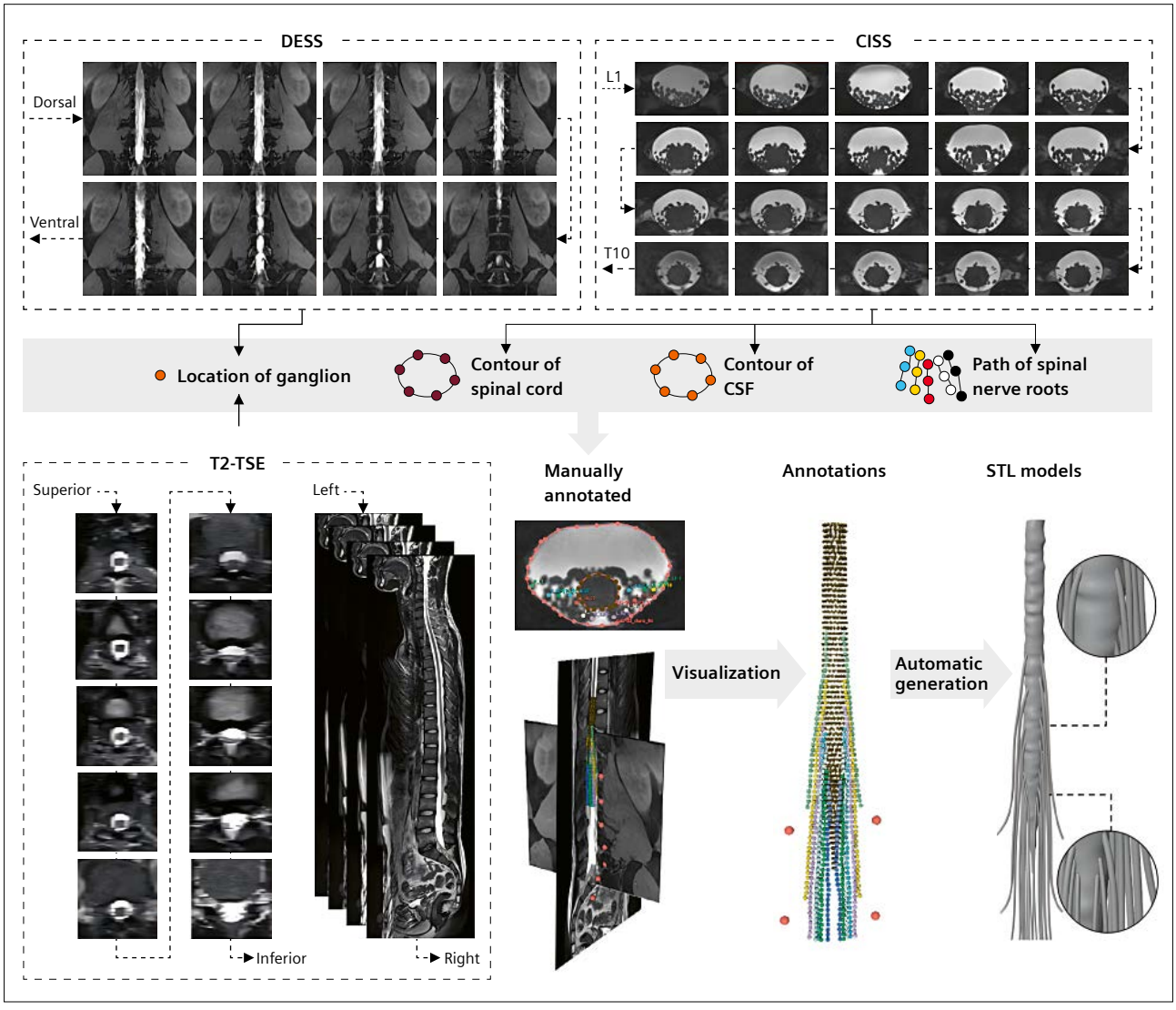

1 Post-processing and annotation workflow.

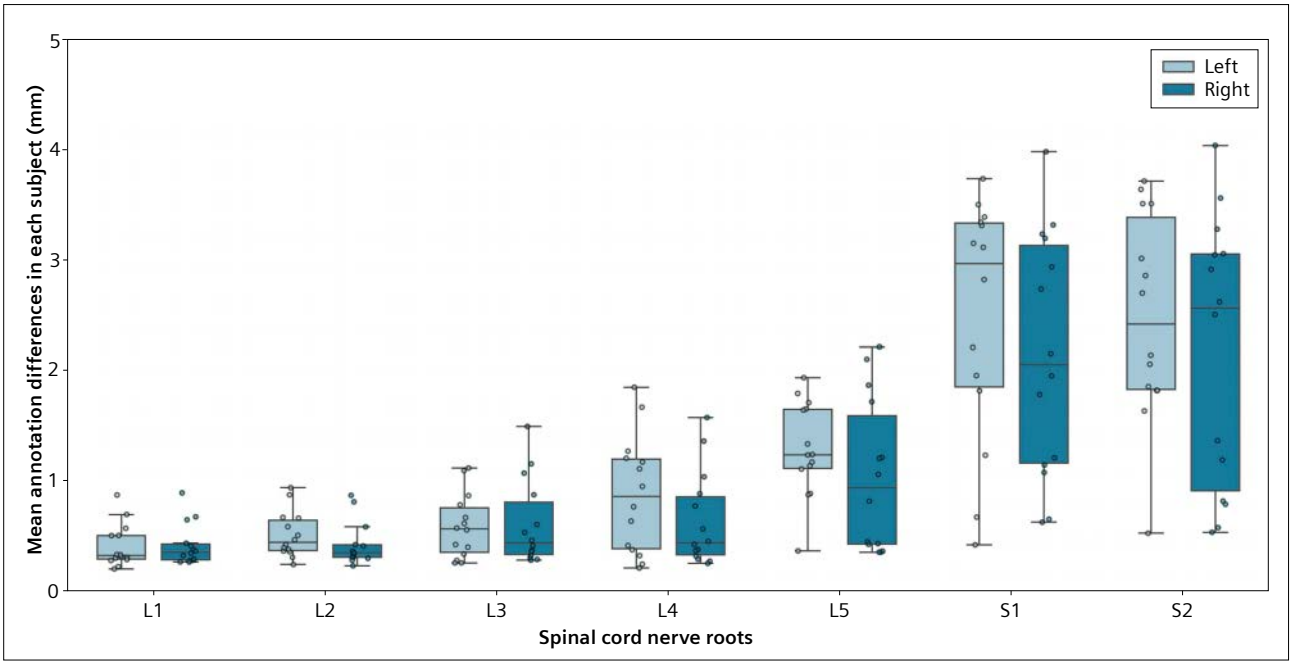

2 Mean differences in annotations from two annotators for each subject, focusing on the L1 to S2 spinal cord nerve roots. Each data point represents the average annotation difference across different imaging slices. The differences were specifically measured by calculating the three-dimensional distances between the coordinates of corresponding points in the two sets of annotations.

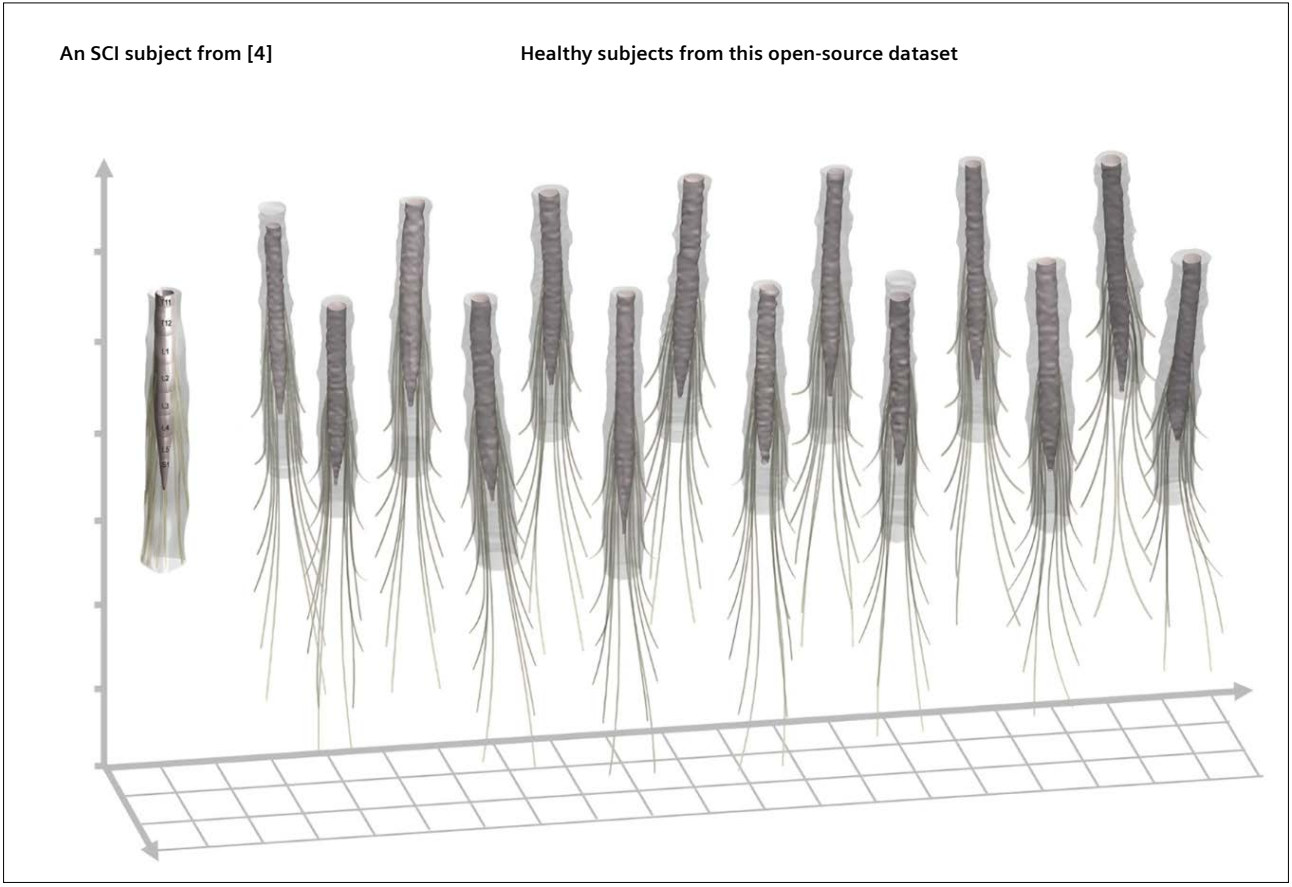

3 Visualization of 3D reconstructed models highlighting the dura, cerebrospinal fluid, and nerve roots spanning from L1 to S2.

The nerve root annotations were quantitatively analyzed to assess interparticipant variability. Statistical measures, including mean trajectory deviations and standard deviations, were computed for key landmarks along the L1 to S2 segments. Variability was minimal in the upper segments (L1–L3) but increased in the caudal regions (S1–S2), reflecting natural anatomical diversity. Although the annotation differences for the S1 and S2 nerve roots are relatively larger, they remain smaller than the width of the Medtronic 5-6-5 paddle lead (10 mm; Medtronic, Minneapolis, MN, USA), which is widely used in EES — an important application that requires spine MRI.

Using annotated data, we generated 3D models of the lumbosacral spine, including nerve roots, white-matter boundaries, and cerebrospinal fluid using the open-source modeling software Blender (v4.0.2; Blender, Amsterdam, the Netherlands) [3]. These models are accessible for visualization and computational simulations. The models revealed consistent anatomical structures among healthy participants, providing a baseline for comparisons with pathological cases.

Quality control and annotation consistency

Notably, the data in this dataset were collected from healthy subjects. As observed in Figure 3, the overall morphology of the spinal cord in healthy subjects does not substantially differ from that of a patient (from a previous study [4]) with SCI. Overall, we hope our dataset can be used to evaluate the performance of advanced algorithms on general healthy subjects. An algorithm generalized well across healthy subjects is expected to achieve satisfactory performance on patient data.

Model-based application: Parameter optimization in EES

As shown in Figure 4, the spinal cord models provided by this dataset can be used for finite-element modeling to simulate the electric field distribution generated by the stimulation paddle across different spinal cord roots, which helps in parameter adjustment and optimization. For example, the primary muscle required for left hip

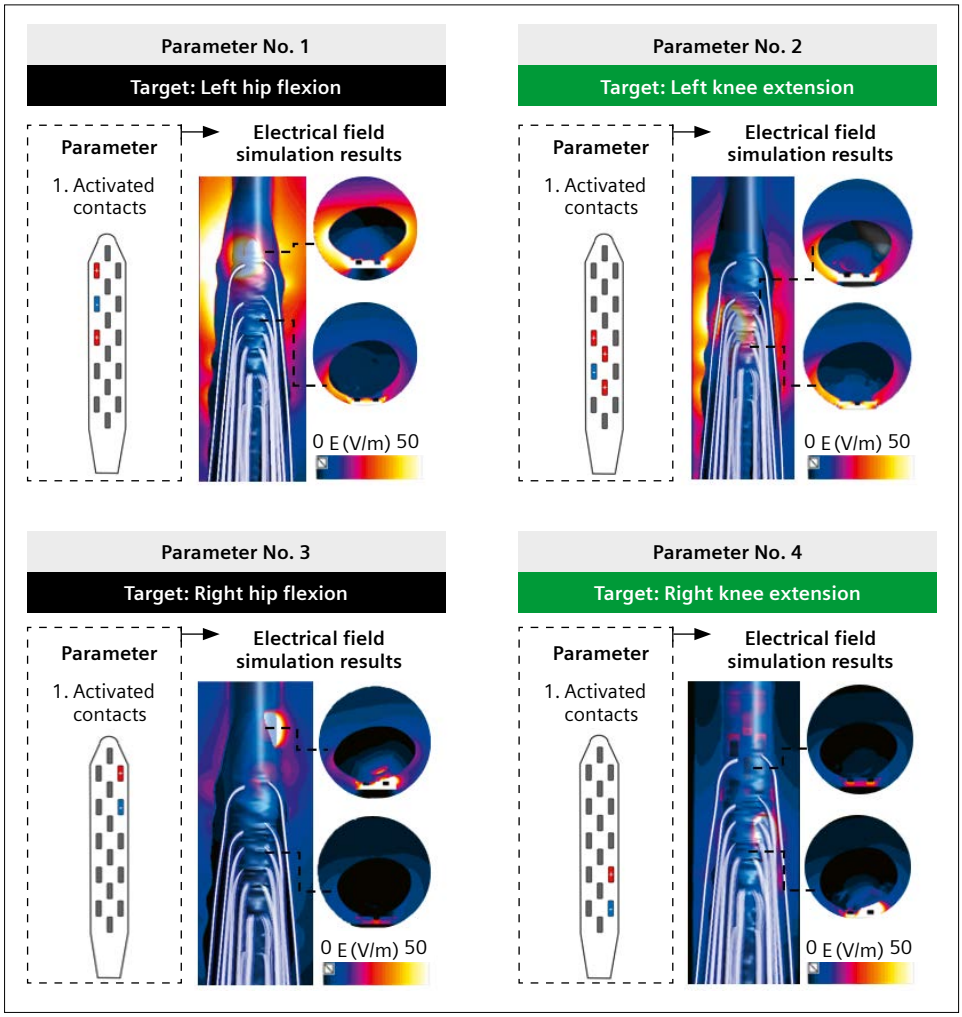

4 Results of the finite-element simulation for four typical parameters based on a spinal cord model.

flexion is the left iliopsoas muscle, which corresponds to the spinal nerve root at the left L1. The results of the finite-element simulation in Figure 5 show that the activated-contacts combination using Parameter No. 1 achieves better activation selectivity for the left L1 nerve root.

Pilot clinical extension: Imaging of SCI patients

To expand the utility of the dataset, a pilot study incorporating MRI data from an SCI patient was conducted. The patient's imaging was acquired using the same protocol as the healthy participants. The patient is a 33-year-old male, diagnosed with paraplegia for 21 months, classified as ASIA-B, with the injury site at T8. The scanning section was below the injury site. As shown in Figure 5, there is no significant difference between the SCI patient's spinal cord model and the healthy participant models in this dataset. However, more spinal data from SCI patients needs to be collected and statistical tests conducted to confirm the specific differences.

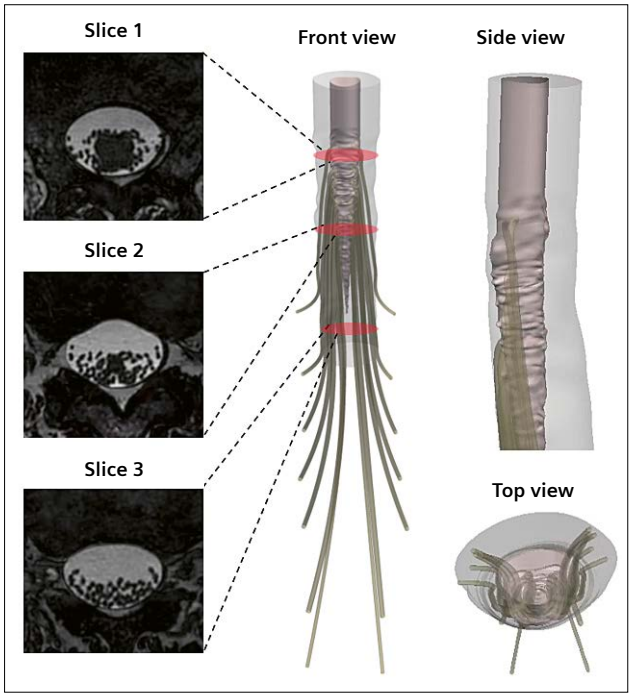

5 Visualization of spinal cord injury (SCI) patient data. The SCI patient model has a similar shape and structure to the healthy spinal cord model provided in this dataset, with differences being difficult to discern.

Existing literature indicates that while the unaffected areas of the spinal cord in SCI patients may undergo some atrophy or demyelination complications, these do not significantly affect the overall macroscopic morphology of the spinal cord. A study measuring the spinal cord cross-sectional area at the C1–C2 levels in 14 patients with injury levels ranging from C3 to C7 found that the cord area was 77.5 ± 3.2 mm^2 in controls and 68.8 ± 12.1 mm^2 in patients [5, 6]. On average, the spinal cord area in SCI patients shrunk by 11.2%, which is a small difference and does not hinder the implementation of the pipeline from imaging to modeling in this study.

Potential applications of the dataset and future development

This open-access dataset offers a valuable foundation for advancing neuromodulation technologies, particularly in the context of personalized spinal cord stimulation. The high-resolution MRI scans and detailed anatomical annotations support precise targeting of spinal nerve roots, which is critical for spatiotemporal epidural electrical stimulation.

The 3D models reconstructed from 14 healthy participants enable the development of machine learning algorithms for automated nerve root detection and spinal model generation — key steps toward efficient, individualized treatment planning [7]. In addition, these models facilitate finite-element simulations to evaluate how stimulation fields propagate through spinal tissues and to assess inter-individual variability in therapeutic response.

While the dataset primarily includes healthy subjects, the inclusion of an SCI case demonstrates its translational potential. By integrating patient-specific imaging into the modeling pipeline, clinicians and researchers can optimize stimulation parameters preoperatively, reducing the reliance on time-consuming manual adjustments during surgery and enhancing the precision of neuromodulation therapies.

Conclusion

This open-access lumbosacral MRI dataset fills a critical gap in spinal imaging resources, offering high-resolution views of nerve roots and anatomical annotations. It serves as a platform for enhancing research in spinal cord neuromodulation and related fields.

Data availability

The dataset is hosted on Figshare. It is organized according to the Brain Imaging Data Structure (BIDS) standards, and includes raw and processed data alongside quality metrics.

Acknowledgments

This work was supported by Fudan University and the Shanghai Municipal Science and Technology Major Project. We thank the participants for their contributions, and the Zhangjiang International Brain Imaging Center for imaging support.

References

1 Rowald A, Komi S, Demesmaeker R, Baaklini E, Hernandez-Charpak SD, Paoles E, et al. Activity-dependent spinal cord neuromodulation rapidly restores trunk and leg motor functions after complete paralysis. Nat Med. 2022;28(2):260–271.
2 Canbay S, Gürer B, Bozkurt M, Comert A, Izci Y, Başkaya MK. Anatomical relationship and positions of the lumbar and sacral segments of the spinal cord according to the vertebral bodies and the spinal roots. Clin Anat. 2014;27(2):227–33.
3 Joshua-M-maker. Joshua-M-maker/SpineNerveModelGenerator [Internet]. GitHub. 2025 [cited 2025 Dec 15]. Available from: https://github.com/Joshua-M-maker/SpineNerveModelGenerator.
4 Mesbah S, Herrity A, Ugiliweneza B, Angeli C, Gerasimenko Y, Boakye M, et al. Neuroanatomical mapping of the lumbosacral spinal cord in individuals with chronic spinal cord injury. Brain Commun. 2022;5(1):fcac330.
5 Cohen-Adad J, El Mendili MM, Lehéricy S, Pradat PF, Blancho S, Rossignol S, et al. Demyelination and degeneration in the injured human spinal cord detected with diffusion and magnetization transfer MRI. Neuroimage. 2011;55(3):1024–33.
6 Lundell H, Barthelemy D, Skimminge A, Dyrby TB, Biering-Sørensen F, Nielsen JB. Independent spinal cord atrophy measures correlate to motor and sensory deficits in individuals with spinal cord injury. Spinal Cord. 2011;49(1):70–5.
7 Liu J, Zhang W, Zhou Y, Xu L, Chu YH, Jia F. An open-access lumbosacral spine MRI dataset with enhanced spinal nerve root structure resolution. Sci Data. 2024;11(1):1131.

Ying-Hua Chu, Ph.D.
Lead Research Scientist
MR Research Collaboration Team
Siemens Healthineers Ltd.
Shanghai
China
yinghua.chu@siemens-healthineers.com

Contact

Fumin Jia, Ph.D.
Associate Professor
Institute of Science and Technology
for Brain-inspired Intelligence
Fudan University
Guanghua building
220 Handan Road
Shanghai
China
jfmin@fudan.edu.cn

Clinical Experience with a Coil-Integrated Head Fixation System in the Context of Intraoperative Magnetic Resonance Imaging for Intracranial Lesions

Greta Bohr, B.A.[1]; Dirk Freudenstein, M.D.[2]

[1] NORAS MRI products GmbH, Höchberg, Germany
[2] Department of Neurosurgery, RKH Klinikum Ludwigsburg, Germany

Introduction

Introduced into clinical practice more than 30 years ago, intraoperative magnetic resonance imaging (ioMRI) has become an indispensable tool, particularly for resection guidance in neurosurgery [1–3]. Nevertheless, the use of ioMRI imposes specific demands on personnel and technical infrastructure, especially with respect to head fixation systems and MRI coils: They determine not only surgical precision, but also image quality, safety, and workflow efficiency.

Head holders provide excellent cranial fixation and precise adjustment of extension and rotation angles according to the operative strategy. Also, they are essential for achieving optimal accuracy when frameless navigation systems are employed [4]. Integrated solutions combining MR-compatible head fixation systems with dedicated coils substantially improve imaging quality and surgical workflow. The limitations regarding head rotation and angulation that were present in early models have since been markedly reduced.

At RKH Klinikum Ludwigsburg, a triple-room ioMRI concept based on the 1.5T MAGNETOM Aera (Siemens Healthineers, Erlangen, Germany) was established in 2017. Until recently, the integrated 8-channel FLEXIBILITY OR Head Holder (NORAS MRI products, Höchberg, Germany) with three to seven fixation points had been used in all cases. In the following, we report on a three-month evaluation of the integrated three-pin LUCY OR Head Holder & 8-Ch Coil (NORAS MRI products, Höchberg, Germany).

Methods

From mid-October 2025 to mid-January 2026, a total of 20 microsurgical procedures were performed using the LUCY OR head fixation system. Workflow requirements, economic efficiency, and technical implementation were systematically evaluated.

1 Intraoperative MR imaging with the LUCY OR Head Holder & 8-Ch Coil on a 1.5T MAGNETOM Aera.

Workflow

Following patient positioning and anesthesia, the dedicated head holder is mounted and adjusted according to the planned surgical approach. The patient's head is positioned and fixed in the desired orientation, ensuring both mechanical stability and optimal access to the surgical site (Fig. 2A).

After fixation, the lower 4-channel coil element is inserted under the patient's head, and the holders for the upper coil element and the navigation reference are attached and aligned (Fig. 2B).

Before proceeding, a collision check is performed using a bore gauge to confirm safe clearance for intraoperative transfer into the MR bore (Fig. 2C). The navigation system

2 Workflow with the LUCY OR Head Holder & 8-Ch Coil. **(2A)** Adjusted head holder with the positioned patient. **(2B)** Placement of the lower 4-channel coil element and navigation reference. **(2C)** Collision check using the bore gauge. **(2D)** Setting up the navigation system. **(2E)** Surgical site with retractors. **(2F)** Easy draping and placement of the upper 4-channel coil element thanks to the dedicated sterile concept. **(2G)** After the checklist has been reviewed, the patient is ready for transport to the MR room. Draping and coil placement usually take less than 10 minutes.

3 Case presentation (1.5T MRI datasets). **(3A)** Preoperative T1 sequences with gadolinium showing the progressive glioblastoma in the lateral perirolandic region. **(3B)** The intraoperative MRI demonstrated residual tumor, predominantly within the precentral gyrus. Resection was continued until a motor-evoked-potential (MEP) stimulation threshold of 2 mA was reached. **(3C)** The early postoperative MRI shows the contrast-enhancing tumor remnants that were intentionally left in place for functional reasons, in keeping with the principle of maximal safe resection.

(Brainlab SE, Munich, Germany) is then initialized to enable accurate registration for reliable intraoperative guidance (Fig. 2D). After sterile preparation and exposure of the surgical field, retractors are positioned (Fig. 2E).

For ioMRI, the surgical site is easily draped according to a dedicated sterile concept. Then the upper 4-channel coil element is placed, completing the 8-channel configuration with optimal proximity to the anatomy for high-quality intraoperative imaging (Fig. 2F).

A structured review of the safety checklist is then carried out. After this, the patient is ready for transport to the MR room (Fig. 2G). Notably, draping and final coil placement usually require less than 10 minutes, demonstrating the efficiency and reproducibility of the setup within a routine intraoperative workflow.

Results

During the three-month evaluation period, 16 glioblastoma resections were performed, including four awake craniotomies. Three procedures were carried out in the prone position, while the others were in supine and lateral. Head rotation ranged from 15° to 60°. In four cases, a transsphenoidal pituitary tumor resection was conducted with a head angulation of up to 30°.

In all cases, the system design enabled an efficient and comfortable workflow while ensuring patient safety throughout the intervention. The head holder provides a robust and stable pinning mechanism that is suitable for different head sizes. The fixation system is height-adjustable and allows rotation, swiveling, tilting, and movement along the z-axis, as well as lateral displacement. Despite being based on a three-pin configuration, fixation remained stable during all procedures and throughout transport into and out of the scanner. Mounting and removing the coils was quick and straightforward and did not interfere with head fixation or life-support equipment, irrespective of patient positioning. The setup includes a dedicated sterile concept, and the head holder allows for easy and efficient cleaning. [5]

Case presentation

In a 70-year-old patient with progressive glioblastoma located in the lateral perirolandic region (primary resection in June 2024, followed by the Stupp protocol), a maximally safe resection was performed under neurophysiological monitoring with ioMRI-guided resection control. Due to the highly eloquent location of tumor components with blood-brain barrier disruption, and the presence of early motor-evoked potentials at a low stimulation threshold (2 mA), complete resection was not feasible from a functional perspective.

The postoperative course was uneventful and without neurological deficits (Karnofsky performance score of 90%). Subsequently, fractionated stereotactic radiotherapy (30 Gy in six fractions) was administered and well tolerated.

This case shows how maximal safe resection was achieved by using ioMRI to increase the extent of cytoreduction, and intraoperative neuromonitoring to preserve neurological function.

Conclusion

Compared with the previous model, the LUCY OR head fixation system with integrated coils demonstrated marked improvements in handling, greater flexibility across all axes while maintaining stability, and consistently high imaging quality. These findings have been confirmed in routine neurosurgical practice. This is particularly relevant for lateral approaches requiring head rotation of more than 30°, such as in insular tumor surgery or during awake craniotomies.

In our experience, the LUCY system offers more straightforward handling in these settings, especially for surgeons accustomed to three point head holders.

References

1 Jolesz FA, Blumenfeld SM. Interventional use of magnetic resonance imaging. Magn Reson Q. 1994;10(2):85–96.
2 Mislow JM, Golby AJ, Black PM. Origins of intraoperative MRI. Neurosurg Clin N Am. 2009;20(2):137–46.
3 Hlavac M, Wirtz CR, Halatsch ME. Intraoperative magnetic resonance imaging. HNO. 2017;65(1):25–29.
4 Beuriat PA, Jacquesson T, Jouanneau E, Berhouma M. Headholders' - complications in neurosurgery: A review of the literature and recommendations for its use. Neurochirurgie. 2016;62(6):289–294.
5 Bohr G, Roessler K. Evolution and Clinical Relevance of a Dedicated Head Holder & Coil Solution for Intraoperative MRI-guided Neurosurgery. ↗ MAGNETOM Flash. 2025;92:62–65.

Contact

Dr. Dirk Freudenstein, M.D.
Attending Neurosurgeon
Department of Neurosurgery
RKH Klinikum Ludwigsburg
Posilipostr. 4
71640 Ludwigsburg
Germany
dirk.freudenstein@rkh-gesundheit.de

Greta Bohr, B.A.
NORAS MRI products GmbH
Leibnizstr. 4
97204 Höchberg
Germany
Greta.Bohr@noras.de

Integrating MRI into Radiotherapy: Insights from Clinical Implementation of an MRI-Guided Workflow for Prostate Cancer

Philipp Schubert, M.D.; Juliane Szkitsak, Ph.D.; Rainer Fietkau, M.D.; Christoph Bert, Ph.D.; Florian Putz, M.D.

Department of Radiation Oncology, Universitätsklinikum Erlangen, Friedrich-Alexander-Universität Erlangen-Nürnberg, Erlangen, Germany

Introduction

Since 2019, the Department of Radiation Oncology at Universitätsklinikum Erlangen has had a dedicated magnetic resonance imaging (MRI) in radiotherapy (RT) program. To facilitate optimal integration of MRI into MR-guided RT protocols, a 1.5T MAGNETOM Sola RT Pro Edition was installed in our department. An interdisciplinary team consisting of radiation oncologists, medical physicists, and radiation therapy technologists (RTTs) collaboratively manage all MR imaging related to RT treatment planning. This specialized approach enables the implementation of RT-optimized imaging setups, tailored protocols, and streamlined imaging-to-treatment workflows designed explicitly to meet RT requirements. Additionally, comprehensive daily, weekly, and monthly quality assurance measures guarantee MRI studies of consistently high quality, providing a reliable basis for precise treatment planning. Beyond its crucial role in planning, the 1.5T MRI system is also used in collaboration with the Institute of Diagnostic Radiology, allowing convenient diagnostic examinations and follow-up imaging for patients treated in our clinic.

MR-guided treatment planning offers several significant advantages, notably the superior soft tissue contrast provided by MRI compared to computed tomography (CT). This enhanced contrast facilitates more precise and personalized delineation of target volumes and improves sparing of organs at risk (OARs), particularly in prostate cancer RT [1, 2]. Synthetic CT (sCT) has enabled MR-only workflows, eliminating the need for traditional CT scans in RT

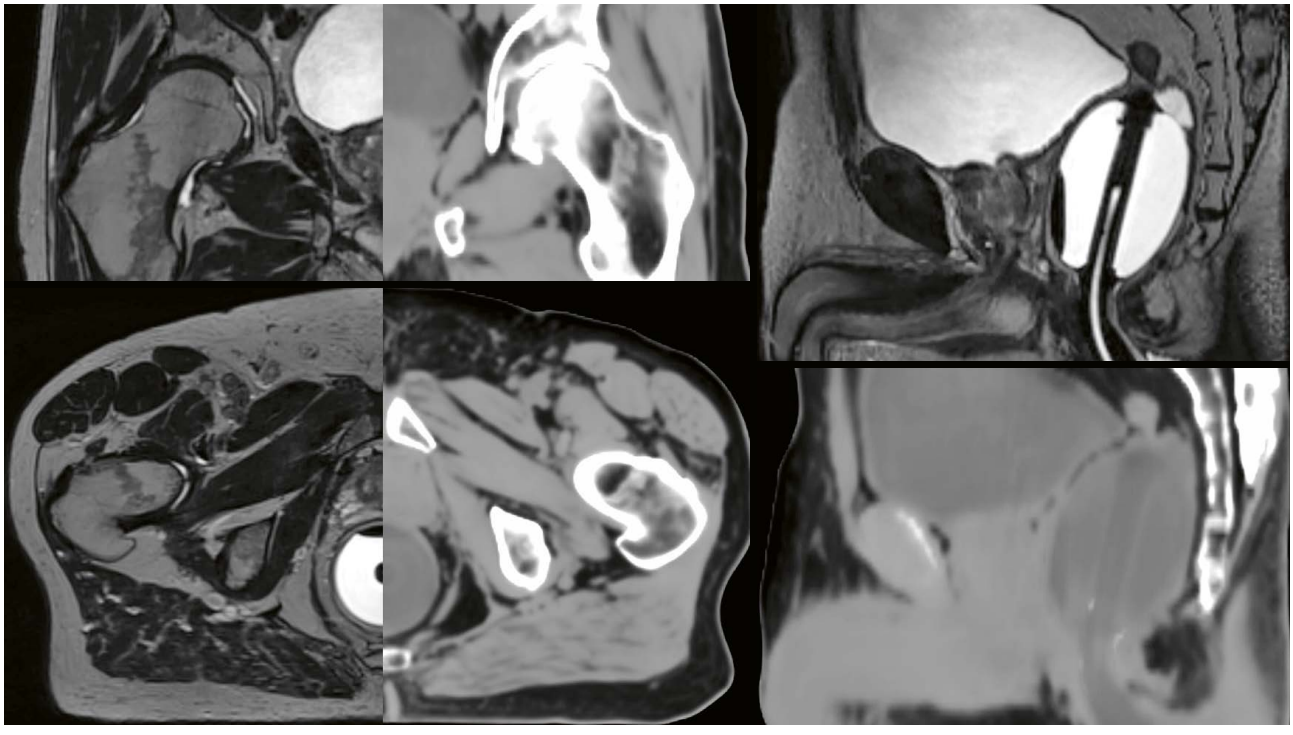

1 MR-only treatment planning using 3D T2w SPACE and synthetic CT. Note the correct reconstruction of water density for the rectal balloon.

planning. These workflows use MRI alone, with AI algorithms generating the necessary sCT images required for dose calculation. Synthetic CT can streamline treatment planning and reduces patient exposure to additional imaging procedures while eliminating registration uncertainties (Fig. 1). One of the key areas where MRI has significantly improved RT precision is in the treatment of prostate cancer. Prostate tumors often have poor visibility on CT imaging due to insufficient soft tissue contrast, complicating accurate delineation of the target area [3]. This limitation is particularly critical in advanced RT techniques such as stereotactic body radiotherapy (SBRT), where high-dose, hypofractionated regimens demand exceptionally precise targeting. Employing a combination of MRI sequences — including 2D T2-weighted turbo spin echo (T2w TSE), diffusion-weighted imaging (DWI), and dynamic contrast-enhanced T1-weighted GRASP sequences — optimizes localization and delineation of intraprostatic tumors. This approach enables targeted dose escalation to the tumor while simultaneously reducing radiation exposure to adjacent OARs, thereby enhancing treatment efficacy and minimizing toxicity [3]. Notably, a large Phase III trial demonstrated that MR-guided high-dose boosting to intraprostatic lesions reduced biochemical treatment failure rates by more than half (hazard ratio 0.45, $p < 0.001$), highlighting the substantial clinical impact of MR-guided RT planning [1].

A major challenge in prostate RT is the reduction of genitourinary side effects. These effects can significantly impact a patient's quality of life. Erectile dysfunction (ED) is one of the most prevalent toxicities following RT for prostate cancer. It results from endovascular injury, direct neuronal damage, and radiation-induced fibrosis [4]. The neurovascular bundle (NVB), penile bulb (PB), corpora cavernosa (CC), and pudendal arteries (PA) are functionally critical structures, and studies have demonstrated clear dose-toxicity relationships for these tissues. For instance, a mean dose exceeding 20 Gy to the penile bulb or 36 Gy to the pudendal arteries has been associated with an increased risk of post-RT ED [5]. Recent studies have demonstrated the feasibility of MR-guided neurovascular-sparing prostate RT, with promising long-term functional outcomes. For example, Spratt et al. reported that 90% of patients remained sexually active five years after vessel-sparing radiotherapy using MR-based contouring [5]. However, widespread adoption of this approach has been limited by challenges such as MRI accessibility, contouring expertise, and time constraints. Conventional CT-based planning is insufficient for accurately identifying and contouring these delicate structures, due to the limited soft tissue contrast. High-resolution 3D TSE T2w SPACE allows for detailed delineation of anatomical structures for RT treatment planning. Moreover, deep learning MR-based auto-contouring solutions hold the potential to improve accessibility to vessel-sparing radiotherapy and focal dose boost.

With the increasing availability of RT-optimized MRI scanners, the optimal integration of MRI into MR-guided RT treatment protocols is becoming an ever-more important topic. In this article, we outline our experience in establishing an MRI workflow for RT treatment planning, leveraging the capabilities of MR in RT technology from Siemens Healthineers. We describe how dedicated protocols, patient positioning strategies, and deep-learning-supported contouring approaches can contribute to improved RT treatment precision. By sharing our insights, we aim to contribute to the ongoing development of MRI-based RT workflows and to highlight the potential of MR-guided treatment planning for enhancing oncological and functional outcomes in prostate cancer patients.

2 Imaging setup in RT treatment position for prostate cancer patients.

MR-imaging setup in treatment position

Patients receive MRI for RT planning in the RT treatment position to ensure optimal alignment with subsequent therapy sessions (Fig. 2). This approach enhances the accuracy of the target and of the OAR delineation, and improves the reproducibility for patient positioning during treatment. To realize the RT treatment position, a flat tabletop (INSIGHT, CQ Medical, Avondale, PA, USA) and MR-compatible positioning aids are employed. A Body 18 coil within an INSIGHT coil holder is positioned above the patient's pelvic region.

Pre-MRI patient preparation

To standardize bladder and rectal conditions, all patients follow a structured preparation protocol prior to the MRI examination and all subsequent RT sessions. This includes:

- Bladder-filling protocol: Patients are instructed to drink a specified volume of water before the scan to ensure consistent bladder filling, as bladder volume can significantly impact prostate position and dosimetric planning.
- Rectal preparation: A rectal balloon (Balloon Rectal Tube, 10 mm/210 mm, Teleflex, Malaysia) is inserted before imaging and filled with 80 mL of water to standardize rectal geometry, reduce prostate motion, and improve treatment reproducibility [6, 7]. This step is particularly important for high-precision techniques such as SBRT, where small changes in prostate position can impact dose delivery and dose distribution [8, 9].
- Pharmacological preparation: To reduce bowel peristalsis and associated image artifacts, patients receive an intravenous injection of butylscopolamin unless contraindicated. Additionally, an intravenous contrast agent is administered to enhance the visualization of the intraprostatic tumor and lymph node metastases on T1w sequences.

MRI acquisition protocol

The primary MRI sequence for treatment planning is a 3D T2w SPACE sequence with Compressed Sensing (CS) acceleration, acquired with an isotropic voxel resolution of 1.0 × 1.0 × 1.0 mm^3 and a large field of view (FOV) to cover the pelvic region. The T2w SPACE forms the main sequence for treatment planning and is used for general OAR and target volume definition. We also use the T2w SPACE for neurovascular delineation, including the neurovascular bundles and internal pudendal arteries (see below).

Due to its superior in-plane resolution and soft tissue contrast, an additional 2D T2w TSE sequence with Deep Resolve Boost is employed for intraprostatic tumor delineation. DWI is performed using ZOOMit reduced-FOV single-shot echo-planar imaging (EPI) to help identify the intraprostatic tumor for focal dose escalation. A dynamic T1w GRASP VIBE sequence with fat suppression is used to assess dynamic contrast enhancement of intraprostatic lesions. Information from the 2D T2w TSE, the DWI, and the dynamic T1w GRASP is combined to delineate the intraprostatic tumor using the multimodal image viewing capabilities

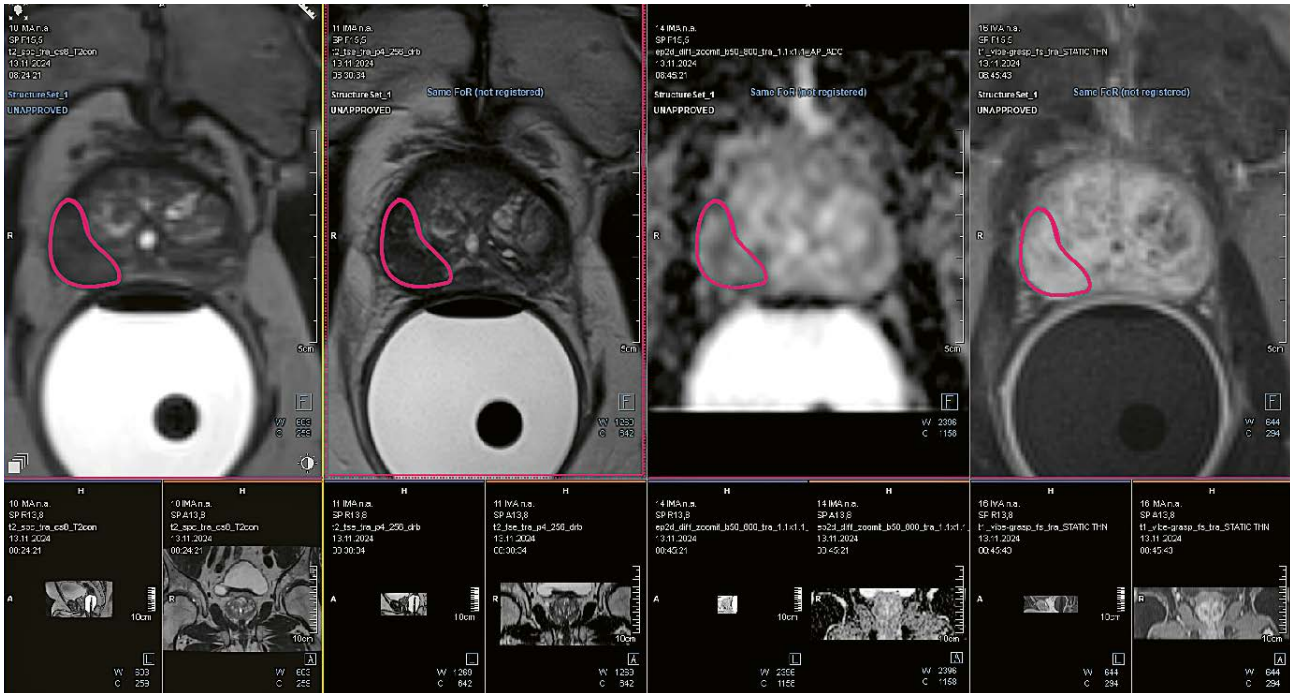

3 Multiparametric contouring of the intraprostatic tumor using 3D T2w SPACE, T2w TSE DRB, ZOOMit EPI DWI, and dynamic T1-GRASP in *syngo*.via RT Image Suite.

of *syngo*.via RT Image Suite (Fig. 3). Finally, in patients with suspected or known lymph node metastases, a high-resolution, large-FOV 3D T1w VIBE with Dixon fat saturation is used. All protocols are transversal to ensure optimal compatibility with RT treatment planning systems.

This combination of RT imaging setup, dedicated patient preparation, and RT-optimized protocols aims to maximize the benefits of MRI in RT, particularly for specialized RT treatment modalities such as SBRT and vessel-sparing prostate radiotherapy.

Name of protocol	sCTp1-Dixon-HR	t2_spc_tra_cs8_T2con	t2_tse_tra_p4_256_drb	t2_tse_sag_p4_256_drb	ep2d_diff_zoomit	t1_vibe-grasp_fs_tra_2.1s_3mm	t1_vibe_dixon_tra_p2_352_lymph_nodes
Acquisition type	3D	3D	2D	2D	2D	3D	3D
Orientation	Transverse	Transverse	Transverse	Sagittal	Transverse	Transverse	Transverse
Field of view (cm^2)	50.0 × 37.5	44.8 × 32.0	20 × 20	20 × 20	8.8 × 24.0	24.0 × 24.0	25.5 × 32.0
Acquisition matrix	320 × 240	448 × 320	256 × 256	256 × 256	42 × 114	224 × 224	280 × 352
Acquisition in-plane resolution (mm^2)	1.56 × 1.56	1.0 × 1.0	0.78 × 0.78	0.78 × 0.78	2.11 × 2.11	1.07 × 1.07	0.91 × 0.91
Slice thickness (mm)	2.0	1.0	3.0	3.0	3.0	3.0	2.0
Slice resolution (%)	66%	100%	/	/	/	79%	100%
Echo time (ms)	2.39 / 4.77	255	97	97	51	1.83	2.39 / 4.77
Repetition time (ms)	6.23	2200	7410	6060	3500	4.09	6.91
Flip angle (°)	15	120 / 90	160 / 90	160 / 90	90	12	10
Averages	5	1	4	4	1	1	3
Gradient nonlinearity distortion correction	3D	3D	3D	3D	3D	3D	3D
Shimming of B0 inhomogeneities	Patient-specific	Patient-specific	Patient-specific	Patient-specific	Patient-specific	Patient-specific	Patient-specific
Readout bandwidth (Hz)	1120	558	199	201	1828	500	470
Acceleration factor	4 (CAIPIRINHA)	8 (CS)	4 (GRAPPA)	4 (GRAPPA)	None	CS	2 (CAIPIRINHA)
Deep Resolve Boost	No	No	Yes	Yes	No	No	No
Acquisition time (min)	04:12	05:27	05:13	04:16	04:07	04:16	07:35
Contrast agent	None	None	None	None	None	Gadovist	Gadovist
RT planning indication	Synthetic CT	Main sequence for MR-only contouring, OAR delineation	Intraprostatic tumor delineation	Optional: Urogenital diaphragm (lower target volume boundary)	Intraprostatic tumor delineation	Intraprostatic tumor delineation	Optional: Nodal metastases delineation

Table 1: Sequence protocol parameters for prostate cancer treatment planning. CS: Compressed Sensing

Optimizing MR imaging for RT planning: Lessons learned and practical improvements

Over the course of implementing MRI for RT treatment planning in prostate cancer, we identified several modifications to improve image quality and geometric accuracy. One significant adjustment was the optimization of the medium used for filling the rectal balloon. Initially, air was used as a filling material, following the conventional CT-based workflow, but we observed that this led to increased distortions, particularly in DWI. To mitigate this, we transitioned to filling the rectal balloon with water (Fig. 4). This change significantly improved signal homogeneity and reduced susceptibility artifacts, leading to more reliable diffusion images and better visualization of intraprostatic diffusion restrictions.

Improved single-shot EPI distortion correction was subsequently introduced via an in-house postprocessing

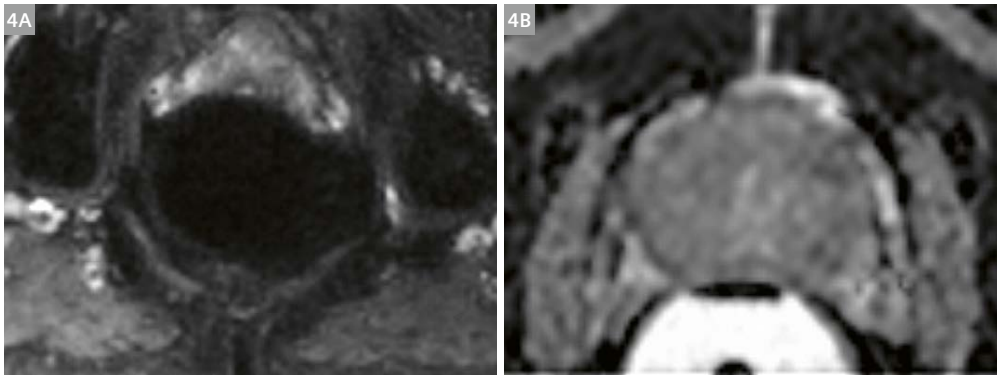

4 Air vs. water in the rectal balloon.
(4A) Air-filled rectal balloon;
(4B) water-filled rectal balloon.

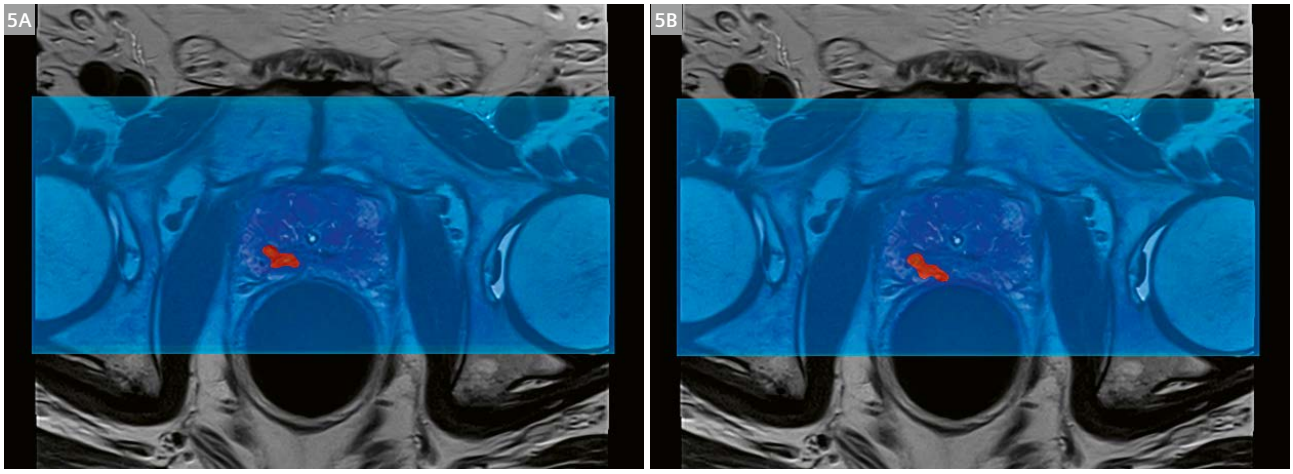

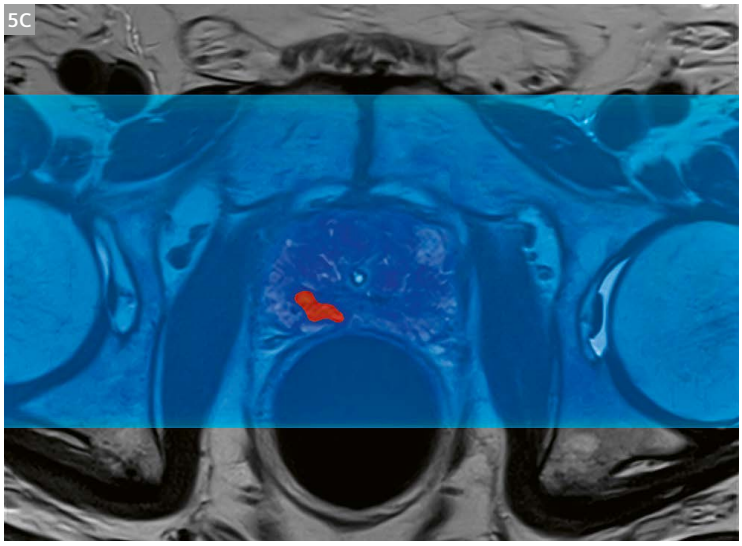

5 In-house distortion correction of single-shot EPI using a reversed gradient polarity method (PyHySCO). The figure shows a 2D T2w TSE sequence with the ZOOMit EPI (b800 TraceW) overlaid with a blue-to-orange colormap in a patient with a small intraprostatic tumor.
(5A) ZOOMit EPI acquired in anterior-posterior (AP) phase-encoding direction.
(5B) ZOOMit EPI acquired in posterior-anterior (PA) phase-encoding direction.
(5C) Corrected EPI.
Note: The corrected EPI shows the best correspondence to the T2w signal hypointensities.

solution. Geometric distortions in EPI along the phase-encoding direction can complicate the precise localization of intraprostatic tumors for target volume definition. To mitigate these issues, we implemented a reversed gradient polarity correction method using the GPU-enabled susceptibility artifact distortion correction python library PyHySCO [10]. An in-house application was built that loads the two EPI series with opposite phase-encoding direction in DICOM format and outputs corrected series (Fig. 5).

Another important observation during the implementation of our MR-based planning protocol was the sequential order between fiducial marker implantation and planning MRI acquisition. It was observed that performing the MRI after marker placement could compromise intraprostatic tumor delineation. These early post-interventional scans often revealed localized hemorrhage around the fiducials, as well as artifacts on DWI. Such effects may mimic or obscure intraprostatic lesions, thus hampering accurate tumor delineation. To address this, the MR-guided prostate treatment planning workflow was changed to perform any fiducial marker implantation after planning MRI.

Introducing artificial intelligence for MRI-guided radiotherapy planning

The integration of artificial intelligence (AI) into MRI-guided RT planning is transforming the way treatment is designed and optimized. At the Department of Radiation Oncology at Universitätsklinikum Erlangen, we have implemented deep learning approaches to enhance image analysis and support EBRT and brachytherapy planning [11]. We recently introduced MR-based autocontouring for OARs[1] in male pelvis patients via the *syngo*.via VC10A CUT version (Siemens Healthineers, Forchheim, Germany). In prostate cancer patients, we observed a significantly reduced manual workload, with MR-based OAR autocontouring being particularly valuable for MR-only workflows (Fig. 6).

An interesting novel application for AI in radiotherapy is the automated contouring of delicate neurovascular

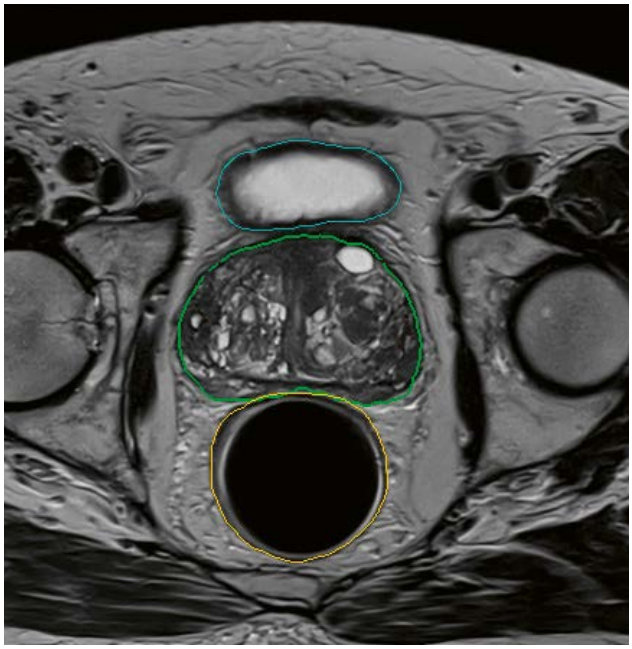

6 MR-based OAR autocontouring for the male pelvis using *syngo*.via VC10A CUT[1] in clinical treatment planning.

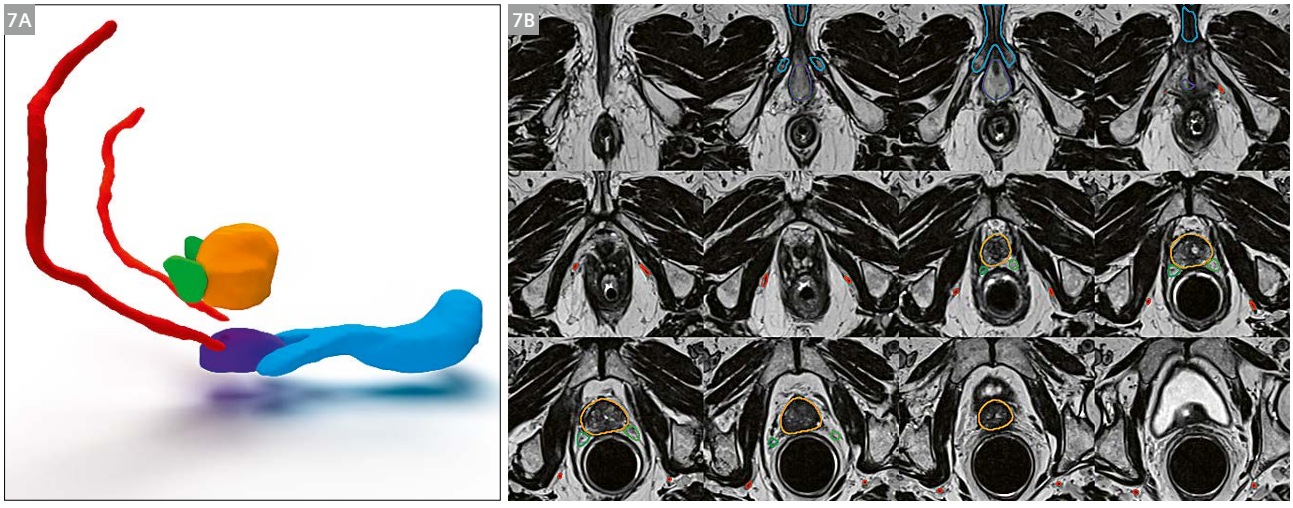

7 Deep learning neurovascular OAR autocontouring on high-resolution T2w SPACE for a prostate cancer test case. **(7A)** 3D rendering of autosegmented neurovascular OARs. **(7B)** Transverse cross-sections. The nnU-net model was trained in-house on 40 manually delineated T2w SPACE datasets to autosegment the internal pudendal artery (red), the neurovascular bundle (green), the corpora cavernosa (blue), the prostate (orange), the penile bulb (violet), and the seminal vesicles (green).

[1] *Work in progress. The application is currently under development and is not for sale in the U.S. and in other countries. Its future availability cannot be ensured.*

OARs that are visible thanks to the detailed image information provided by MRI. Traditional manual segmentation of high-resolution image datasets is time-consuming and prone to interobserver variability. Deep learning architectures, such as 3D U-Net [12], can assist in automatically delineating the OARs and target volumes. We developed and validated an in-house model for automatic segmentation of neurovascular OARs in high-resolution 3D T2w SPACE datasets based on the nnU-net pipeline [13], confirming its robustness and accuracy (Fig. 7). The model can autosegment neurovascular OARs including the internal pudendal arteries, penile bulb, and neurovascular bundles with high accuracy, and is currently being introduced into our clinical treatment workflow. Similar solutions will be interesting to integrate into commercial solutions to facilitate vessel-sparing radiotherapy in prostate cancer.

As well as supporting OAR delineation, AI could also play an important role in identifying dominant intraprostatic lesions (DILs) for focal dose escalation. Multiparametric MRI can enable personalized treatment planning for precisely targeting high-risk tumor regions with selective dose escalation. Techniques such as the simultaneous integrated boost (SIB) enable focused intensification of the radiation dose directly to these critical areas, improving biochemical cure rates in prostate cancer [1]. However, radiation oncologists frequently lack expert knowledge on interpreting multiparametric prostate images. Deep learning applications might serve as a robust decision-support tool throughout this process. We are currently evaluating the *syngo*.via Prostate AI Frontier[1] application for automatic segmentation of intraprostatic lesions for RT treatment planning. The Prostate AI Frontier application can detect and autosegment intraprostatic tumors by combining T2w, DWI, and contrast-enhanced T1w input series (Fig. 8). Clinical integration of similar autosegmentation solutions could increase precision and standardization in prostate cancer RT, while reducing manual planning time to facilitate single-day treatment planning and adaptive MR-guided protocols.

Conclusion

Integrating MRI into RT planning has significantly advanced prostate cancer treatment. Superior soft tissue contrast enables precise delineation of the prostate, accurate identification of dominant intraprostatic lesions, and clear differentiation of surrounding organs, resulting in highly personalized treatment strategies. At our center, we developed a combined MRI planning and RT treatment planning workflow, which includes standardized patient preparation, dedicated imaging in the treatment position, synthetic CT, and deep learning postprocessing. While implementing the comprehensive MR-guided planning protocol, we learned to optimize multiple aspects. This included changing the medium used for filling the rectal balloon, avoiding fiducial implantation before MRI, and implementing an in-house solution for reversed gradient polarity correction of single-shot EPI sequences. The recent

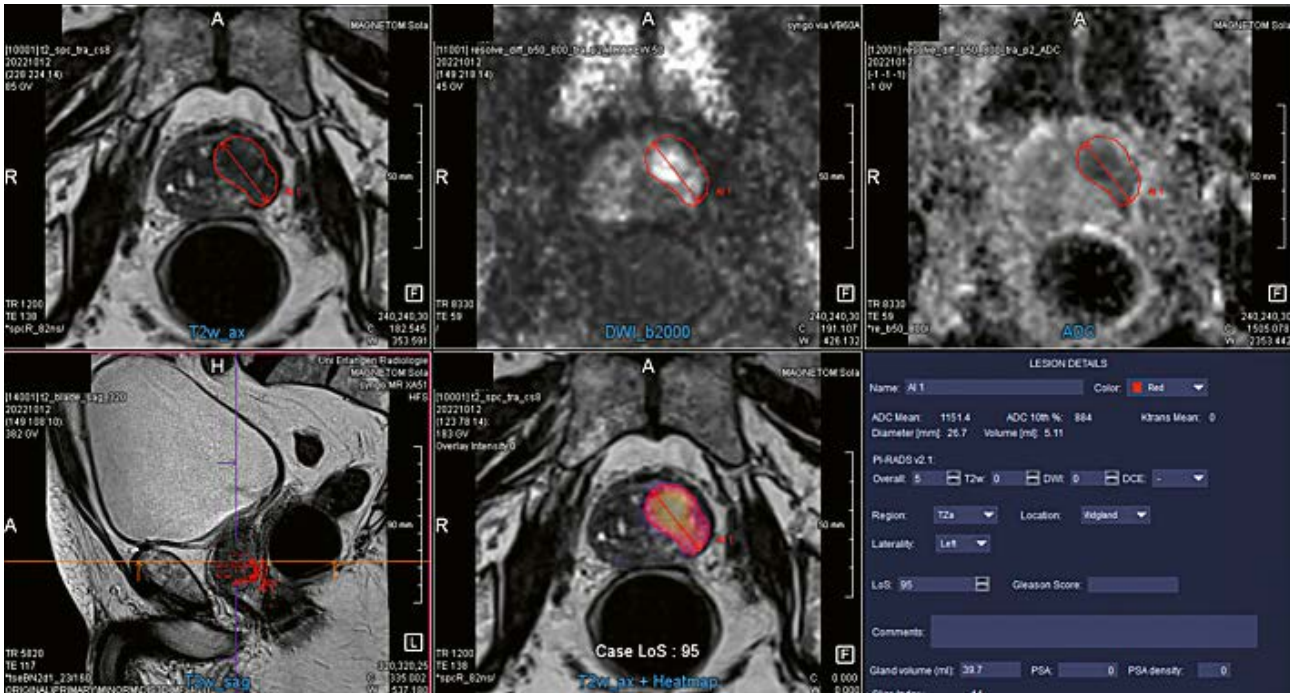

8 The *syngo*.via Prostate AI Frontier[1] application can autodetect and autosegment intraprostatic tumors on multiparametric MRI input data. AI applications could improve accessibility to MR-guided focal dose escalation in prostate cancer.

incorporation of MR-based pelvic OAR autocontouring has considerably reduced clinical workload and is particularly promising for MR-only workflows. Combining RT-optimized MRI with AI postprocessing applications could be crucial in facilitating advanced MR-guided treatment concepts such as focal dose boost and neurovascular sparing.

References

1 Kerkmeijer LGW, Groen VH, Pos FJ, Haustermans K, Monninkhof EM, Smeenk RJ, et al. Focal Boost to the Intraprostatic Tumor in External Beam Radiotherapy for Patients With Localized Prostate Cancer: Results From the FLAME Randomized Phase III Trial. J Clin Oncol. 2021;39(7):787-796.

2 Spratt DE, Lee JY, Dess RT, Narayana V, Evans C, Liss A, et al. Vessel-sparing Radiotherapy for Localized Prostate Cancer to Preserve Erectile Function: A Single-arm Phase 2 Trial. Eur Urol. 2017;72(4):617-624.

3 Moore-Palhares D, Ho L, Lu L, Chugh B, Vesprini D, Karam I, et al. Clinical implementation of magnetic resonance imaging simulation for radiation oncology planning: 5 year experience. Radiat Oncol. 2023;18(1):27.

4 Zelefsky MJ, Eid JF. Elucidating the etiology of erectile dysfunction after definitive therapy for prostatic cancer. Int J Radiat Oncol Biol Phys. 1998;40(1):129-33.

5 Le Guevelou J, Sargos P, Ferretti L, Supiot S, Pasquier D, Crehange G, et al. Sexual Structure Sparing for Prostate Cancer Radiotherapy: A Systematic Review. Eur Urol Oncol. 2024;7(3):332-343.

6 Böckelmann F, Hammon M, Lettmaier S, Fietkau R, Bert C, Putz F. Penile bulb sparing in prostate cancer radiotherapy: Dose analysis of an in-house MRI system to improve contouring. Strahlenther Onkol. 2019;195(2):153-163.

7 Böckelmann F, Putz F, Kallis K, Lettmaier S, Fietkau R, Bert C. Adaptive radiotherapy and the dosimetric impact of inter- and intrafractional motion on the planning target volume for prostate cancer patients. Strahlenther Onkol. 2020;196(7):647-656.

8 Jaccard M, Lamanna G, Dubouloz A, Rouzaud M, Miralbell R, Zilli T. Dose optimization and endorectal balloon for internal pudendal arteries sparing in prostate SBRT. Phys Med. 2019;61:28-32.

9 Hamstra DA, Mariados N, Sylvester J, Shah D, Gross E, Hudes R, et al. Sexual quality of life following prostate intensity modulated radiation therapy (IMRT) with a rectal/prostate spacer: Secondary analysis of a phase 3 trial. Pract Radiat Oncol. 2018;8(1):e7-e15.

10 Julian A, Ruthotto L. PyHySCO: GPU-enabled susceptibility artifact distortion correction in seconds. Front Neurosci. 2024;18:1406821.

11 Grigo J, Karius A, Hanspach J, Mücke L, Laun FB, Huang Y, et al. Toward a deep learning-based magnetic resonance imaging only workflow for postimplant dosimetry in I-125 seed brachytherapy for prostate cancer. Brachytherapy. 2024;23(1):96-105.

12 Ronneberger O, Fischer P, Brox T. U-Net: Convolutional networks for Biomedical Image Segmentation. In: Navab N, Hornegger J, Wells W, Frangi A, editors. Medical Image Computing and Computer-Assisted Intervention – MICCAI 2015. MICCAI 2015; 2015, Oct 5-9; Munich, Germany. Cham, Switzerland: Springer; 2015. p. 234-241.

13 Isensee F, Jaeger PF, Kohl SAA, Petersen J, Maier-Hein KH. nnU-Net: a self-configuring method for deep learning-based biomedical image segmentation. Nat Methods. 2021;18(2):203-211.

Philipp Schubert, M.D.

Florian Putz, M.D.

Contact

Florian Putz, M.D.
Senior Physician and Senior Researcher
Department of Radiation Oncology
Universitätsklinikum Erlangen
Universitätsstraße 27
91054 Erlangen
Germany
Tel.: +49 9131 8534080
florian.putz@uk-erlangen.de

How Deep Learning Reconstruction Impacts Radiomics Features in Abdominal MRI

Jingyu Zhong, M.D.[1,2]; Yang Song, Ph.D.[3]; Minda Lu[4]; Dominik Nickel, Ph.D.[5]

[1] Department of Imaging, Tongren Hospital, Shanghai Jiao Tong University School of Medicine, Shanghai, China
[2] Shanghai Key Laboratory of Flexible Medical Robotics, Tongren Hospital, Institute of Medical Robotics, Shanghai Jiao Tong University, Shanghai, China
[3] MR Research Collaboration Team, Siemens Healthineers, Shanghai, China
[4] MR Application, Siemens Healthineers, Shanghai, China
[5] Research & Clinical Translation, Magnetic Resonance, Siemens Healthineers, Erlangen, Germany

Why did we conduct the research?

Magnetic resonance imaging (MRI), especially T2-weighted imaging with fat suppression (T2 FS) or without (T2WI), plays a pivotal role in abdominal imaging [1]. However, conventional MRI protocols have the inherent limitation of prolonged acquisition time, which may lead to motion artifacts [2, 3]. One solution is the half-Fourier acquisition single-shot turbo spin echo (HASTE) technique, which shortens the acquisition time. However, this comes at the cost of reduced signal-to-noise ratio, reduced image contrast, and reduced sharpness [4, 5]. To address this drawback, HASTE with deep learning reconstruction (DLR)[1] was introduced to accelerate the acquisition and shorten echo trains for improved T2 weighting [6, 7].

Radiomics, which extracts quantitative features from medical images for clinical decision-making, has gained in popularity [8, 9]. Yet it faces challenges caused by its sensitivity to acquisition parameters, reconstruction algorithms, and post-processing techniques [10–12]. DLR enables acceptable image quality and faster acquisitions, and it is therefore expected to be widely adopted in the future. However, the influence of DLR and the combined effects of DLR and accelerated acquisition on radiomics features have not yet been investigated. It is necessary to evaluate in advance the potential changes that the new technique could cause to radiomics features.

Our study provides a basis for future research into establishing radiomics models using images from an accelerated HASTE sequence with DLR. We investigated the impact of DLR and accelerated acquisitions on the robustness of radiomics features in abdominal scans acquired using a HASTE sequence.

How did we conduct the research?

We performed abdominal MRI scans on volunteers with no history of abdominal surgery or malignancies (Fig. 1). We used a 3T MRI system (MAGNETOM Vida, Siemens Healthineers, Erlangen, Germany) with an 18-channel body matrix coil and the integrated spine array. We ran the research HASTE sequence[1] three times with different orientations and contrasts: axial T2W, axial T2 FS, and coronal T2W. Each protocol was acquired and reconstructed four times: (1) clinical reference acquisition with standard reconstruction (REF + STD), (2) clinical reference acquisition with deep learning reconstruction (REF + DLR), (3) accelerated acquisition with standard reconstruction (ACC + STD), and (4) accelerated acquisition with deep learning reconstruction (ACC + DLR) (Table 1). The clinical reference acquisition with standard reconstruction (REF+STD) served as the reference standard for the evaluation. The impact of accelerated acquisition and DLR were then assessed by quantifying how these two factors changed radiomics features.

To extract the radiomics features, the regions of interest (ROIs) were drawn for 10 anatomical sites with rigid registrations. The ROIs, which had a fixed diameter of 15 pixels (approximately 15 mm), were placed on 10 anatomical sites: the left and right lobes of the liver, the body of the pancreas, the center of the spleen, the left and right kidneys, the left and right psoas major muscles, the first lumbar vertebra, and the subcutaneous fat tissue. The ROIs were selected to cover as much as possible of the parenchyma of the organ or tissue, avoiding contact with the vessels, ducts, and lesions. Ninety-three radiomics features, including histogram-based and texture features from the original image, were extracted using PyRadiomics after z-score normalization. All these features were extracted in line with the Image Biomarker Standardization Initiative (IBSI).

[1] *Work in progress. The application is currently under development and is not for sale in the U.S. and in other countries. Its future availability cannot be ensured.*

Image acquisition

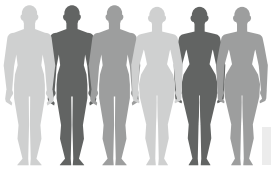

Screen

18 participants who volunteered to undergo abdominal MRI scan during January 2024

Exclusion

Claustrophobia (n = 1)

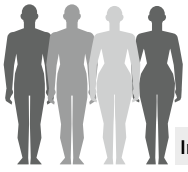

Inclusion

17 participants for evaluation

3 sequences × 4 scans

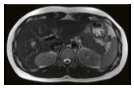

Axial T2WI

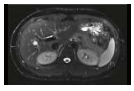

Axial T2FS

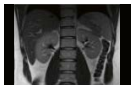

Coronal T2WI

No	Accelerated acquisition	Deep learning reconstruction	Breath holds
1	No	No	11
2	No	Yes	11
3	Yes	No	8
4	Yes	Yes	8

Radiomics analysis

Manual segmentation

10 ROIs with a diameter of 15 mm

Copy with a rigid registration

- left and right lobe of liver
- body of pancreas
- center of spleen
- left and right kidney
- left and right psoas major
- the first lumbar vertebra
- subcutaneous fat tissue

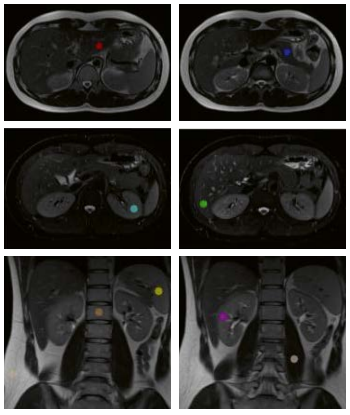

Feature extraction

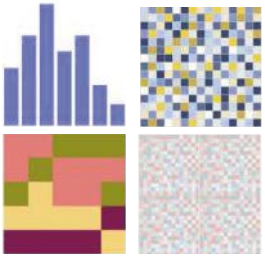

Statistical analysis

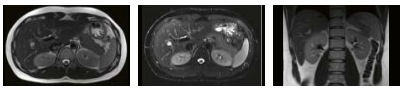

Axial T2WI Axial T2FS Coronal T2WI

Reproducibility

Reference standard
REF acquisition + Std. reconstruction

Versus

REF acquisition + DL reconstruction
Acc. acquisition + Std. reconstruction
Acc. acquisition + DL reconstruction

ICC, CCC

$$ICC = \frac{\sigma_a^2}{\sigma_a^2 + \sigma_c^2}$$

$$\rho_c = \frac{2\rho\sigma_x\sigma_y}{\sigma_a^2 + \rho_y^2 + (\mu_x - \mu_y)^2}$$

Variability

10 ROIs

REF acquisition + Std. reconstruction
REF acquisition + DL reconstruction
Acc. acquisition + Std. reconstruction
Acc. acquisition + DL reconstruction

CV, QCD

$$CV = \frac{\sigma}{\mu}$$

$$\%QCD = \frac{Q3 - Q1}{Q3 + Q1} \times 100$$

1 Study workflow
The study had three steps: image acquisition, radiomics analysis, and statistical analysis.
REF = original; Std. = standard; Acc. = accelerated; DL = deep learning; ICC = intraclass correlation coefficient; CCC = concordance correlation coefficient; CV = coefficient of variation; QCD = quartile coefficient of dispersion

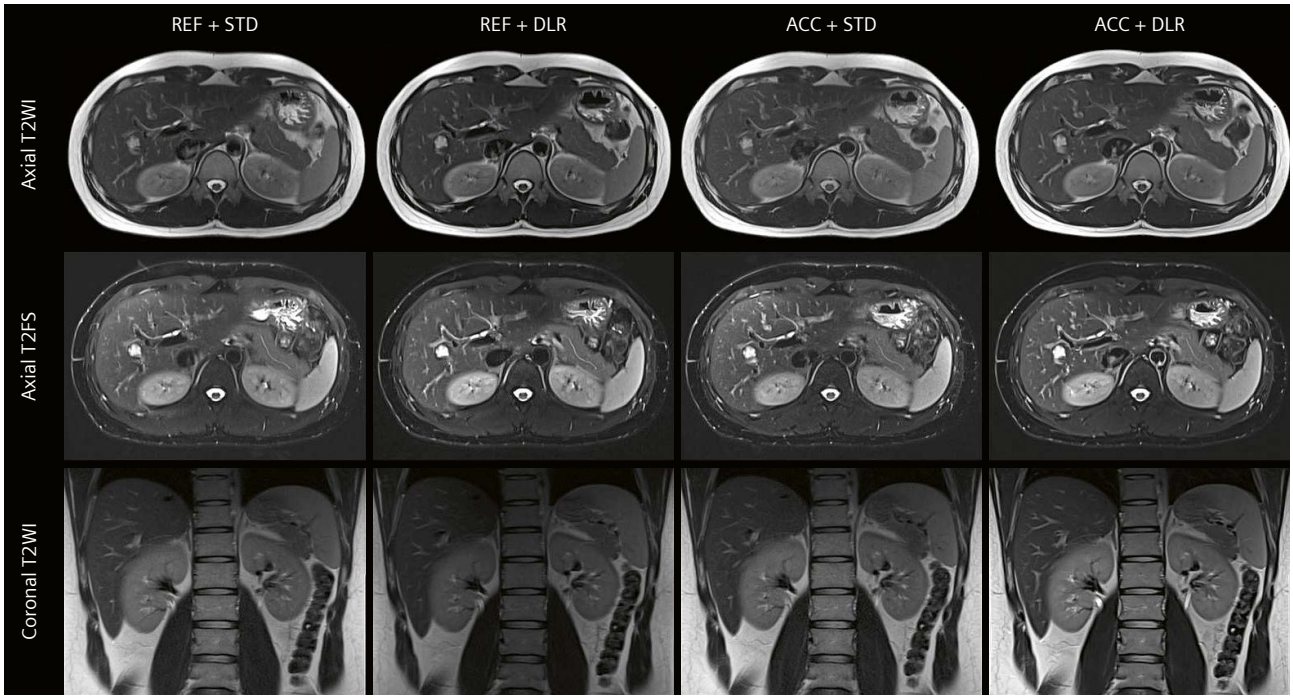

2 The representative case was four scans of three sequences from a 29-year-old male participant with a height of 1.86 m, a weight of 80 kg, and a body mass index of 23.1 kg/m². He had no history of abdominal surgery or cancer, and no current acute abdominal injury or disease. The conventional abdominal MRI scan identified a hepatic cystic lesion, but it was situated outside the region of interest.

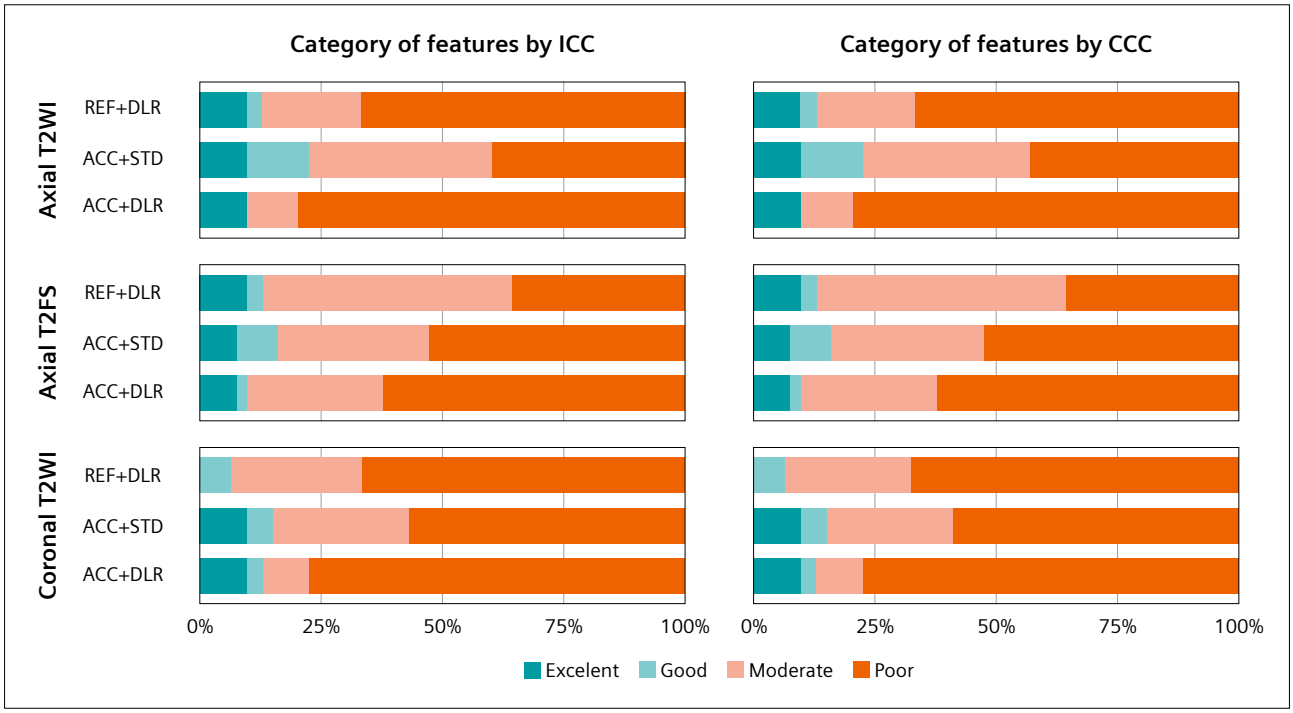

3 Reproducibility of radiomics features according to intraclass correlation coefficient (ICC) and concordance correlation coefficient (CCC) values.

The reproducibility was evaluated with the intraclass correlation coefficient (ICC) and the concordance correlation coefficient (CCC), using REF+STD as the reference. The variability between four scans was assessed by coefficient of variation (CV) and quartile coefficient of dispersion (QCD).

How might deep learning reconstruction impact radiomics features in abdominal MRI?

One author of this study (JZ) also participated in the study and served as a representative case. The REF+STD is used as the reference standard for the image quality and showed good signal-to-noise ratio, reduced image contrast, and reduced sharpness for assessment. The hepatic cystic lesion was clearly visible on the REF+STD images. The REF+DLR provided even better contrast and sharpness for the lesion characterization. However, the ACC+STD did not show satisfactory image quality due to the increased image noise, blurry edges of the lesion, and suboptimal contrast. The image quality of ACC+DLR was greatly improved thanks to DLR, even for the accelerated acquisition protocol. Therefore, we suspected that both the accelerated acquisition protocol and DLR could change the radiomics features. However, for both, the changed radiomics features might be recovered.

Unfortunately, the radiomics features were not recovered. Compared to the REF+STD images, the REF+DLR, ACC+STD, and ACC+DLR images showed substantial change in the radiomics features. Our study found that the median (first and third quartile) of overall ICC and CCC values were 0.451 (0.305, 0.583) and 0.450 (0.304, 0.582). The overall percentage of radiomics features with ICC > 0.90 and CCC > 0.90 was 8.1% and 8.1%, which was considered acceptable (Fig. 3). The median (first and third quartile) of overall CV and QCD values was 9.4% (4.9%, 17.2%) and 4.9% (2.5%, 9.7%). The overall percentage of radiomics features with CV < 10% and QCD < 10% was 51.9% and 75.0%, which was considered acceptable (Fig. 4).

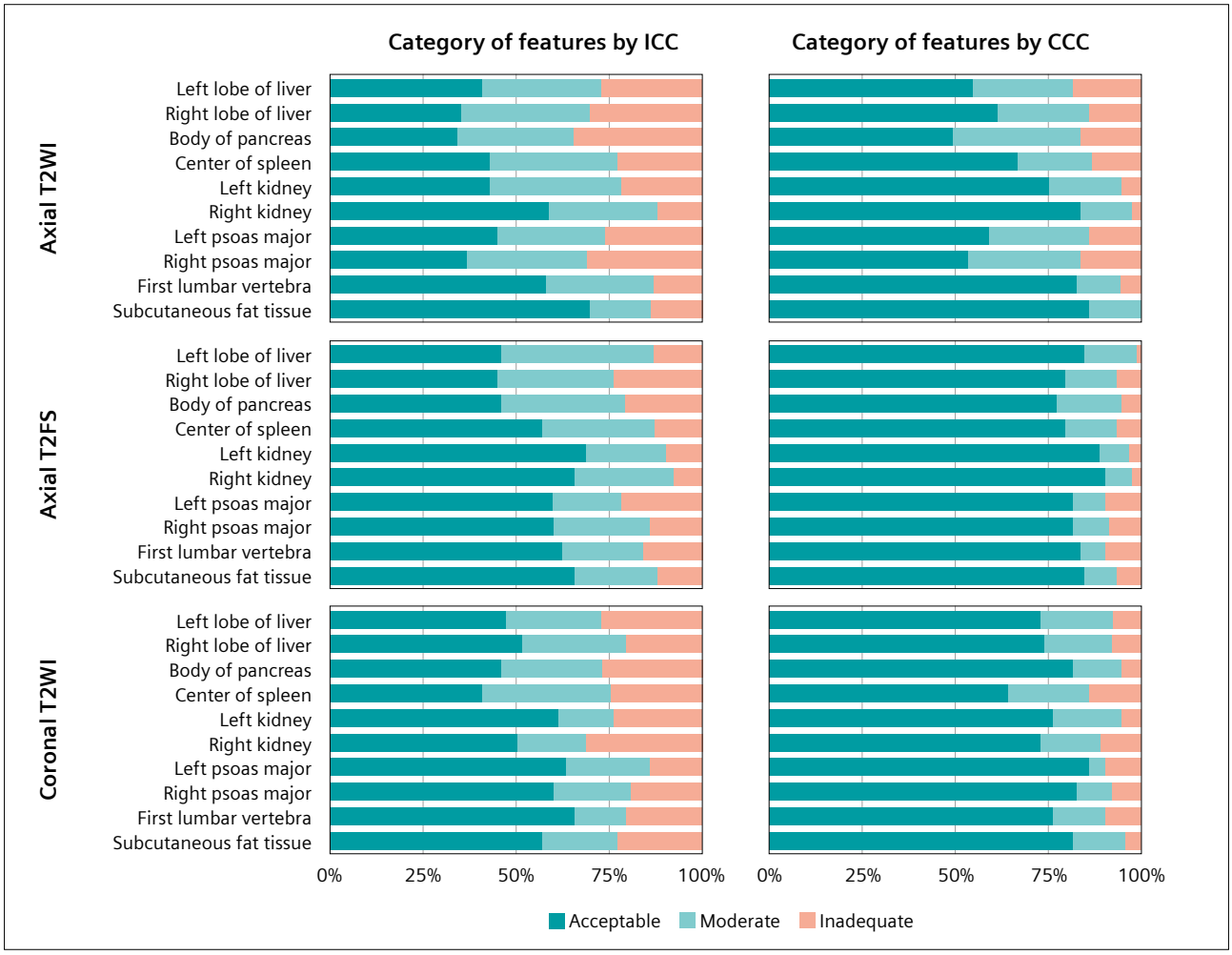

4 Variability of radiomics features according to coefficient of variation (CV) and quartile coefficient of dispersion (QCD) values.

Our study showed that the radiomics features were significantly influenced by the accelerated acquisition and DLR. The reproducibility of radiomics features was low between the standard and accelerated acquisitions, and between the standard and DLR acquisitions. Although the REF+STD and ACC+DLR images remained unchanged to the naked eye, the in-depth radiomics features did change. The brittle changes might be too small to be detected by the naked eye.

What should we do before introducing deep learning reconstruction into radiomics analysis?

We expected that DLR would allow faster acquisition with higher image quality and comparable diagnostic performance. The DLR algorithm used in our study reconstructed images using a variational network to generate images with higher signal-to-noise ratio and thereby allow faster acquisition with higher parallel imaging acceleration. The algorithm enhanced the image contrast and reduced the image noise for diagnostic purposes. However, it was not designed to keep the values of the radiomics features stable. We hypothesized that the increased image noise caused by accelerated acquisition and the reduced image noise from DLR might offset each other and make the radiomics features more reproducible. However, the combination of these two factors did not result in stable values of the radiomics features. Although the subjective image-quality and diagnostic assessments favored the accelerated acquisition with DLR, the radiomics analysis for different acquisition protocols and reconstruction algorithms was not interchangeable.

To reduce the impact on the generalizability of radiomics analysis, we need to try something different to harmonize DLR and non-DLR images. First, standardize protocols: Radiomics analysis relies on consistent image acquisition to ensure feature reproducibility. Our study revealed that protocol variations, even minor differences in repetition time, echo time, and parallel imaging factors, can cause severe variations in texture features like the gray-level co-occurrence matrix (GLCM) contrast. To mitigate this, we suggest a standardization framework in at least a multi-scanner or multi-center study. This approach can harmonize data at the very beginning without concerns about changing the in-depth information due to the later pre-processing steps. However, it cannot be used here, because the DLR itself is a game-changer in MRI scanning.

Second, choose appropriate image pre-processing before performing radiomics analysis: It is hard to use a standardized protocol across multiple centers. Even with standardized protocols, image pre-processing is critical to address residual variability. Our workflow only used z-score normalization, but other workflows may integrate bias field correction, anisotropic diffusion filtering, and so on. These steps reduce intensity inhomogeneity and noise, and they may change the information in the image. It is necessary to assess their influence as well. By treating pre-processing as an integral step rather than an afterthought, radiomics models gain resilience to acquisition-specific noise patterns, ensuring features reflect true biological heterogeneity rather than technical variability.

Third, use only radiomics features with higher reproducibility and less variability: Feature selection bridges raw data and actionable biomarkers. Ideally, we would only use features that have acceptable reproducibility and variability to establish the radiomics models. We did find that some features are robust against many factors. Further, if these features are biologically relevant to lesion properties, corresponding radiomics models will achieve greater generalizability across diverse clinical settings. However, the question is whether these features are informative enough to establish a radiomics model. We need to balance the robustness of features and the diagnostic performance of models. Prioritizing stability and biological relevance will make radiomics models more generalizable across diverse clinical settings.

Conclusion

Deep learning reconstruction is a double-edged sword for radiomics. While it addresses critical bottlenecks in MRI workflows, its feature perturbations demand rigorous validation. By adhering to standardized protocols and investing in robustness testing, the radiology community can harness the full potential of DLR without compromising the diagnostic promise of radiomics.

References

1 Klessen C, Asbach P, Kroencke TJ, Fischer T, Warmuth C, Stemmer A, et al Magnetic resonance imaging of the upper abdomen using a free-breathing T2-weighted turbo spin echo sequence with navigator triggered prospective acquisition correction. J Magn Reson Imaging. 2005;21(5):576–82.
2 Nanko S, Oshima H, Watanabe T, Sasaki S, Hara M, Shibamoto Y. Usefulness of the application of the BLADE technique to reduce motion artifacts on navigation-triggered prospective acquisition correction (PACE) T2-weighted MRI (T2WI) of the liver. J Magn Reson Imaging. 2009;30(2):321–6.
3 Nakayama Y, Yamashita Y, Matsuno Y, Tang Y, Namimoto T, Kadota M, et al. Fast breath-hold T2-weighted MRI of the kidney by means of half-Fourier single-shot turbo spin echo: comparison with high resolution turbo spin echo sequence. J Comput Assist Tomogr. 2001;25(1):55–60.
4 Lee MG, Jeong YK, Kim JC, Kang EM, Kim PN, Auh YH, et al. Fast T2-weighted liver MR imaging: comparison among breath-hold turbo-spin-echo, HASTE, and inversion recovery (IR) HASTE sequences. Abdom Imaging. 2000;25(1):93–9.
5 Schlemper J, Caballero J, Hajnal JV, Price AN, Rueckert D. A deep cascade of convolutional neural networks for dynamic MR image reconstruction. IEEE Trans Med Imaging. 2018;37(2):491–503.
6 Hammernik K, Klatzer T, Kobler E, Recht MP, Sodickson DK, Pock T, et al. Learning a variational network for reconstruction of accelerated MRI data. Magn Reson Med. 2018;79(6):3055–3071.
7 Herrmann J, Gassenmaier S, Nickel D, Arberet S, Afat S, Lingg A, et al. Diagnostic confidence and feasibility of a deep learning accelerated HASTE sequence of the abdomen in a single breath-hold. Invest Radiol. 2021;56(5):313–319.
8 Volpe S, Mastroleo F, Krengli M, Jereczek-Fossa BA. Quo vadis radiomics? Bibliometric analysis of 10-year Radiomics journey. Eur Radiol. 2023;33(10):6736–6745.
9 Kocak B, Baessler B, Cuocolo R, Mercaldo N, Pinto Dos Santos D. Trends and statistics of artificial intelligence and radiomics research in radiology, nuclear medicine, and medical imaging: bibliometric analysis. Eur Radiol. 2023;33(11):7542–7555.
10 Kocak B, Baessler B, Bakas S, Cuocolo R, Fedorov A, Maier-Hein L, et al. CheckList for EvaluAtion of Radiomics research (CLEAR): a step-by-step reporting guideline for authors and reviewers endorsed by ESR and EuSoMII. Insights Imaging. 2023;14(1):75.
11 Kocak B, Akinci D'Antonoli T, Mercaldo N Alberich-Bayarri A, Baessler B, Ambrosini I, et al. METhodological RadiomICs Score (METRICS): a quality scoring tool for radiomics research endorsed by EuSoMII. Insights Imaging. 2024;15(1):8.
12 Akinci D'Antonoli T, Cuocolo R, Baessler B, Pinto Dos Santos D. Towards reproducible radiomics research: introduction of a database for radiomics studies. Eur Radiol. 2024;34(1):436-443.

Contact

Jingyu Zhong, M.D., Ph.D.
Department of Imaging
Tongren Hospital
Shanghai Jiao Tong University
School of Medicine
No. 1111 Xianxia Road
Shanghai 200336
China
ZJY4623@shtrhospital.com

Imaging the Early Fetal Brain Using Deep Resolve in 3T MRI

Andrea Righini, M.D.[1]; Giana Izzo, M.D.[1]; Filippo Arrigoni, M.D.[1]; Chiara Doneda, M.D.[1]; Cecilia Parazzini, M.D.[1]; Domenico Zacà, Ph.D.[2]; Ilaria Balba, M.Sc.[2]

[1] Pediatric Radiology and Neuroradiology Department, Children's Hospital V. Buzzi, Milan, Italy
[2] Siemens Healthineers, Milan, Italy

Introduction

Fetal magnetic resonance imaging (MRI)[1] is contributing to progress on neurodevelopment within the clinical neurosciences [1]. While state-of-the-art ultrasound scanning produces images with excellent spatial resolution of the fetal brain even below a gestational age (GA) of 24 weeks, MRI based on T2-weighted single-shot sequences (e.g., HASTE) provides optimal contrast resolution of the various components of the brain mantle. However, despite making such progress, MRI has been affected in the last two decades by limited in-plane resolution (around 1 mm^2) [2]. This limitation impacts the diagnostic confidence of neuroradiologists when investigating small fetal brain structures, especially in countries where diagnostic efforts mostly focus on GAs in the range of 19 to 24 weeks due to legal constraints on pregnancy terminations. For these reasons, increasing spatial resolution is highly desirable.

Technique

In recent years, artificial-intelligence (AI) applications in MRI have made it possible to accelerate acquisitions and increase resolution using various image reconstruction and denoising algorithms [3].

In our department, we have started using Deep Resolve, an AI-driven image reconstruction technology, on our 3-Tesla MAGNETOM Vida scanner. Deep Resolve increases spatial resolution, and our aim is to acquire more-detailed T2-weighted HASTE images, which are the pillar of fetal neuro MRI.

	T2 HASTE	T2 HASTE with Deep Resolve
Acquisition time	20 s	13 s
TR/TE	2200 ms / 104 ms	1150 ms / 76 ms
Concatenations	1	1
FOV	260 mm	220 mm
Phase FOV	100%	100%
Base resolution	320	256
Phase resolution	65%	100%
In-plane res. acquisition	(1.25 × 0.81) mm^2	(0.86 × 0.86) mm^2
In-plane res. reconstructed	(0.81 × 0.81) mm^2	(0.43 × 0.43) mm^2
Slice thickness	3 mm	2.5 mm
Distance factor	20%	10%
Gap	0.6 mm	0.3 mm
Slices	9	11
Phase oversampling	60%	100%
GRAPPA	None	2
Gradient mode	Fast	Normal
Turbo factor	208	256
Echo spacing	6.50 ms	6.32 ms
Bandwidth	446 Hz/Px	630 Hz/Px

Table 1: Main parameters of the original HASTE protocol and the optimized version with Deep Resolve.

[1] *Siemens Healthineers disclaimer: MR scanning has not been established as safe for imaging fetuses and infants less than two years of age. The responsible physician must evaluate the benefits of the MR examination compared to those of other imaging procedures. Note: This disclaimer does not represent the opinion of the authors.*

Since our institution mostly deals with fetuses of an early GA (19–24 weeks), we used this approach with a higher in-plane resolution (about 0.5 mm^2). In what follows, we present some promising examples.

It is worth noting that, while applying AI-based technology to acquire higher-resolution images in small fetuses is challenging, these cases may benefit the most from strategies to improve spatial resolution.

The original HASTE sequence was designed with a specific combination of parameters to achieve an optimal balance between signal quality and spatial resolution. A reasonable compromise is typically obtained by disabling parallel imaging while increasing phase oversampling. This raises the signal-to-noise ratio (SNR) and minimizes wrap-around artifacts caused by the unpredictable orientation of the fetal brain.

However, increasing phase oversampling and reducing parallel imaging inherently introduces global blurring. This is due to the increase in echo spacing, an expected behavior in single-shot sequences. The implementation of Deep Resolve significantly mitigates this effect through two complementary mechanisms: a denoising boost and the enhancement of effective resolution provided by the sharpening model. Moreover, Deep Resolve enables the use of a higher receiver bandwidth. This helps reduce chemical-shift artifacts between adjacent tissues and thereby improves the delineation of anatomical boundaries.

Deep Resolve operates when *k*-space undersampling is enabled, which explains why the GRAPPA acceleration factor shifts from "None" to "2" in the optimized protocol. This also suggests a potential further optimization strategy: increasing the parallel imaging factor from 2 to 3. Such an adjustment would improve image quality on two fronts by providing more effective denoising in undersampled regions and by further reducing echo spacing. These modifications, however, also require corresponding adaptation of the echo time, which declines as the echo train length becomes shorter.

In Table 1, we report the main parameters of our current T2-weighted HASTE protocol with the Deep Resolve algorithm.

Results

In Figure 1, we report a case with mild undefined and borderline brain dysmorphism. Establishing the presence or absence of malformation of the inner ear may corroborate the suspicion of a genetic condition if the labyrinth also proves to be abnormal.

As an additional example of the use of Deep Resolve, the depiction of the structures of the posterior fossa also benefit from higher-resolution images (Fig. 2). The result is better visualization of cerebellar foliation and the ability to more confidently assess structures like the taenia-tela choroidea complex, which plays a pivotal role in the characterization of cystic malformations (e.g., differential diagnosis of Dandy-Walker spectrum versus Blake's pouch cyst, which is caused by failed perforation of the foramen of Magendie).

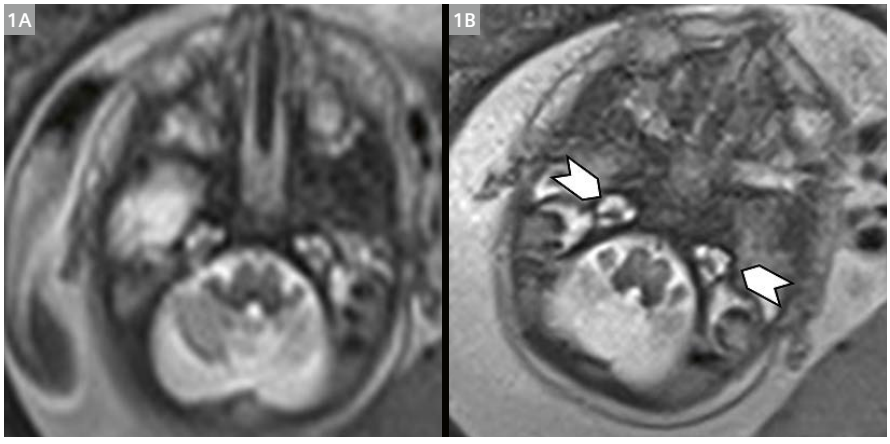

1 Axial T2-weighted HASTE of a fetus at 21 weeks gestational age, with 3 mm thick slices at 3 Tesla: **(1A)** 1 mm^2 in-plane resolution, **(1B)** corresponding slice acquired with Deep Resolve (0.86 × 0.86 mm^2 in-plane resolution, 2.5 mm slice thickness). The structures of the labyrinth of the inner ear are depicted with greater clarity and detail after Deep Resolve application (arrowheads).

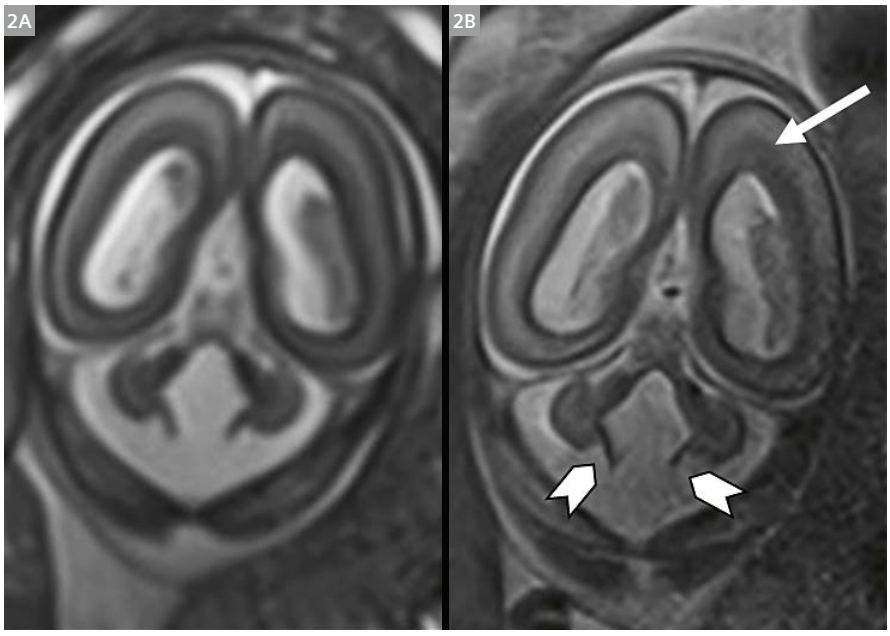

2 Coronal T2-weighted HASTE with 3 mm thick slices at 3T from a fetus of 19 weeks gestational age with posterior fossa anomaly on ultrasonography: **(2A)** 1 mm^2 in-plane resolution, **(2B)** corresponding section acquired with Deep Resolve (0.86 × 0.86 mm^2 in-plane resolution, 2.5 mm slice thickness). The lateral and caudal dislocation of the tela choroidea in a Dandy-Walker spectrum case is better depicted with Deep Resolve (arrowheads). Note also the sharper appearance of the border between different layers of the brain mantle (arrow).

Discussion and conclusion

The preliminary cases presented here demonstrate how using deep learning in MR image reconstruction can benefit a complex field such as fetal neuro MRI. Extensive quantitative studies comparing images with and without AI techniques or with different AI grading now need to be performed.

Although Deep Resolve offers significant advantages in MR image reconstruction, it is important to also consider the possible drawbacks of this novel approach. For instance, exaggerated fetal motion may degrade the image quality, and image inhomogeneity may arise if the fetal head is not located in the best area for coil sensitivity.

Furthermore, signal inhomogeneity in the field of view can be an issue. However, since the abdomen is generally smaller when the fetus is younger, this kind of image degradation is less likely, especially if using high-density coils. This is the case at our institution, where we prefer the 18-channel UltraFlex coil, which adapts to the smaller dimension of the abdomen prior to the third trimester of pregnancy.

Other approaches to enhancing spatial resolution in fetal MRI may enter clinical practice in the near future. These include small-field-of-view techniques (e.g., multichannel RF transmission) once they have been adapted for T2-weighted acquisition rather than echo-planar acquisition. Adding AI methods to this approach may also further enhance image quality.

Contact

Andrea Righini, M.D.
Radiologia e Neuroradiologia Pediatrica
Ospedale dei Bambini V. Buzzi
Via Castelvetro 32
20154, Milan
Italy
andrea.righini@asst-fbf-sacco.it

References

1 Griffiths PD, Bradburn M, Campbell MJ, Cooper CL, Graham R, Jarvis D, et al. Use of MRI in the diagnosis of fetal brain abnormalities in utero (MERIDIAN): a multicentre, prospective cohort study. Lancet. 2017;389(10068):538–546.
2 Jang M, Gupta A, Kovanlikaya A, Scholl JE, Zun Z. High-resolution anatomical imaging of the fetal brain with a reduced field of view using outer volume suppression. Magn Reson Med. 2024;92(4): 1556–1567.
3 Wilpert C, Russe MF, Weiss J, Voss C, Rau S, Strecker R, et al. Deep Learning Reconstruction Combined With Conventional Acceleration Improves Image Quality of 3 T Brain MRI and Does Not Impact Quantitative Diffusion Metrics. Invest Radiol. 2025;60(8):526–534.

CMR in Light of the 2025 ESC Guidelines on Myocarditis and Pericarditis: Opportunities and Challenges

Andreas Schuster[1]; Jan Gröschel[2]; Johannes Kowallick[3]; Valentino Collini[4]; Massimo Imazio[4]; Jeanette Schulz-Menger[2]

[1] FORUM Medizin, Kardiologie, Rosdorf, Germany
[2] Charité – Universitätsmedizin Berlin, corporate member of Freie Universität Berlin and Humboldt-Universität zu Berlin; ECRC (Experimental and Clinical Research Center), Berlin, Germany; DZHK (German Centre for Cardiovascular Research), partner site Berlin, Berlin, Germany; Deutsches Herzzentrum der Charité Berlin, Germany; Cardiology and Nephrology, HELIOS Hospital Berlin-Buch, Berlin, Germany
[3] FORUM Medizin, Radiologie, Rosdorf, Germany
[4] Department of Medicine, University of Udine, and Cardiothoracic Department, University Hospital Santa Maria della Misericordia, ASUFC, Udine, Italy

Clinical impact of the 2025 ESC Guidelines on routine management of patients with myocarditis

The release of the 2025 European Society of Cardiology (ESC) Guidelines for the management of myocarditis and pericarditis signals a watershed moment in cardiac imaging. These guidelines fundamentally reshape the diagnostic landscape, placing cardiovascular magnetic resonance (CMR) at the forefront of routine clinical practice [1]. This paradigm shift necessitates a comprehensive understanding of the updated guidelines and a critical reassessment of current practices for clinicians.

The core message is clear: Non-invasive evaluation of myocardial inflammation has reached a new level of sophistication and importance (Fig. 1). The guidelines champion a holistic approach to inflammatory heart disease, moving beyond the limitations of solely relying on invasive procedures. There are essential changes affecting clinicians, particularly imaging specialists, that need to be considered to ensure that patient care fully benefits from these advancements.

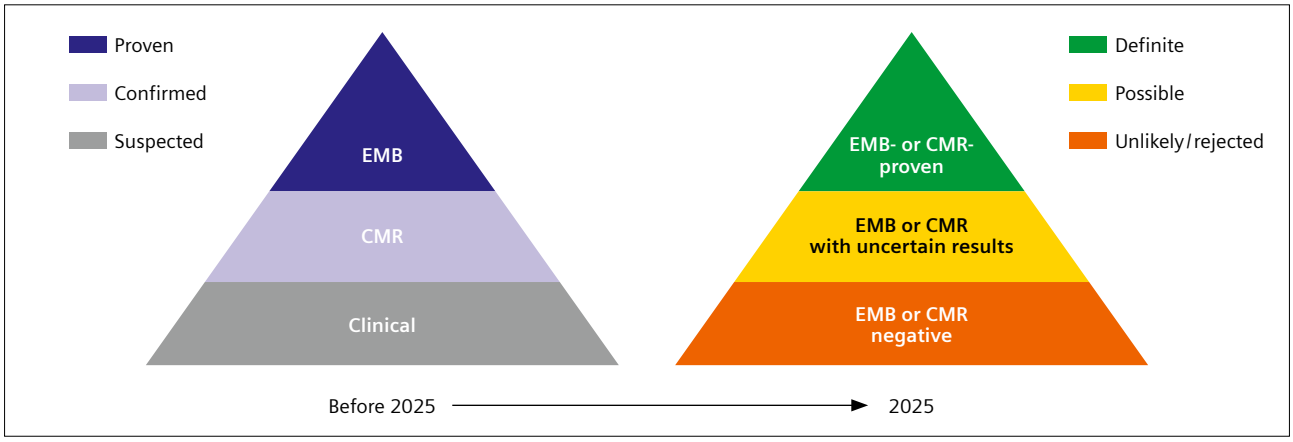

1 Visualization of the diagnostic criteria for myocarditis according to the current ESC guidelines [1]. A paradigm shift has occurred in the clinical diagnosis of myocarditis: Both cardiovascular magnetic resonance (CMR) and endomyocardial biopsy (EMB) can establish a definitive diagnosis, but are applied in different clinical contexts.

The shifting diagnostic paradigm: Embracing "IMPS" and updated imaging criteria

The 2025 guidelines introduce the term "inflammatory myopericardial syndrome" (IMPS) [1]. This recognizes the clinical spectrum of disease, ranging from simple myocarditis, through mixed forms, to simple pericarditis. IMPS serves as a framework for initiating a diagnostic workup that considers both myocardial and pericardial involvement, and urges clinicians to be aware of the overlapping nature of these conditions (Table 1).

This approach directly impacts imaging protocols and interpretation. Instead of narrowly focusing on fulfilling specific criteria for myocarditis *or* pericarditis, imaging specialists should now consider the possibility of both, and tailor imaging acquisitions and analyses accordingly. This necessitates incorporating specific imaging sequences that can detect both myocardial and pericardial inflammation, including sequences to assess edema and tissue characterization [2, 3].

Moreover, the guidelines solidify the importance of the Lake Louise criteria (LLC) for the CMR diagnosis of myocarditis [4, 5]. It is imperative for imaging specialists to thoroughly familiarize themselves with the updated LLC and understand the nuances. Furthermore, since myocardial inflammation can arise from various causes, imaging results must also be weighed in the relevant clinical context rather than solely relying on abnormal imaging parameters [6]. This not only involves acquiring high-quality images, but also recognizing the patterns and distribution of myocardial edema, assessing non-ischemic scar distribution, and accurately evaluating ventricular function to aid in the non-invasive diagnosis of myocarditis.

Inflammatory Myopericardial Syndrome		
If diagnostic criteria for myocarditis and/or pericarditis are fulfilled		
	Myocarditis	**Pericarditis**
Definite	Clinical presentation and CMR- or EMB-proven	Clinical presentation with >1 additional criterion
Possible	Clinical presentation with at least 1 additional criterion CMR- or EMB-uncertain or not available	Clinical presentation with 1 additional criterion
Unlikely/rejected	Only clinical presentation without additional criteria	Only clinical presentation without additional criteria
Additional criteria beyond clinical presentations		
	Myocarditis	**Pericarditis**
Clinical	Non-specific findings	Pericardial rubs
ECG	ST-T changes	PR depression, widespread ST-segment elevation
Biomarkers	Troponin elevation	C-reactive protein elevation
Imaging	Abnormal strain, wall motion, reduced EF Myocardial oedema and/or LGE (CMR findings)	New or worsening pericardial effusion Percardial oedema and/or LGE (CMR findings)

Table 1: Diagnostic criteria and classification for inflammatory myopericardial syndrome.
CMR, cardiovascular magnetic resonance; ECG, electrocardiogram; EF, ejection fraction; EMB, endomyocardial biopsy; IMPS, inflammatory myopericardial syndrome; LGE, late gadolinium enhancement; LLC, Lake Louise criteria
Clinical presentations include chest pain or infarct-like symptoms, arrhythmias, heart failure, aborted sudden cardiac death.
Cardiovascular magnetic resonance categories:
proven = 2 out of 2 updated LLC fulfilled; uncertain = only 1 out of 2 updated LLC fulfilled; rejected = negative CMR.

From biopsy-driven to CMR-centric: A new diagnostic era

The most significant change is the transition from endomyocardial biopsy (EMB) as a primary diagnostic tool to CMR as the leading modality for initial assessment in appropriate cases.

Traditionally, EMB played a central role in confirming the diagnosis of myocarditis [7]. Although EMB remains crucial for specific scenarios and when tissue analysis is required, it is no longer the first step for the vast majority of patients with suspected myocarditis. EMB is now reserved for cases in which its findings would specifically alter management strategies, such as directing targeted therapies or identifying the underlying cause of the myocardial disease. Imaging specialists should therefore proactively guide clinical decision-making by emphasizing the strengths and limitations of CMR in identifying myocardial inflammation, assessing the extent and severity of disease, and excluding other potential causes of cardiac dysfunction. Skillful application of these insights will enable more informed patient management, allowing clinical cardiologists to make appropriate referral decisions for EMB if required.

These scenarios may include high-risk myocarditis (e.g., with hemodynamic or arrhythmic instability) or when specific histopathologic diagnoses (e.g., giant cell myocarditis) are needed to guide targeted therapy. EMB is also appropriate in moderate-risk cases that do not respond to conventional treatments when a viral or specific cause is suspected and impacts decision-making. It is important to note that the relative fraction of these scenarios is relatively small given the large number of myocarditis patients that can be sufficiently managed based on non-invasive imaging only.

Unmasking inherited risks: The interplay of genetics and inflammatory heart disease

A further significant advancement of the guidelines is the recognition of the influence of genetics on inflammatory heart conditions. The guidelines now recommend obtaining a detailed family history in cases of recurrent IMPS to uncover potential inherited causes, assess inheritance patterns, and identify at-risk relatives. Genetic testing should be considered, especially with a family history of IMPS, inherited cardiomyopathy, or unexplained sudden cardiac death, as certain genetic variants can increase susceptibility to IMPS or influence disease severity. Notably, there is an overlap between genes associated with inherited cardiomyopathies, such as arrhythmogenic right ventricular cardiomyopathy (ARVC) and dilated cardiomyopathy (DCM), and those that may predispose a person to myocardial inflammation. This highlights the need to consider genetic testing in cases where IMPS presents atypically or with a strong family history, potentially unveiling an underlying inherited risk [8, 9].

Risk stratification and return-to-activity: Guiding a safe resumption

CMR plays a crucial role in risk stratification, identifying those at higher risk for adverse events and guiding recommendations for a safe return to physical activity and work. By characterizing myocardial damage and assessing potential arrhythmogenic substrates (e.g., using late gadolinium enhancement, LGE), CMR provides clinicians with essential information for evaluating prognoses and guiding management decisions. Imaging specialists should proactively communicate the presence of concerning CMR findings — such as extensive LGE, significant ventricular dysfunction, or evidence of ongoing inflammation — in their reports. These findings should be carefully considered in the context of other clinical data to determine the appropriate level of monitoring, treatment, and activity restrictions for each patient.

In general, the guidelines recommend surveillance including imaging. Specifically, they provide a detailed follow-up schedule for patients diagnosed with IMPS, differentiating between myocarditis and pericarditis cases. Clinical evaluations, alongside specific testing, are consistently recommended at each follow-up interval — within one month, at three to six months, at 12 months, and beyond. Detailed recommendations regarding CMR for myocarditis include a one-month scan or within three to six months, then a second CMR at six to 12 months, and a long-term follow-up if required depending on the results of the initial scans [1, 10].

One of the less-discussed but equally important roles of CMR is its ability to definitively exclude both myocarditis and pericarditis in patients with suspected symptoms. A negative CMR scan, when combined with a thorough clinical evaluation, can provide significant reassurance to patients and clinicians, ruling out myocardial and/or pericardial inflammation as a cause of their symptoms.

For imaging specialists, this requires clear and confident communication of negative CMR findings in their reports. This will minimize unnecessary anxiety and enable prompt investigation for other potential causes of chest pain, dyspnea, or arrhythmias [11]. It is also important to identify and rule out other potential causes of symptoms, including acute coronary syndrome (ACS), as appropriate.

The updated Lake Louise criteria in clinical practice: Application, technical challenges, and confounding factors

The ESC guidelines emphasize the use of the updated LLC for the detection of myocarditis [1]. While the original LLC were based on T2-weighted sequences, early gadolinium enhancement sequences, and LGE [12], the updated LLC incorporate parametric mapping [4] (Fig. 2). With this refinement, sensitivity is greatly increased [13]. Currently, the diagnosis of acute myocarditis can be made when a T1 criterion (T1 mapping, LGE, or extracellular volume) and a T2 criterion (T2-weighted imaging or T2 mapping) are fulfilled (Figs. 3 and 4). It should be noted that even in the absence of one criterion, the diagnosis of myocarditis is still possible in the proper clinical scenario. If not all criteria are fulfilled, diagnostic accuracy is lower but remains above 75%. Importantly, T2-based criteria specifically reflect the current activity of the disease. Although parametric mapping has revolutionized the approach to IMPS in CMR, certain issues remain. Consensus statements from the Society for Cardiovascular Magnetic Resonance (SCMR) provide guidance regarding acquisition and analysis [14], yet inter-scanner and inter-vendor differences remain [15]. Promising research has been published regarding post-hoc standardization, but further prospective approaches should aim to overcome the need for additional post-processing steps [16]. In addition to standardization across sequences, scanners, and vendors, other patient- and acquisition-related factors must also be considered. Artifacts, such as those caused by motion or metallic objects, can impair image quality. Therefore, careful quality assurance is essential to identify and exclude non-diagnostic images [17].

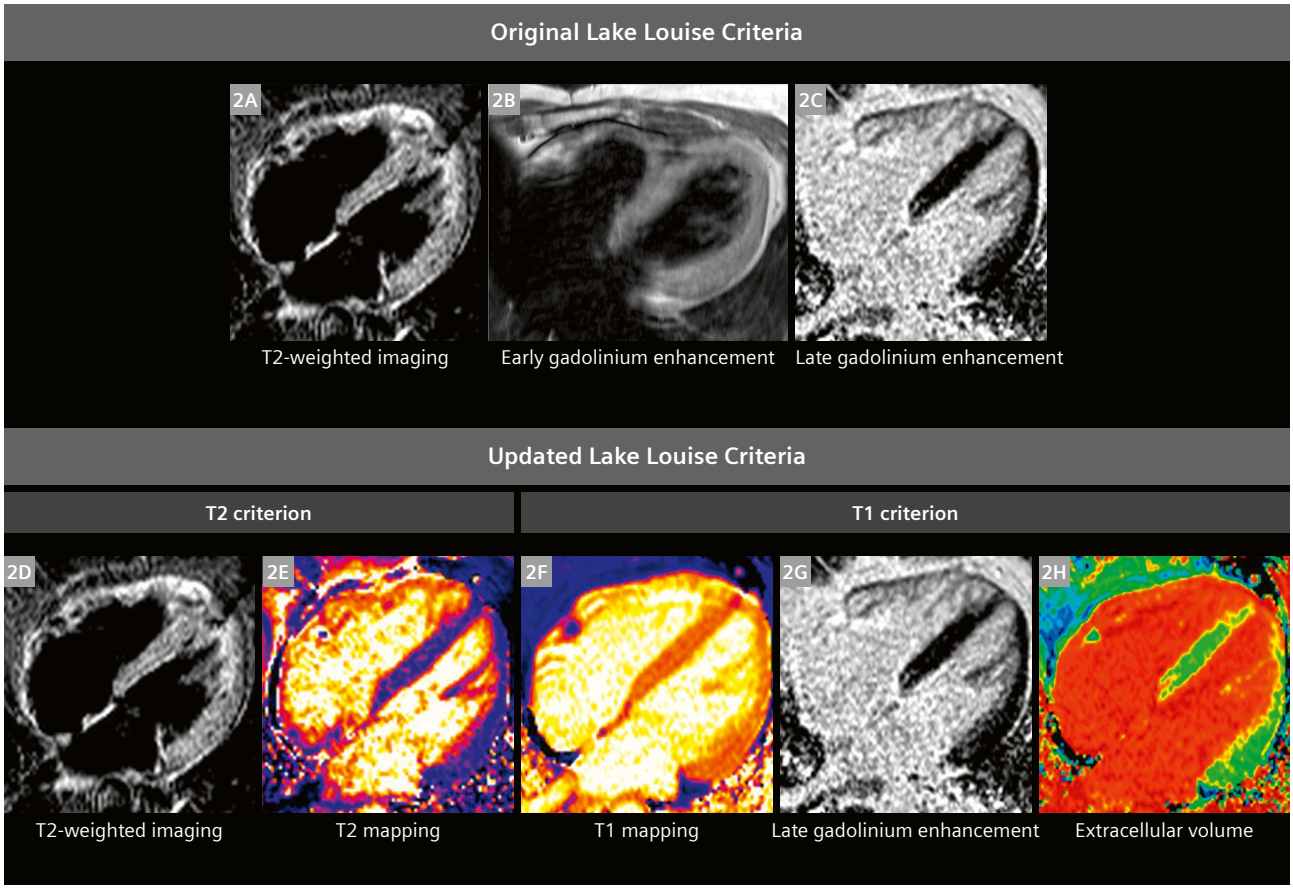

2 Example images comparing the former Lake Louise criteria (top row) with the updated Lake Louise criteria (bottom row). Top row: **(2A)** T2-weighted imaging based on a TIRM sequence, **(2B)** early gadolinium enhancement based on a T1-weighted gradient echo sequence, **(2C)** late gadolinium based on a PSIR sequence. Botton row: **(2D)** T2-weighted imaging based on a TIRM sequence, **(2E)** T2 mapping based on a bSSFP sequence, **(2F)** T1 mapping based on a MOLLI sequence, **(2G)** late gadolinium enhancement based on a PSIR sequence, **(2H)** extracellular volume map based on pre- and post-contrast MOLLI-based T1 mapping sequences.
Images acquired on a 1.5T MAGNETOM Avanto Fit at Charité Campus Berlin-Buch.

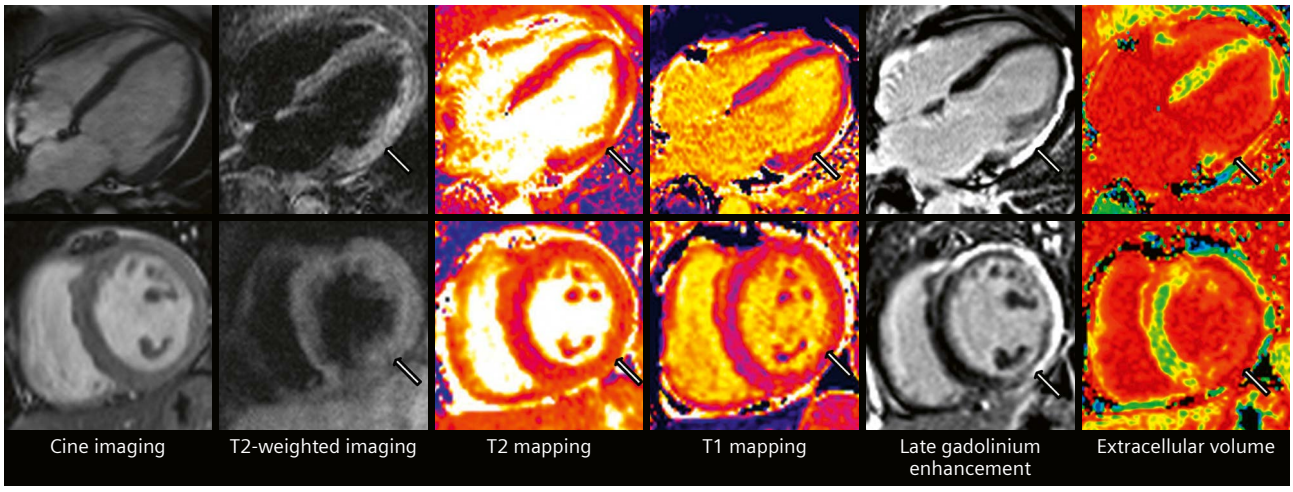

3 Cardiovascular magnetic resonance (CMR) findings in a 56-year-old woman presenting with dyspnea and elevated NT-proBNP. CMR demonstrates features consistent with acute myocarditis. Cine imaging showed reduced left ventricular systolic function with global hypokinesia. T2-weighted imaging and T2 mapping revealed increased myocardial signal and elevated T2 values, indicating myocardial edema (arrows). Native T1 mapping showed diffusely increased relaxation times. Late gadolinium enhancement imaging demonstrated extensive subepicardial enhancement of the lateral wall extending into the anteroseptal region, confirming active myocardial injury. PET-CT was unremarkable and genetic testing is pending.
Images acquired on a 1.5T MAGNETOM Avanto Fit at Charité Campus Berlin-Buch.

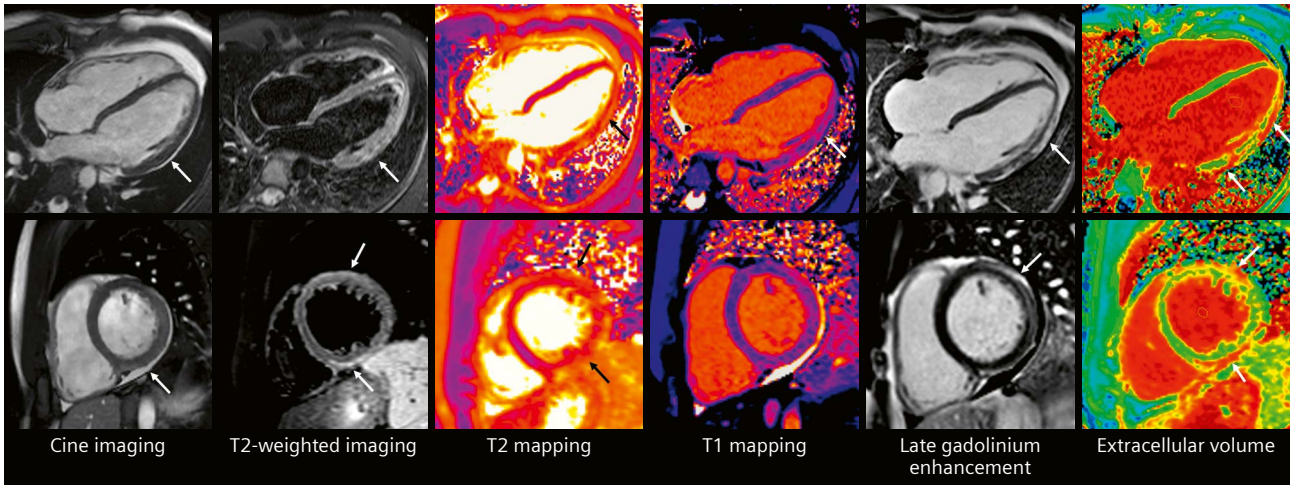

4 Cardiovascular magnetic resonance findings in a 28-year-old man presenting with chest pain and dyspnea. Elevated troponin levels were detected. CMR findings are characteristic of acute myocarditis. There was preserved left ventricular systolic function on Compressed Sensing cine imaging (LV EF: 55%; GLS: 15.9%) in the presence of a small pericardial effusion (arrows). STIR T2-weighted imaging and T2 mapping revealed increased myocardial signal and elevated T2 values indicative of myocardial edema (arrows). Native T1 mapping showed diffusely increased relaxation times. Free-breathing LGE imaging demonstrated characteristic subepicardial enhancement of the lateral wall and extending into the anterolateral and inferolateral region, confirming active myocardial injury.
Images acquired on a 1.5T MAGNETOM Sola at FORUM Medizin, Rosdorf, Germany.

Future perspectives

In the 2025 ESC Guidelines for the management of myocarditis and pericarditis, a considerable number of recommendations are classified as Class I, but are supported only by Level C evidence. This reflects strong agreement within the writing group, as the voting on recommendations is a secret process. However, a high level of evidence is missing, since prospective and outcome-oriented multicenter studies are lacking. This can be an opportunity for our community to generate the data, as this may define the next stage of evidence-based management for IMPS.

Our community generally agrees that efficient and reproducible CMR examinations are essential, and that the updated LLC provide a corresponding consensus protocol [4]. At the same time, CMR protocols should be tailored to the clinical question. In follow-up studies that focus primarily on disease activity, it may be reasonable to reconsider the routine use of contrast agents, as parametric mapping, T2 imaging, and cine techniques can provide reliable information. Such an approach emphasizes both clinical relevance and resource efficiency.

Innovation has always been a hallmark of the CMR community. Novel pulse sequences and AI-based analytic tools are constantly being developed, opening new doors in cardiac imaging. Yet every new technique must undergo systematic validation. This requires coordinated efforts and robust tools, including quality assurance pipelines and possibly a gold-standard dataset driven by SCMR. While we can be proud of what we have achieved with CMR so far, even greater progress is possible by pooling our efforts.

References

1 Schulz-Menger J, Collini V, Gröschel J, Adler Y, Brucato A, Christian V, et al. ESC Guidelines for the management of myocarditis and pericarditis. Eur Heart J. 2025;46(40):3952–4041.

Contact

Professor Jeanette Schulz-Menger, M.D.
University Medicine Berlin
Charité Campus Buch, ECRC
HELIOS Clinics Berlin-Buch
Department of Cardiology and Nephrology
Lindenberger Weg 80
13125 Berlin, Germany
Tel.: +49 30 040153536
jeanette.schulz-menger@charite.de

Professor Andreas Schuster, M.D., Ph.D.
Forum Medizin GbR
An der Ziegelei 1
37124 Rosdorf
Germany
Tel.: +49 551 89069840
andreas.schuster@forum-medizin-goettingen.de
https://forum-medizin-goettingen.de/

2 Kramer CM, Barkhausen J, Bucciarelli-Ducci C, Flamm SD, Kim RJ, Nagel E. Standardized cardiovascular magnetic resonance imaging (CMR) protocols: 2020 update. J Cardiovasc Magn Reson. 2020;22(1):17.
3 Schulz-Menger J, Bluemke DA, Bremerich J, Flamm SD, Fogel MA, Friedrich MG, et al. Standardized image interpretation and post-processing in cardiovascular magnetic resonance 2020 update: Society for Cardiovascular Magnetic Resonance (SCMR): Board of Trustees Task Force on Standardized Post-Processing. J Cardiovasc Magn Reson. 2020;22(1):19.
4 Ferreira VM, Schulz-Menger J, Holmvang G, Kramer CM, Carbone I, Sechtem U, et al. Cardiovascular Magnetic Resonance in Nonischemic Myocardial Inflammation: Expert Recommendations. J Am Coll Cardiol. 2018;72(24):3158–3176.
5 Writing Committee, Drazner MH, Bozkurt B, Cooper LT, Aggarwal NR, Basso C, et al. 2024 ACC Expert Consensus Decision Pathway on Strategies and Criteria for the Diagnosis and Management of Myocarditis: A Report of the American College of Cardiology Solution Set Oversight Committee. J Am Coll Cardiol. 2025;85(4):391–431.
6 Hua A, Domenech-Ximenos B, Lopez B, Sanna G, Chiribiri A, Rajani R, et al. Diagnostic utility of the revised Lake Louise criteria in myocarditis associated with active autoimmune rheumatic disease. J Cardiovasc Magn Reson. 2025;27(2):101916.
7 Schultheiss HP, Kühl U, Cooper LT. The management of myocarditis. Eur Heart J. 2011;32(21):2616–25.
8 Gasperetti A, Muller SA, Peretto G, Asatryan B, Protonotarios A, Laredo M, et al. Prognostic Role of Myocarditis-Like Episodes and Their Treatment in Patients With Pathogenic Desmoplakin Variants. Circulation. 2025;152(14):978–989.
9 Piriou N, Marteau L, Kyndt F, Serfaty JM, Toquet C, Le Gloan L, et al. Familial screening in case of acute myocarditis reveals inherited arrhythmogenic left ventricular cardiomyopathies. ESC Heart Fail. 2020;7(4):1520–1533.
10 Aquaro GD, Ghebru Habtemicael Y, Camastra G, Monti L, Dellegrottaglie S, Moro C, et al. Prognostic Value of Repeating Cardiac Magnetic Resonance in Patients With Acute Myocarditis. J Am Coll Cardiol. 2019;74(20):2439–2448.
11 Writing Committee Members, Gulati M, Levy PD, Mukherjee D, Amsterdam E, Bhatt DL, et al. 2021 AHA/ACC/ASE/CHEST/SAEM/SCCT/SCMR Guideline for the Evaluation and Diagnosis of Chest Pain: A Report of the American College of Cardiology/American Heart Association Joint Committee on Clinical Practice Guidelines. J Am Coll Cardiol. 2021;78(22):e187–e285.
12 Friedrich MG, Sechtem U, Schulz-Menger J, Holmvang G, Alakija P, Cooper LT, et al. Cardiovascular magnetic resonance in myocarditis: A JACC White Paper. J Am Coll Cardiol. 2009;53(17):1475–87.
13 Luetkens JA, Faron A, Isaak A, Dabir D, Kuetting D, Feisst A, et al. Comparison of Original and 2018 Lake Louise Criteria for Diagnosis of Acute Myocarditis: Results of a Validation Cohort. Radiol Cardiothorac Imaging. 2019;1(3):e190010.
14 Messroghli DR, Moon JC, Ferreira VM, Grosse-Wortmann L, He T, Kellman P, et al. Clinical recommendations for cardiovascular magnetic resonance mapping of T1, T2, T2* and extracellular volume: A consensus statement by the Society for Cardiovascular Magnetic Resonance (SCMR) endorsed by the European Association for Cardiovascular Imaging (EACVI). J Cardiovasc Magn Reson. 2017;19(1):75.
15 Gröschel J, Trauzeddel RF, Müller M, von Knobelsdorff-Brenkenhoff F, Viezzer D, Hadler T, et al. Multi-site comparison of parametric T1 and T2 mapping: healthy travelling volunteers in the Berlin research network for cardiovascular magnetic resonance (BER-CMR). J Cardiovasc Magn Reson. 2023;25(1):47.
16 Viezzer D, Hadler T, Gröschel J, Ammann C, Blaszczyk E, Kolbitsch C, et al. Post-hoc standardisation of parametric T1 maps in cardiovascular magnetic resonance imaging: a proof-of-concept. EBioMedicine. 2024;102:105055.
17 Fenski M, Gröschel J, Gatehouse P, Kolbitsch C, Schulz-Menger J. Artifacts in cardiac T1 and T2 mapping techniques – Influence on reliable quantification. J Cardiovasc Magn Reson. 2025;101934.

What happens when you have an MRI scan?

Help your little patients lose their fear — with Lottie

Lottie is an adventurous little lamb that loves to skateboard. But poor Lottie had an accident and may have broken her ankle. Now instead of leaping, she can only limp. Lottie is off to the hospital for an MRI scan. This engaging story by Professor Rolf Vosshenrich and Sylvia Graupner explains to children what it's like to have an MRI scan in a way they can understand.

We offer Lottie's story as a children's book in 21 languages (PDF) and as video in 6 languages. You can also order hard copies of the book in German, English, and Spanish.

The material is available at
www.siemens-healthineers.com/magnetom-world

Go to **> Publications > MR Basics**

syngo NATIVE TrueFISP Non-Contrast MR Angiography: Pulmonary Arteries

Marcelo Fernandes Arêas

Siemens Healthineers, Erlangen, Germany

NATIVE (non-contrast angiography of the arteries and veins) is a contrast-free MR angiography technique for visualizing the vessels of the body. You can find tailored protocols for use in renal arteries and peripheral vessels on the protocol tree from Siemens Healthineers. *syngo* NATIVE TrueFISP is based on the TrueFISP (true fast imaging with steady state precession) sequence, which is a balanced steady-state gradient echo technique. The sequence can be made selective for arteries or veins by appropriate positioning of the inversion pulse, which can be positioned independently from the imaging volume.

The most robust method of performing *syngo* NATIVE TrueFISP is with respiratory triggering. With BioMatrix Technology, the respiratory sensor in the BioMatrix spine coil improves the workflow and increases efficiency.

The following acquisition protocol was performed on a 1.5T MAGNETOM Sola and on a 3T MAGNETOM Cima.X.

We start with the patient positioned headfirst, with the BioMatrix Contour L coil or the BioMatrix Body 18 coil covering the upper abdomen to the thorax. For better localization of the pulmonary arteries, I recommend a T2 TrueFISP sequence for the lungs, in addition to the standard free-breathing localizer. The exam can also be performed with the patient in a feetfirst position.

You can take the NATIVE TrueFISP sequence directly from the protocol tree, as shown in Figure 1.

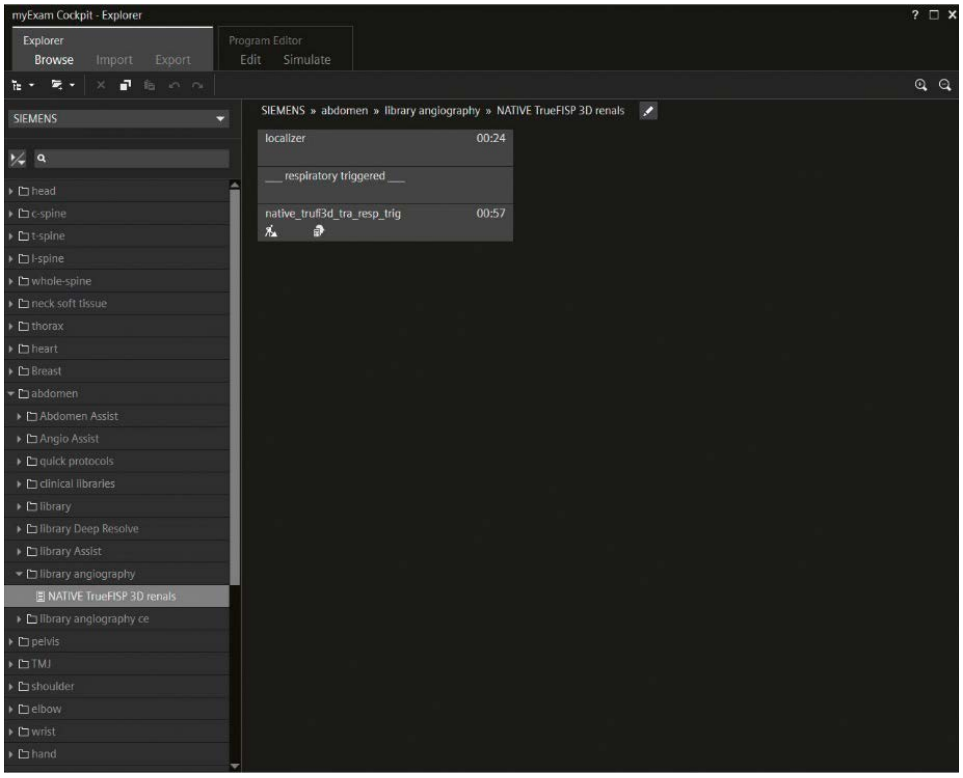

1 The NATIVE TrueFISP sequence in the protocol tree.

Next, align the axial slices with the pulmonary arteries and increase the number of slices as needed. Make sure that the inversion band is positioned perpendicular to the pulmonary vessels (Fig. 2).

You can modify the inversion time of the inversion bands as needed. Note that the optimal range for pulmonary artery values is generally considered to be between 900 and 1100 ms (Fig. 3). The acquisition time will vary depending on the patient's respiratory cycle. The sequence can be performed on either 1.5T or 3T systems. Below are some example results.

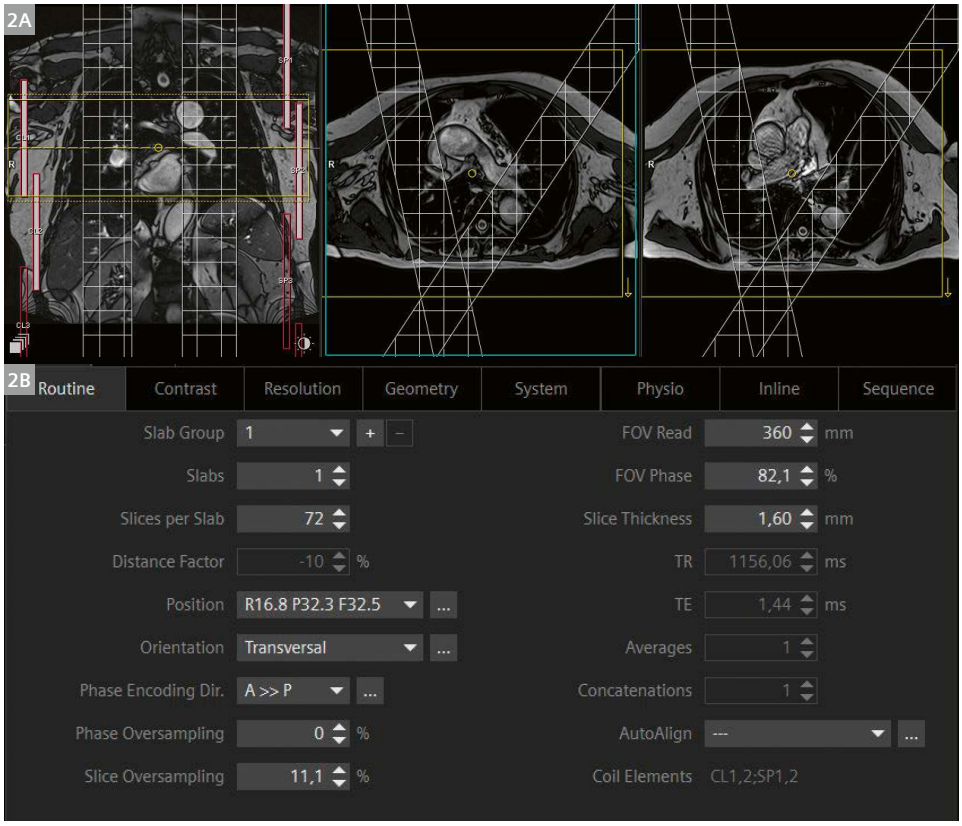

2 Axial slices aligned with the pulmonary arteries **(2A)** and details of alignment on the dashboard **(2B)**.

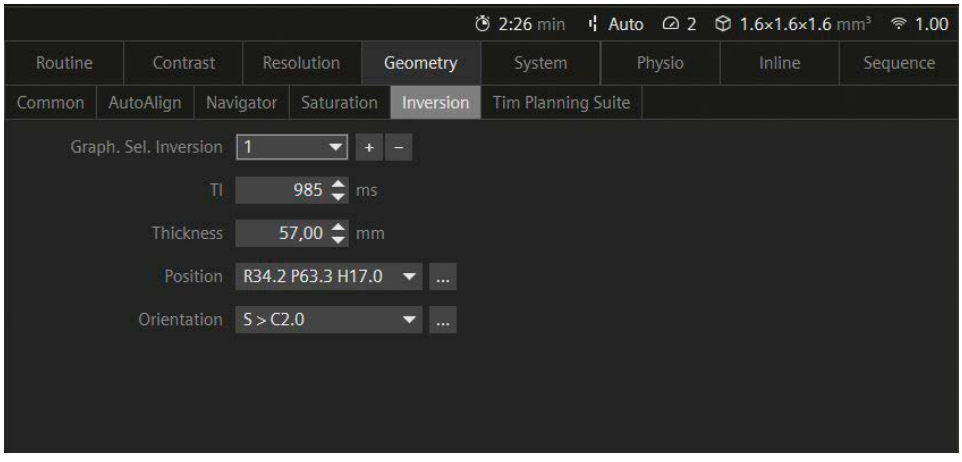

3 Optimal inversion time (TI) of the inversion bands: between 900 and 1100 ms.

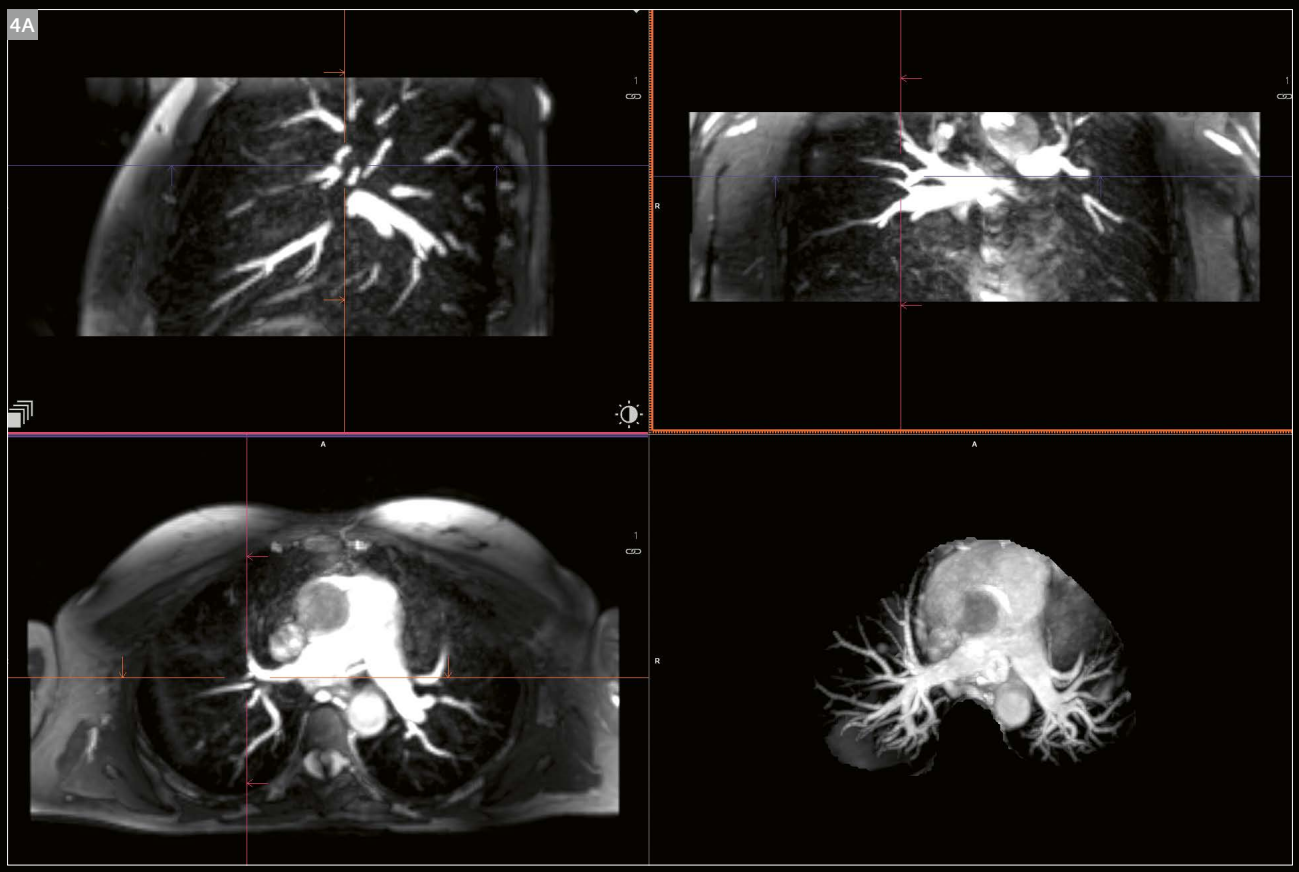
4A
1aaaa6381

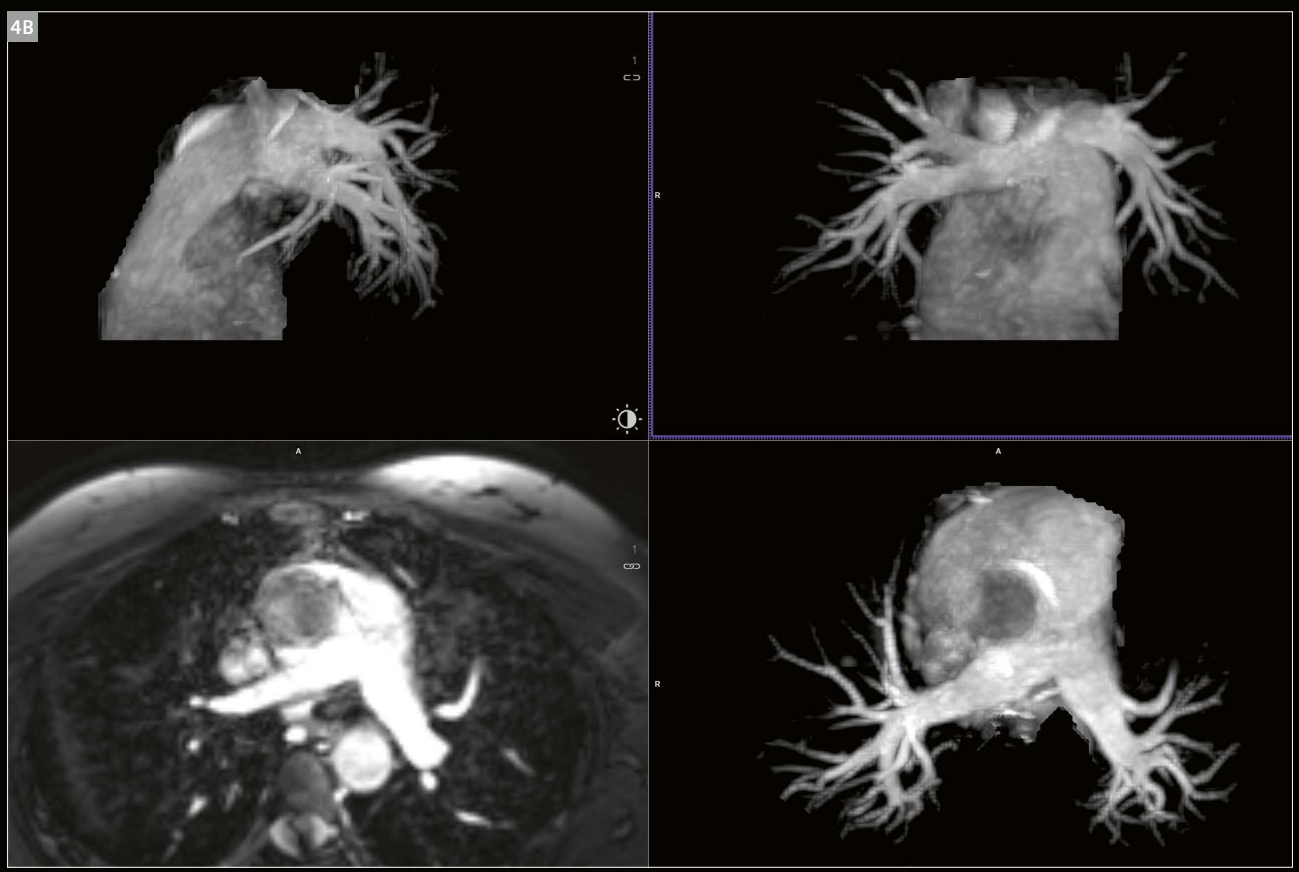
4B
1aaaa6381

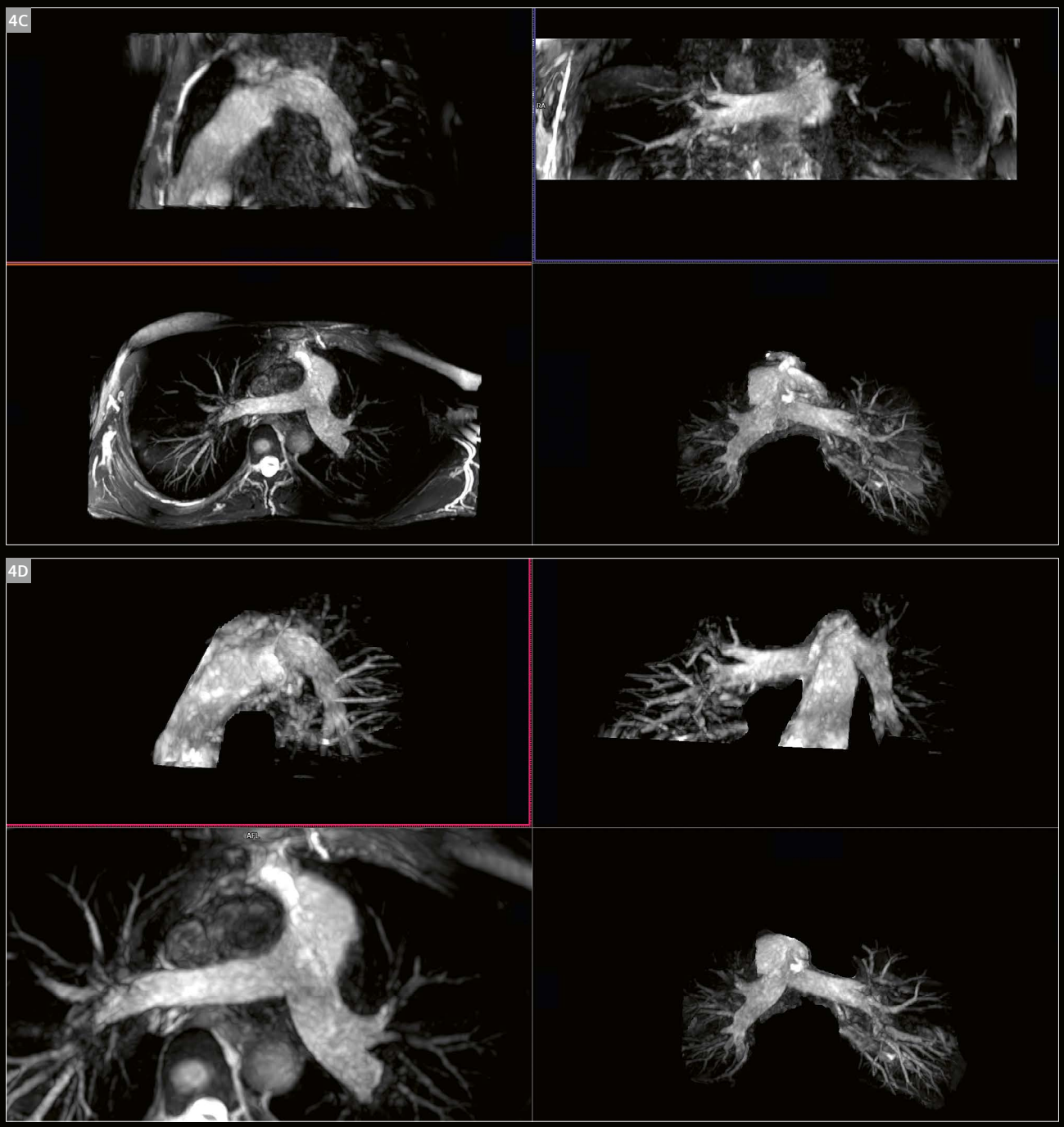

4 Pulmonary arteries scanned with *syngo* NATIVE TrueFISP, a contrast-free MR angiography technique. Images produced on a 1.5T MAGNETOM Sola **(4A, 4B)** and a 3T MAGNETOM Cima.X. **(4C, 4D)** system.

Contact

Marcelo Fernandes Arêas
Siemens Healthineers
SHS DI MR M&S S CVP
Allee am Röthelheimpark 2
91052 Erlangen
Germany
marcelo.areas@siemens-healthineers.com

Meet Siemens Healthineers

Siemens Healthineers: Our brand name embodies the pioneering spirit and engineering expertise that is unique in the healthcare industry. The people working for Siemens Healthineers are totally committed to the company they work for, and are passionate about their technology. In this section we introduce you to colleagues from all over the world — people who put their hearts into what they do.

Daniel Polak, Ph.D.

Daniel Polak holds a B.Sc. and an M.Sc. in physics from Technische Universität Darmstadt and Heidelberg University. He pursued his Ph.D. with direct support from Siemens Healthineers MR in Erlangen, Germany. During his master's and Ph.D. studies, Daniel completed research appointments at both Harvard Medical School and the Massachusetts Institute of Technology (MIT) in Boston, MA, USA. Through these collaborative research experiences, Daniel established a broad network of professional relationships in the United States that continue to shape his career. After earning his doctorate, Daniel joined the global Siemens Neuro pre-development team, where he led the development of a retrospective motion-correction technique for brain MRI. This technology — BioMatrix Motion Sensor — was launched as part of the MAGNETOM Cima.X platform, in which it contributes to improved image quality and clinical reliability in neuroimaging. In 2025, Daniel transitioned to the U.S. organization at Siemens Healthineers as a senior key expert scientist, supporting a newly established portfolio of collaborative neuroimaging projects with Stanford University. In this role, he continues to bridge innovative research and clinical translation, strengthening new partnerships and advancing next-generation MRI technologies.

How did you first come into contact with MRI?
My first experience with MRI was for my master's thesis, while visiting the Athinoula A. Martinos Center for Biomedical Imaging in Boston. Working in such a vibrant and fast-paced academic environment was both challenging and inspiring. I was fortunate to receive exceptional mentorship that not only shaped my technical expertise but also inspired my scientific thinking. Only a few months into my research project, I had the opportunity to attend the ISMRM annual scientific meeting in Singapore. Engaging with researchers from around the world and witnessing the breadth of innovation in MRI deepened my enthusiasm for the biomedical imaging field. These experiences ultimately inspired me to pursue a Ph.D. and continue building my career in MRI research.

What are the most important developments in healthcare?
In medicine today, imaging plays an increasingly central role — not only in diagnosis, but also in monitoring disease progression and guiding emerging treatment options, for example in Alzheimer's disease. As a result, the number of procedures is rising worldwide and this trend is expected to accelerate further due to individualized treatments and an aging population. At the same time, healthcare systems face growing pressure from workforce shortages and declining reimbursement rates. Technology providers can help address these challenges by delivering intelligent solutions that support the entire patient workflow — from patient preparation and image acquisition to interpretation and reporting. I have contributed to the development of advanced MRI techniques designed to make scans more robust and reproducible. One recent example is a method that corrects for patient motion artifacts. Such innovations are particularly valuable for pediatric and elderly patients, who are often the most likely to move during scans. However, this is only one piece of a much larger puzzle. Looking ahead, a broad range of advanced algorithms and workflow-integrated tools will be essential to meaningfully support clinical practice — and will ultimately enhance efficiency, diagnostic confidence, and patient outcomes.

What would you do if you could spend a month doing whatever you wanted?
Having recently moved into a role where I support our research collaboration with Stanford University, I've begun an exciting new chapter in my career. I am exactly where I want to be, both professionally and personally. I have the privilege of working closely with professors and students on a wide range of cutting-edge research topics, expanding my expertise beyond neuroimaging and gaining valuable insights across multiple areas of radiology. I truly appreciate the close partnership and how warmly Stanford has welcomed me into its academic community. Being embedded in such an intellectually inspiring environment is deeply motivating.

Living in Silicon Valley adds yet another dynamic dimension. Experiencing the future of technology first-hand — from the latest advances in artificial intelligence to autonomous vehicles and robotics — fuels my curiosity and drive. At the same time, I cherish the Bay Area lifestyle. The Mediterranean climate means I can play tennis outdoors even in winter. I also have breathtaking nature right on my doorstep, so I can easily go on scenic hikes, enjoy the ocean views, and take weekend trips to California's amazing national parks.

Silvia Arroyo Camejo, Ph.D.

Silvia Arroyo Camejo was born in Berlin, Germany. She developed an early interest in physics, writing a book about quantum physics at age 17 ("Skurrile Quantenwelt", Springer Nature, 2006). She went on to study physics at Humboldt-Universität zu Berlin in Germany, at Massachusetts Institute of Technology in the U.S., and at the University of Vienna in Austria, specializing in atomic physics and quantum optics. In 2015, she completed her Ph.D. at the Max Planck Institute for Biophysical Chemistry and at Heidelberg University in Germany, on the topic of quantum information, quantum sensing, and super-resolution microscopy on nitrogen-vacancy centers in diamond.

Silvia has been with Siemens Healthineers since 2017. Her role in software predevelopment at MR allows her to combine her passion for physics, technology, and medicine.

What do you find motivating about your job?
I have always been very motivated by complex problems. Even as a young teenager, I liked to solve physics, math, and logic puzzles and I was fascinated to learn about the world and how it works. That's what eventually led me to study physics.

Now, I am lucky to work in software predevelopment at MR, where I can contribute to our goal of making our MR scanners more intelligent and autonomous. I love being able to tackle a mix of technical, medical, and regulatory challenges with a great, diverse team here at Siemens Healthineers.

Ultimately, my greatest pleasure and privilege is to interact with our clinical and research customers, discuss their everyday challenges, learn from them, and try to develop the best possible solutions to support their vital work. Our customers' input and feedback is probably the most crucial initiator of any development activity I undertake — and it's the final benchmark to gauge whether we were successful.

I am driven every day by this challenging mix of topics, the continuous exchange with clinical and research customers, and last but not least the importance of our goal to make our scanners more autonomous.

What are the biggest challenges in your job?
It's perhaps not the biggest challenge, but the hardest truth of working in predevelopment is this: We encounter so many interesting and exciting topics and possibilities every week. We constantly come up with new ideas for how we could improve or extend our solutions. But despite our passion for innovation and our love of optimization, we must always be mindful that time is finite. We must prioritize and focus on the most important and promising activities and features so we can bring them to a sufficiently mature state and reach the prototype level within a reasonable time. This is the only way to create real value that makes a difference in clinical practice in the not-too-distant future. Getting this balance right is oftentimes tough, but extremely important.

What are the most important developments in healthcare?
I currently see two major topics:

1) Connecting the diverse, independent IT systems (and some remaining paper-based systems) that are used for planning, managing, and documenting the patient's journey through the hospital. Generative AI may play a key part in connecting and automating information flow through the system, and thus enable healthcare providers to have the right information available where it is needed to optimally diagnose and treat patients. This is going to be a big improvement in efficiency for healthcare providers and in quality of care for patients.
2) The increasing demand for diagnostic imaging procedures coupled with the increasing shortage of qualified personnel (in particular MR technologists) is creating a need for more autonomous, intelligent scanners that can take over some of the tasks an MR technologist has to perform today. This will ensure that patients receive timely diagnosis and treatment with a high, standardized quality of care. I am very happy to be part of this journey and to contribute to the development of these future, more intelligent MR scanners.

How did you first come into contact with MRI?
I had my first touchpoints with MRI when I was still working in fundamental physics, on quantum sensing and quantum computing. I drew methodological inspiration for my work on spin physics from the admirable, established body of work on nuclear magnetic resonance (NMR) and MRI. I remember being deeply intrigued by the way MRI skillfully plays with spin physics and combines this with substantial medical value in a beautiful way.

What would you do if you could spend a month doing whatever you wanted?
This may sound strange, but I don't think I would want to do anything differently. I really enjoy both my professional work and my private life as they are right now. My work on developing autonomous scanning with great colleagues and in very close collaboration with our clinical and research partners is the perfect mix for me.

On the personal side, my husband and I are blessed with an 11-month-old girl, who is extremely curious and always learning. If anything, I wish the day had more than 24 hours so I could do even more of everything I love. And sometimes a bit more sleep would also be nice, but I guess that will come back, when my daughter is a bit older. 😊

Get to know us

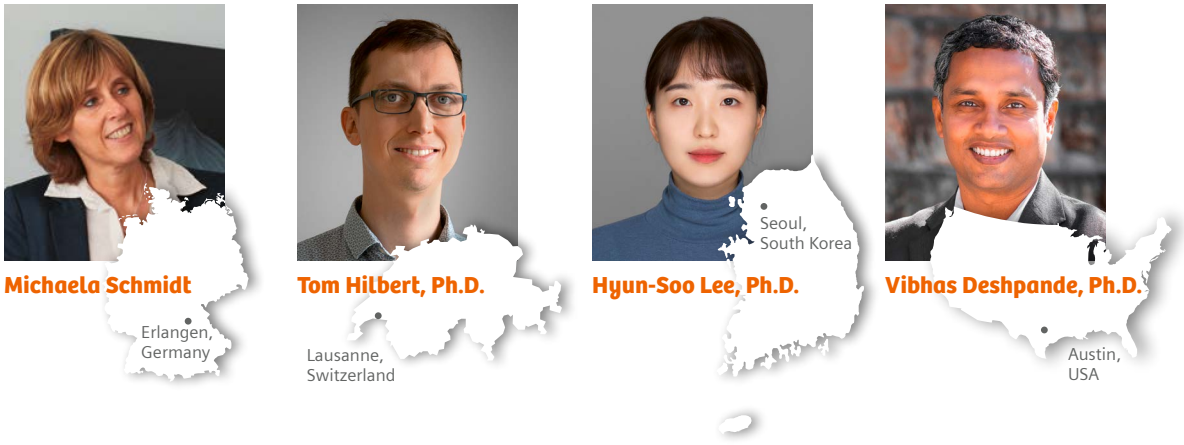

Find more portraits of our colleagues around the world!

www.magnetomworld.siemens-healthineers.com/meet-siemens-healthineers

The entire editorial staff at University of Cape Town (UCT), Cape Town, South Africa and at Siemens Healthineers extends their appreciation to all the radiologists, technologists, physicists, experts, and scholars who donate their time and energy — without payment — in order to share their expertise with the readers of MAGNETOM Flash.

MAGNETOM Flash — Imprint

Publisher:
Siemens Healthineers AG
Magnetic Resonance,
Karl-Schall-Str. 6, D-91052 Erlangen, Germany

Editor-in-chief:
Antje Hellwich
antje.hellwich@siemens-healthineers.com

Guest Editor:
Professor Ernesta Meintjes, Ph.D.
Department of Human Biology
Faculty of Health Sciences
University of Cape Town
Anzio Road, Observatory
Cape Town, 7925
South Africa

Editorial Board:
André Fischer, Ph.D.; Kera Westphal, Ph.D.;
Heiko Meyer, Ph.D.; Wellesley Were; Katie Grant, Ph.D.

Review Board:
Gaia Banks, Ph.D.; Tassiana Marini, Ph.D.;
Christian Mühlhäusser; Christian Schuster, Ph.D.;
Aurélien Stalder, Ph.D.; Gregor Thörmer, Ph.D.

Copy Editing:
Sheila Regan, Jen Metcalf, UNIWORKS,
www.uni-works.org
(with special thanks to Kylie Martin)

Layout:
Agentur Baumgärtner,
Friedrichstr. 4, D-90762 Fürth, Germany,
www.agentur-baumgaertner.com

PrePress and Image Editing, Production:
Sandra Birner, Andrea tom Felde, Jennifer Klancar,
Paul Linssen, Siemens Healthineers AG

Printer:
Schmidl & Rotaplan Druck GmbH,
Hofer Str. 1, D-93057 Regensburg, Germany

MAGNETOM Flash includes reports in the English language on magnetic resonance: diagnostic and therapeutic methods and their application as well as results and experience gained with corresponding systems and solutions. It introduces from case to case new principles and procedures and discusses their clinical potential. The statements and views of the authors in the individual contributions do not necessarily reflect the opinion of the publisher.

The information presented in these articles and case reports is for illustration only and is not intended to be relied upon by the reader for instruction as to the practice of medicine. Any health care practitioner reading this information is reminded that they must use their own learning, training and expertise in dealing with their individual patients. This material does not substitute for that duty and is not intended by Siemens Healthcare to be used for any purpose in that regard. The drugs and doses mentioned herein are consistent with the approval labeling for uses and/or indications of the drug. The treating physician bears the sole responsibility for the diagnosis and treatment of patients, including drugs and doses prescribed in connection with such use. The Operating Instructions must always be strictly followed when operating the MR system. The sources for the technical data are the corresponding data sheets. Results may vary.

We welcome your questions and comments about the editorial content of MAGNETOM Flash. Please contact us at
magnetomworld.team@siemens-healthineers.com

Manuscripts as well as suggestions, proposals and information are always welcome; they are carefully examined and submitted to the editorial board for attention. MAGNETOM Flash is not responsible for loss, damage, or any other injury to unsolicited manuscripts or other materials. We reserve the right to edit for clarity, accuracy, and space. Include your name, address, and phone number and send to the editors, address above.

MAGNETOM Flash is also available online:

www.magnetomworld.siemens-healthineers.com

Not for distribution in the US

On account of certain regional limitations of sales rights and service availability, we cannot guarantee that all products included in this brochure are available through the Siemens Healthineers sales organization worldwide. Availability and packaging may vary by country and is subject to change without prior notice. Some/All of the features and products described herein may not be available in the USA.

The information in this document contains general technical descriptions of specifications and options as well as standard and optional features which do not always have to be present in individual cases, and which may not be commercially available in all countries. Due to regulatory reasons their future availability cannot be guaranteed. Please contact your local Siemens Healthineers organization for further details.

Siemens Healthineers reserves the right to modify the design, packaging, specifications, and options described herein without prior notice. Please contact your local Siemens Healthineers sales representative for the most current information.

Note: Any technical data contained in this document may vary within defined tolerances. Original images always lose a certain amount of detail when reproduced.

Siemens Healthineers Headquarters
Siemens Healthineers AG
Siemensstr. 3
91301 Forchheim, Germany
Phone: +49 9191 180
siemens-healthineers.com

Published by Siemens Healthineers AG · Order No. A91MR-01000-0004M-7600 · Printed in Germany · 17686 0426 ·